UNIVERSITY OF OSLO
Faculty of Mathematics and Natural Sciences;
Department of Geosciences; Meteorology and Oceanography Section

Sensitivity of the Modeled Arctic Sea-Ice Extent and Thickness to Changes in Various Parametrizations

Master Thesis in Geosciences

Helene Birkelund Erlandsen

15th June 2010

Sensitivity of the Modeled Arctic Sea Ice Extent and Thickness to Changes in Various Parametrizations

Helene Birkelund Erlandsen

Master Thesis in Geosciences

Discipline: "Meteorology and Oceanography"

Department of Geosciences

Faculty of Mathematics and Natural Sciences

UNIVERSITY OF OSLO

15th June 2010

Tutors: Lars Petter Røed (met.no[1]/UiO metos[2]), Jens Debernard (met.no)
This work is published digitally through DUO Digitale Utgivelser ved UiO
http://www.duo.uio.no
It is also catalogued in BIBSYS (http://www.bibsys.no/english)

[1]the Norwegian Meteorological Institute

[2]The University of Oslo, Faculty of Mathematics and Natural Sciences, Department of Geosciences, Meteorology and Oceanography Section

Abstract

Seven experiments are conducted on a coupled ice-ocean model in order to gain insight in the sensitivity of the modeled Arctic sea-ice extent and thickness to crucial changes in the parametrization of the models albedo scheme and thermodynamics. In addition to a control experiment there are three sensitivity experiments which change how the snow/ice-albedo is parametrized. The first replaced the model's albedo scheme with a more basic one, while the remaing two made changes to the existing albedo scheme. Two experiments are conducted which altered the lead closing parameter, h_0, affecting the thickness of ice formed in open water. The final sensitivity experiment added an icreament of maximum $1°C$ to the 2 m atmospheric temperature. The ice thickness and extent is most sensitive to the experiment which replaced the model's albedo scheme with a basic one. This led to an increase from the control run in the sea ice extent and thickness of about 22%. Increasing the 2 m atmospheric temperature led to a decrease of 60% in the mean snow thickness. Thus the snow thickness is sensitive to the parametrizations of sensible heat and longwave radiation. The seasonal cycle of the sea ice extent was sensitive to the changes made to the lead closing parameter h_0. This parameter can be used to tune the modeled cycle of the sea ice extent to coincide better with the observed sea ice extent cycle.

Acknowledgements

First and foremost to thank my supervisor Lars Petter Røed(@met.no/metos) for orchestrating my thesis and for great guidance. I would also like to my thank my co-supervisor Jens Debernard(@met.no) for patiently answering all my questions about MI-IM and sharing of his knowledge about sea ice. Also Morten Køltzow(@met.no), who acted as my reserve co-supervisor, deserves great thanks for helping me set up my experiments, bringing forward great ideas for the experiments, and sharing of his knowledge. I would also like to thank Yvonne Gusdal(@met.no) for helping me with finding and using met.no scripts to analyse my data (making climatologies from felt-files, including new files to Diana..), and especially much for preparing two OSI-SAF time-series of sea extent suitable for comparing with the model results. Thanks to Ann Kristin Sperrevik(@met.no) for sharing her latex master-thesis-setup with me. I would also like to thank met.no for giving me access to their software, data and models.

I would also to thank the Norwegian Polar Institute for having me as an assistant during their annual field work in the Fram Strait, September 2010, especially Edmond Hansen and Sebastian Gerland. Working in and on the sea ice, seeing and experiencing it for myself, was a great inspiration for my thesis, and also educational.

My fellow students deserves gratitude for making the two years of being a master student fun, with cabin trips, parties, and all the lunch breaks where serious subjects were frowned upon. Thanks, Magne, for reading over the last few pages of my thesis!

Finally, I would like to thank my family and friends, especially Ole Michael Bjørndal, who makes me laugh, and helps and supports me where he can and motivates me to work hard. Thank you. Also my mom, Gunn Elisabeth Birkelund, deserves a special thanks for pointing out some of my skrive-leifs, helping me seeing things from a supervisors point of view, and for making me want to become a researcher, like her.

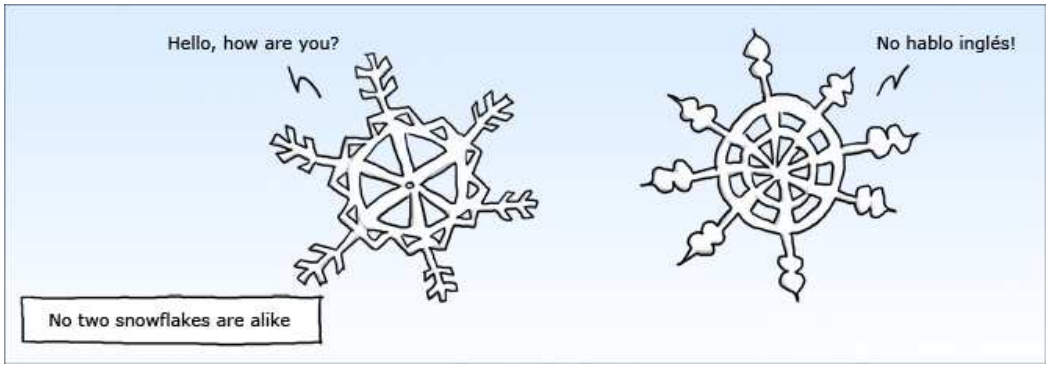

Wulfmorenthaler strip.

Helene B. Erlansen
June 13, 2010

Contents

Abstract ii

Aknowledgements ii

List of Figures vii

List of Tables vii

1 Introduction 1

2 Model Description 3
- 2.1 The Ice Model . . . 3
  - 2.1.1 Relevant Governing Equations . . . 5
- 2.2 The Ice/Snow Albedo Scheme . . . 7
- 2.3 The Ocean Model . . . 8
- 2.4 Initialization and Forcing . . . 10
- 2.5 Hardware, Post-Processing, and Tools . . . 10

3 Sensitivity Experiments 11
- 3.1 Control Experiment . . . 11
- 3.2 Albedo Experiments . . . 12
  - 3.2.1 Alb1 . . . 12
  - 3.2.2 Alb2 . . . 12
  - 3.2.3 Alb3 . . . 14
- 3.3 OW Freezing Experiments . . . 18
  - 3.3.1 Freeze1 . . . 20
  - 3.3.2 Freeze2 . . . 20
- 3.4 Forcing Experiment . . . 20
  - 3.4.1 Temp . . . 20

4 Observations 23
- 4.1 SMMR . . . 24
- 4.2 SSM/I . . . 25
- 4.3 NSIDC Sea Ice Index . . . 25
- 4.4 OSI SAF Global Sea Ice Concentration Reanalysis Product . . . 26
- 4.5 Error Sources . . . 27
  - 4.5.1 Summer Underestimation of the Sea-Ice Concentration . . . 28

5 Results **31**
5.1 Albedo Experiments 31
5.2 Remaining Sensitivity Experiments 32
5.3 All Experiments 36
5.3.1 Snow Thickness 36
5.3.2 Ice Thickness 37
5.3.3 Sea-Ice Extent 37
5.4 Sea-Ice Extent in Comparison to Satellite Observations 43

6 Analysis **51**
6.1 How does the Sensitivity Experiments Compare the Control Experiment and to Observations? 51
6.1.1 Alb1 51
6.1.2 Alb2 53
6.1.3 Alb3 54
6.1.4 Freeze1 55
6.1.5 Freeze2 56
6.1.6 Temp 57
6.2 How does MI-IM's Sea-Ice Extent Compare to Observations? 58
6.3 Observation Uncertainty 59
6.4 A Summary of Each Sensitivity Experiment's Results 60

7 Summary and Key Findings **63**
7.1 Future Work 66

Appendix A **67**

Appendix B **68**

Bibliography **69**

List of Figures

2.1 MI-IM's domain 4
2.2 Figure **a** shows heat fluxes to and from each interface. Figure **b** shows the interface temperatures 5
2.3 The production rates/volume flux from one medium to another. 6
2.4 The snow and ice albedo as a function of h and h_s, T_s and h_s, and T_s and h. 9

3.1 The snow and ice albedo for Alb1, and for Alb2 as a functions of h and h_s, T_s and h_s, and T_s and h. 13
3.2 Various ways of describing the snow cover fraction, f_S, based on the mean snow thickness 14
3.3 Observed relationship between albedo and snow thickness 15
3.4 The snow and ice albedo Alb3 as a function of h and h_s, T_s&h_s, and T_s and h. 17
3.5 The temperature increment used in the forcing experiment 20
3.6 Comparison of temperature for three reanalyses with soundings from the HARA-archive for the period 1979-1996. 22

4.1 The first TIROS TV image 23
4.2 Mean monthly sea-ice concentration for February and August 1985 derived from the SMMR on Nimbus-7. 24
4.3 OSI SAF's and MI-IM's domain. 26
4.4 Comparison between NIC chart's and OSI SAF reanalysis' sea-ice concentration data for the N.H.. 29

5.1 Daily mean ice thickness for the Control exp. and the albedo exp. from 1980 to 1990. 34
5.2 1985-1990 monthly climatology of mean sea-ice thickness for the Control exp. and the albedo exp.. 34
5.3 1985-1990 monthly climatology of sea-ice extent for the Control exp. and the albedo exp.. 34
5.4 1985-1990 monthly climatology of mean ice volume for the Control exp. and the albedo exp.. 34
5.5 Daily mean ice thickness for the Control, OW freezing and forcing experiments from 1980 to 1990. 35
5.6 1985-1990 monthly climatology of mean sea-ice thickness for the Control, OW freezing, and forcing experiments. 35
5.7 1985-1990 monthly climatology of sea-ice extent for the Control, OW freezing, and forcing experiments. 35

5.8 1985-1990 monthly climatology of sea-ice volume for the Control, OW freezing, and forcing experiments. 35
5.9 Climatology of daily mean snow thickness between 1985 and 1990 for all experiments. The red, stapled line shows $h_s = 1.5$ mm, the melt season criteria. 39
5.10 Bias and corr. coeff. for for monthly values of mean snow thickness between 1985-1990 for the experiments. 39
5.11 Bias and ρ for for monthly values of mean ice thickness between 1985-1990 for the experiments. 39
5.12 Bias and ρ for for monthly values of sea-ice extent between 1985-1990 for the experiments. 39
5.13 Snow thickness in May 1990 for the Control and sensitivity experiments. . 40
5.14 sea-ice thickness in March 1990 for the Control and sensitivity experiments. 41
5.15 sea-ice thickness in September 1990 for the Control and sensitivity experiments. 42
5.16 sea-ice extent for the Control and albedo experiments compared to observations. 47
5.17 As described in Figure 5.16, but for the Control, OW freezing and forcing experiments. 47
5.18 Monthly mean modeled bias in sea-ice extent in comparison to OSI SAF data. 47
5.19 The bias, root mean square error and correlation coefficient (ρ) of monthly mean sea-ice extent from July 1987 to December 1990 between model experiments and satellite observations (OSI-SAFv2). 48
5.20 sea-ice concentrations in September 1990 for the Control and sensitivity experiments. 49
5.21 sea-ice extent in July and October 1990 for the Control, Alb1, OW freezing and forcing experiments and from sea-ice concentrations from OSI SAF. . . 50

6.1 The snow cover fraction and the similar expression resulting from weighing the snows albedo towards the underlying snow (given $T_S \leq -2°C$) 54

List of Tables

3.1 An Overview of the Seven Experiments Performed 11
3.2 An overview of the different parametrizations of snow cover fraction 15

5.1 Maximum, minimum and mean values of ice thickness, extent and volume from the 1985-1990 average monthly mean values for the Control experiment and the albedo experiments 32
5.2 Maximum, mean and minimum values of ice thickness, extent and volume from from 1985-1990 monthly mean values for the Control, OW freezing and forcing experiment. 33
5.3 Bias and root mean square error (in brackets) of the sensitivity experiments when compared to the Control experiment (1985-1990). 36
5.4 Snow Free Period and Mean Value of h_s from Daily Climatology (1985-1990) 36
5.5 Correlation coefficient, RMSE and bias of each experiment's sea-ice extent in relation to the Control experiment 38
5.6 Correlation coefficient (ρ), root mean square error (RMSE) and bias of each experiment's eea ice extent in comparison to the OSI SAF sea-ice extent . 43
5.7 Root mean square error (RMSE) and correlation coefficient (ρ) of modeled and observed sea-ice extent from July 1987 to December 1990. 46

6.1 The change in % caused by the experiment on the snow and ice thickness and ice extent. 51
6.2 The difference in % between the observed (OSI SAF) and modeled minimum ice extent. 51

Chapter 1

Introduction

Considered are how sensitive the modeled Arctic sea-ice thickness, extent and snow thickness to crucial changes in the sea-ice parametrizations, such as the albedo scheme and empirical coefficients included in the thermodynamics of the sea-ice model. Seven experiments are conducted and the results from these experiments are compared to determine which of these parameters need further research and tuning. The experiments have been run from 1980 trough 1990. The sea-ice extent produced by each experiment is compared to satellite observations of the sea ice extent, to study which parametrizations induced a sea-ice extent coinciding the most with the observations.

18 000 years ago Scandinavia was covered by ice (*Yokoyama et al.*, 2000). The maintenance of the ice ages is related to the physical properties of ice (*Hartmann*, 1994). Ice and snow has the highest albedo, the ability to reflect incoming sunlight, of all earth's surfaces. This property alters the surface heat budget as less short wave radiation is absorbed at the surface. A higher albedo leads to a lower surface temperature, which encourages ice production, either at the sea surface, in rivers and lakes, or on top of land as frozen precipitation, further increasing the albedo of the surface. A lower albedo leads to a higher surface temperature and consequently less ice and snow covered surfaces, which further decreases the albedo. The interconnection between the surface temperature and the albedo is called the temperature-albedo feedback mechanism, which is a key parameter for understanding the local as well as the global climate.

The observed September sea-ice extent in the Arctic has decreased with 8.9% per decade between 1979 and 2009 (*Perovich et al.*, 2009). It is likely that human activities have had a net warming influence on the climate since 1750 (*Solomon et al.*, 2007). Climate models aim to simulate the present, past and future climate. An important part of these models is the sea-ice model and its coupling to the atmosphere above and the ocean beneath. Predicting the future sea-ice extent is therfore necessary to know the magnitude of the possible changes in the Arctic, due to global warming. In addition, the declining sea-ice extent opens up new shipping routs, reserves of offshore oil and gas, and new (or destroyed) fishing grounds become available for human exploitation. This gives the area an enhanced political and economical value, especially for Norway (*Øseth*, 2010).

Over the past decades climate models are developed to a level in which they are able to reproduce observed past and recent climate changes (*Solomon et al.*, 2007). However,

none, or very few of the climate models included in the Intergovernmental Panel of Climate Change (IPCC) Fourth Assessment Report (AR4) was able to simulate how fast the Arctic sea-ice declined between 1953 to 2006 (*Stroeve et al.*, 2007).

Improved knowledge about the sensitivities of the sea-ice model is therefore important to better simulate future climate change. For this reason six sensitivity experiments in addition to a control experiment are carried out using a coupled sea-ice-ocean model. Three experiments change the albedo parametrization in the model, two alter the value of a parameter controlling the thickness of ice produced in open water, and one experiment increases the 2 m temperature, forcing the coupled ice-ocean model.

The sea-ice model used is the Norwegian Meteorological Institute's Ice Model (MI-IM). It is a dynamic-thermodynamic regional model with an integrated air-sea flux module developed by the Norwegian Meteorological Institute (met.no) (*Røed and Debernard*, 2004). It is coupled with MICOM (*Bleck et al.*, 1992), met.no's version of the Miami Isopycnic Coordinate Model. The atmospheric forcing is derived using input from ECMWF's 45 year reanalysis, ERA-40 (*Uppala et al.*, 2005). The seven experiments simulates the years from 1980 trough 1990.

The sea-ice extent and thickness and the snow thickness produced in each experiment are compared with observations and each other to possibly answer the following research questions: 1)How sensitive are the ice thickness, the minimum ice extent, and the snow thickness to the various parametrizations and to a change in the atmospheric forcing?, 2)How well is the seasonal and inter-annual variation in the Arctic sea-ice extent reproduced in the model?", and finally, 3)Which parameters are most important to determine?.

The thesis is organized as follows. Chapter 2 gives an overview of the sea-ice model MI-IM, used to investigate the above-mentioned questions. It also contains a brief description of the ocean model MICOM, the atmospheric forcing ERA-40, and the initialization of the model runs. The details of each experiment and the motivation for conducting it are explained in Chapter 3. Chapter 4 gives an overview of the satellite products that are used to validate the sea-ice extent produced by the experimental runs. The results are then presented in Chapter 5. The results are discussed in Chapter 6. Chapter 7 contains a summary and offers answers to the research questions identified above.

Chapter 2

Model Description

We have used a stand-alone version of the Oslo Regional Climate Model (ORCM), a fully coupled atmosphere-ice-ocean model as described in *Debernard and Køltzow* (2005). The stand-alone coupled ice-ocean model consist of the Norwegian Meteorological Institute's Ice Model, a dynamic-thermodynamic model described in *Røed and Debernard* (2004) (though the version used here[1] has been improved in some areas). The ocean component is a slightly modified version of the Miami Isopycnic Coordinate Model (MICOM) (*Bleck et al.*, 1992). The coupled ice-ocean model is forced by atmospheric conditions constructed from ECMWF's 45 year reanalysis, ERA-40 (*Uppala et al.*, 2005).

The model domain covers the Arctic Ocean and the Atlantic Ocean, from the southern tip of Florida in the west to Morocco in the east, some of the Mediterranean Sea and the Baltic Sea, as depicted in Figure 2.1. The grid mesh-size is 0.25×0.25 degrees.

2.1 The Ice Model

The Norwegian Meteorological Institute's Ice Model, from now on referred to as MI-IM, has the following prognostic variables: ice stress, $\mathcal{R}$, ice concentration, A, ice volume, hA, ice velocity, $\mathbf{u}$, snow volume, Ah_s, and heat content, E. MI-IM's internal ice stress is based on an elastic-viscous-plastic rheology (EVP) as suggested by *Hunke and Dukowicz* (1997). The EVP rheology allows the ice's adjustment process to take place by elastic wave mechanisms. This does not represent any physical characteristics of the ice as a medium. However it results in a more computational efficient scheme than using the common visco-plastic rheology introduced by *Hibler* (1979). More importantly it avoids the need to employ implicit methods.

The albedo scheme is based on that of *Køltzow* (2007). The thermodynamics follow *Hibler* (1979), *Mellor and Kantha* (1989), and *Häkkinen and Mellor* (1990). In addition, the model includes a prognostic melt heat variable that preserves the heat content and allows ice formed in one place to melt in another. The thermodynamics are modeled with one ice layer and one snow layer. The snow layer has no heat capacity. Advection of prognostic variables is done using MPDATA (*Smolarkiewicz and Margolin*, 1998). This minimizes the

[1] MI-IM.091014

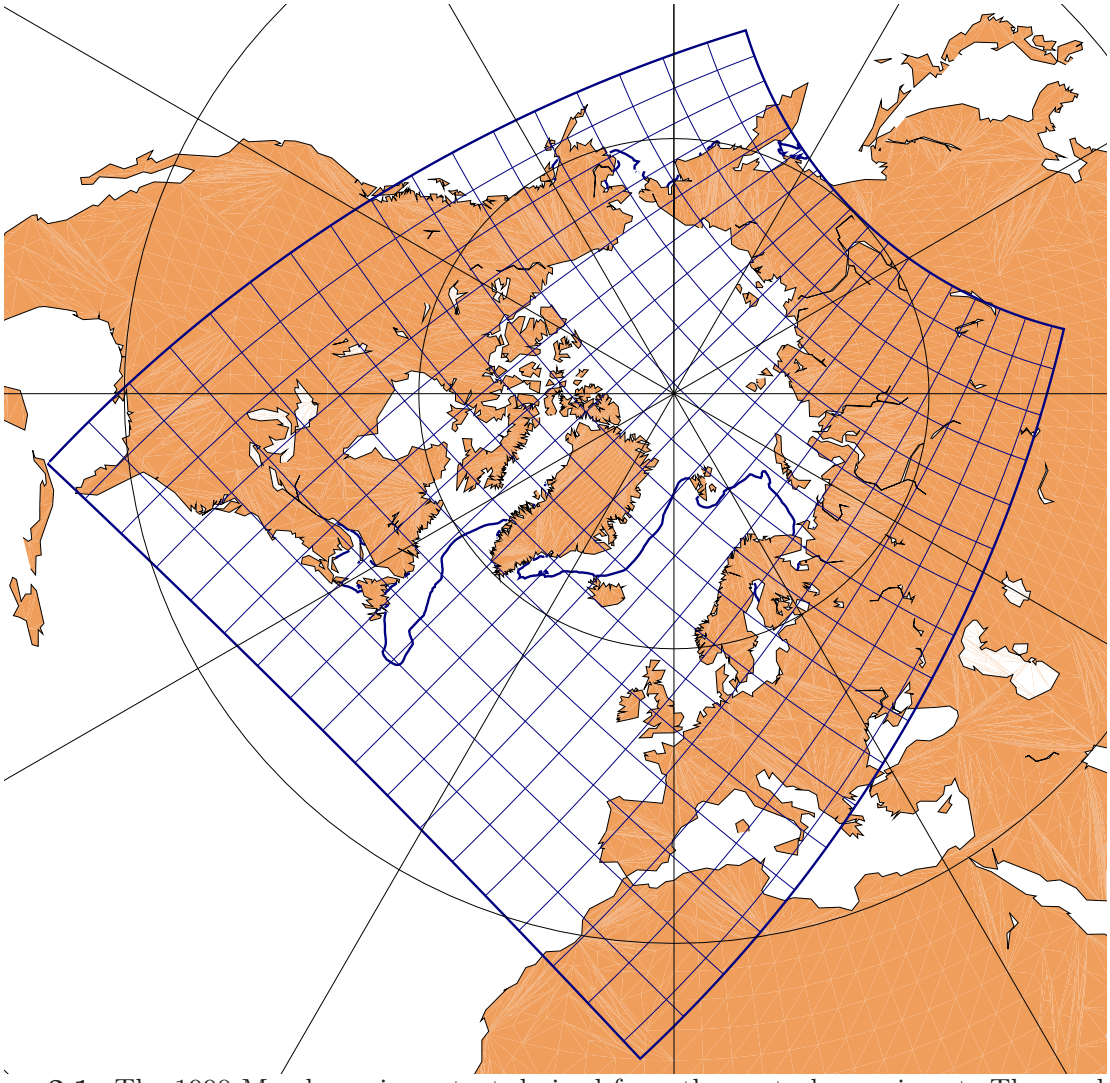

Figure 2.1: The 1990 March sea-ice extent derived from the control experiment. The model domain is marked together with every 20^{th} grid-line and every 30^{th} degree latitude and longitude.

diffusion of steep gradients and helps retain a sharper ice edge in the marginal ice zone (*Røed and Debernard*, 2004).

The flux module integrated in MI-IM exchanges heat, momentum and salt between the ocean, atmosphere and cryosphere. There are up to four important interfaces: the atmosphere-ice/snow interface, the ice-snow interface, the ice-ocean interface, and the ocean-atmosphere interface (Figure 2.2). The parametrizations of the momentum and heat fluxes towards the atmosphere are based on bulk formulas. Appendix B gives an overview of the variables and parameters included in the model.

The boundary conditions of the interfaces are used to calculate the fluxes. The fluxes are defined positive directed upwards. Only the heat fluxes will be further discussed. If no heat is stored at the interface, the interface value must be such that it balances the flux coming in to and going out from the interface. This is always true for the ice-snow interface, as no production or melting of snow or ice takes place here. If the interface temperature is calculated to be equal that of the medium's freezing-/melting point, the temperature is set

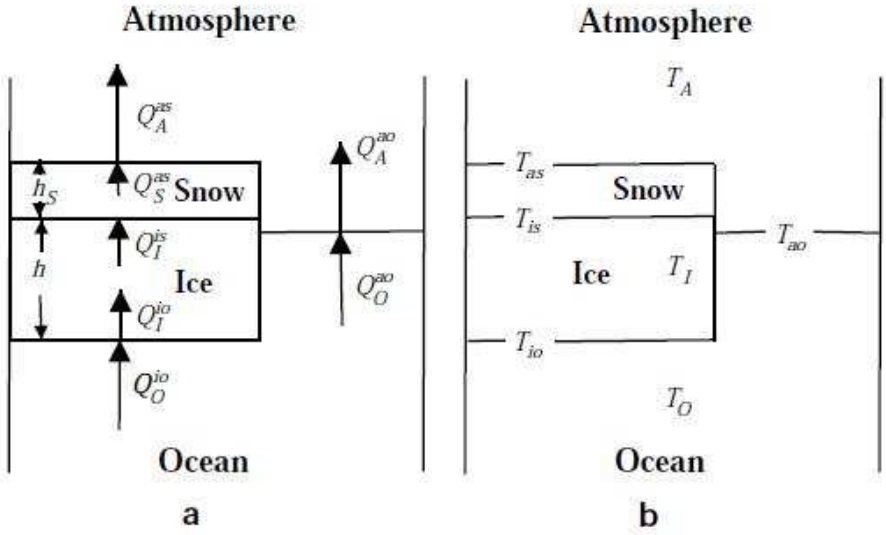

Figure 2.2: Figure **a** shows heat flux (Q_Y^{xy}) to and from each interface.The heat flux's subscript (Y) indicates in which medium the heat flux takes place, while the subscripts (xy) marks which interface the flux is directed. Figure **b** depicts the temperatures used in MI-IM. T_A is the 2m atmospheric temperature, T_I the interior ice temperature, and T_O the upper ocean mixed layer temperature. Also the interface temperatures are shown. In that case the temperature has two indices, indicating the two spheres on each side of the interface. The variables are listed in Appendix B. (Courtesy of *Røed and Debernard* (2004).)

to this value and the remaining heat difference is used to produce ice, or melt ice or snow.

For example, the heat flux coming from the mixed layer to the ocean-atmosphere interface should be balanced by an equal flux going from the ocean-atmosphere interface towards the atmosphere. The interface temperature is calculated to balance these fluxes. The minimum ocean-atmosphere interface temperature possible is the freezing temperature of seawater at the given salinity, T_f. If the interface temperature is calculated to be equal or less than this, the interface temperature is set to T_f and the fluxes are no longer balanced. At this point heat is stored at the interface as sea-ice.

Equally, if the temperature at the atmosphere-snow interface is calculated to be equal to the melting temperature of snow or more, $T_{as} \geq 0°C$, the interface temperature is set to $0°C$, and the flux imbalance are used to melt the layer of snow.

2.1.1 Relevant Governing Equations

The equations concerning the conservation of ice volume and ice concentration differs somewhat from those described in *Røed and Debernard* (2004). As they are particularly relevant for two of the sensitivity experiments they are explained in some detail.

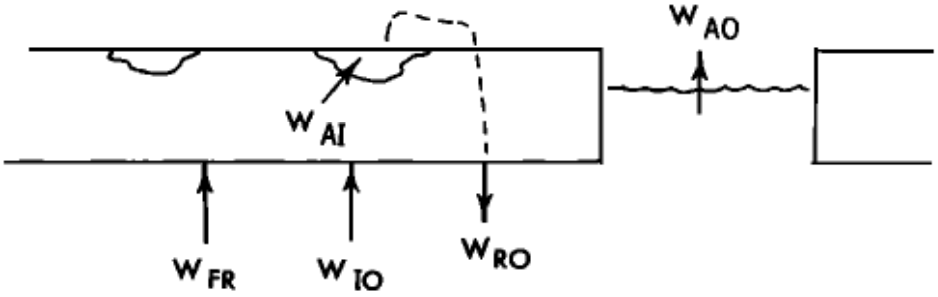

Figure 2.3: The production rates/volume flux from one sphere to another is seawater height per second. The fluxes are positive upwards. W_{io} is the flux from the ocean to the ice or vica versa, W_{ai} the flux across the ice-atmosphere interface (the melt rate, always positive), W_{ao} the flux from the ocean-atmosphere interface, always positive, and W_{fr} is the frazil ice production in the water column.W_{ro} is the runoff. (*Mellor and Kantha*, 1989)

Conservation of Ice Volume

The equation for the conservation of ice volume is:

$$\partial_t(hA) + \nabla \cdot (hA\mathbf{u}) = \frac{\rho_w}{\rho_I}[A(W_{io} - W_{ai}) + (1 - A)W_{ao} + W_{fr}] + \beta(T_O, T_f)hA - AEv \quad (2.1)$$

where hA is the thickness of the ice if it was distributed evenly throughout the unit area, i.e. the equivalent ice thickness or volume per unit area. The ice mass over a unit area is accordingly $\rho_I hA$. h is the mean ice thickness (in the ice covered fraction of a unit area). A is the fraction of a unit area that is covered with ice ($A \epsilon [0\ , 1]$). ρ_w is the density of sea water (=1026 kg/m^3) and ρ_I the density of ice (=900 kg/m^3). The production rates W_{io}, W_{ai}, W_{ao}, and W_{fr} are described in Figure 2.3. As the production rates here are all given in meters of seawater height per second, the production rates are multiplied by ρ_w/ρ_I to get them in meters of ice per second. E_v is the evaporation rate over ice, and β is a lateral melting variable.

The evaporation term, AE_v, and the lateral melting term, $\beta(T_O, T_f)hA$ are not included in the equation for conservation of ice volume in *Røed and Debernard* (2004). The evaporation term is only active when the ice is bare. The lateral melting term, $\beta(T_O, T_f)hA$, decreases from zero with the square of the difference between the upper ocean mixed layer temperature and the freezing temperature of the same water mass.

The different terms in the equation represents the dynamics and thermodynamics influencing the ice mass as well as sources and sinks to the ice mass. The left-hand side of the equation represents the local time rate of change and the lateral divergence of the ice mass flux. On the right-hand side the first term represents how ice melting on the surface (ablation) or at the bottom of ice floes decreases the ice mass, or how ice formed at the bottom of an ice floe (congelation growth) increases the ice mass. The second term represents how the ice mass increases as ice is formed in open water; the third how it increases as frazil ice is produced in the water column.

Conservation of Ice Concentration

It should be noted that in contrast to (2.1) the following equation is empirical.

$$\partial_t A + \nabla \cdot A\mathbf{u} = \frac{\rho_w}{h_0 \rho_I}[W_{fr} + (1 - A)W_{ao}] + \beta(T_O, T_f)A \tag{2.2}$$

On the left-hand side of the equation the first term is the local time rate of change of the ice concentration, while the second term is the divergence. The terms within the brackets on the right-hand side of the equation represents how the ice concentration increases as ice is formed in open water or as frazil ice within the water column. The new ice is reordered to a thickness of h_0, sometimes referred to as a lead closing parameter. It represents the thickness the volume of sea-ice produced in open water and/or as frazil ice is reordered to. The parameter h_0 is set to 0.5 m in the current version of MI-IM. The last term on the right hand side represents how the ice concentration decreases as ice is melted laterally, and is a different term compared to that of *Røed and Debernard* (2004).

2.2 The Ice/Snow Albedo Scheme

An important part of the radiation is the albedo parametrization. The albedo parametrization in MI-IM is based on that of *Køltzow* (2007). It reads:

$$\alpha = f_S \cdot \alpha_s + f_{mp} \cdot \alpha_{mp} + (1 - f_S - f_{mp})\alpha_i \tag{2.3}$$

where f_S is the fraction of the area covered with snow, f_{mp} is the fraction of the area covered with melt ponds, and (1-f_S-f_{mp}) is the fraction of the area covered with bare ice. Likewise is α_s the snow albedo, α_{mp} the melt pond albedo, and α_i the albedo of bare ice.

The fraction of the area covered by snow, f_S, is simply given by:

$$f_S = \min(\sqrt{\frac{h_S}{0.2m}}, 1) \tag{2.4}$$

where h_s is the mean snow thickness.

The albedo of snow depends on the surface temperature. If the surface temperature, T_s is zero degrees Celsius, the snow is melting and consequently has a lower albedo:

$$\alpha_s = \begin{cases} 0.77 & ; \text{if } T_s = 0°C \\ 0.84 & ; \text{if } T_s < 0°C \end{cases}$$

If the snow is thinner than 20 cm the snow albedo is weighted towards the albedo of the underlying ice:

$$\alpha_s = f_S \cdot \alpha_s + (1 - f_S) \cdot \alpha_i \tag{2.5}$$

The melt pond fraction, f_{mp}, and the melt pond albedo, α_{mp}, occurs when the snow cover fraction is less than unity and the surface temperature, T_s[2], is higher than -2°C.

[2] T_s can either be the snow-atmosphere interface temperature, T_{as}, or, if the ice is bare, the ice-atmosphere interface temperature, T_{ai}.

The melt pond fraction depends on the mean snow thickness and the surface temperature:

$$f_{mp} = (1 - f_S)[0.11 \cdot (2 + T_s)] \quad , T_s > -2°C \tag{2.6}$$

The melt pond albedo depends on the surface temperature:

$$\alpha_{mp} = 0.36 - 0.1 \cdot (2 + T_s) \quad , T_s > -2°C \tag{2.7}$$

The ice albedo depends on the surface temperature and the thickness of the ice:

$$\alpha_i = \begin{cases} \min(h, 0.5) \cdot 2 \cdot (0.60 - 0.1) + 0.03 & ; \text{if } T_s = 0°C \\ \min(h, 0.5) \cdot 2 \cdot (0.60 - 0.1) + 0.10 & ; \text{if } T_s < 0°C \end{cases}$$

If the surface is snow covered the albedo varies from 0.84 (when the mean snow thickness is over 20 cm and the snow is not melting) to 0.16 (when the snow thickness is at its minimum and the ice thickness is at its minimum). The melt pond albedo approaches 0.36 as the surface temperature goes towards -2 °C, and decreases to 0.16 when the surface temperature approaches 0 °C. The melt pond fraction varies between zero[3] and 0.22[4]. The albedo of bare ice varies between 0.60 (for non-melting ice thicker than 50 cm) to 0.09 (for melting ice which is 5 cm thin).

The ice/snow albedo is visualized in Figure 2.4. 2.4(a) shows the albedo as a function of snow thickness and ice thickness, given that the surface temperature is -2 °C or less. It decreases sharply when the ice thickness is less than 50 cm and when the snow thickness is less than 20 cm. Figure 2.4(b) shows the albedo as a function of surface temperature and snow thickness, given that the ice thickness is over 50 cm. Figure 2.4(c) and 2.4(d) show the albedo as a function of ice thickness and surface temperature, given respectively a mean snow thickness of 6 cm and 0 cm (no snow). Figure 2.4(b)–(d) depicts how the albedo decreases because of melt ponds when the surface temperature is greater than -2 °C. It is also visible how the albedo decreases when the snow or ice is melting and when the snow and ice becomes thinner.

2.3 The Ocean Model

The ocean model is met.no's version of the Miami Isopycnic Coordinate Model (MICOM). MICOM is a three-dimensional, barotropic-baroclinic, general ocean circulation model which uses potential density as it's vertical coordinate. The model is developed by *Bleck et al.* (1992). The model solves the primitive equations using a split-explicit numerical scheme. It consists of 27 density layers, where the upper layer is a mixed layer. The upper layer interacts with the atmosphere or sea-ice and the interior layers of the ocean model.

The model grid is a rotated spherical grid with a mesh size of 0.25×0.25 degrees. Rivers are included by supplying freshwater "precipitation" of a given salinity to the model (*Røed and Debernard*, 2005). As the model's boundary crosses the Bering Strait, the flux through the

[3]If the mean snow thickness is 20 cm or more or if the surface temperature goes towards -2 °C

[4]When the snow cover fraction and surface temperature equals zero

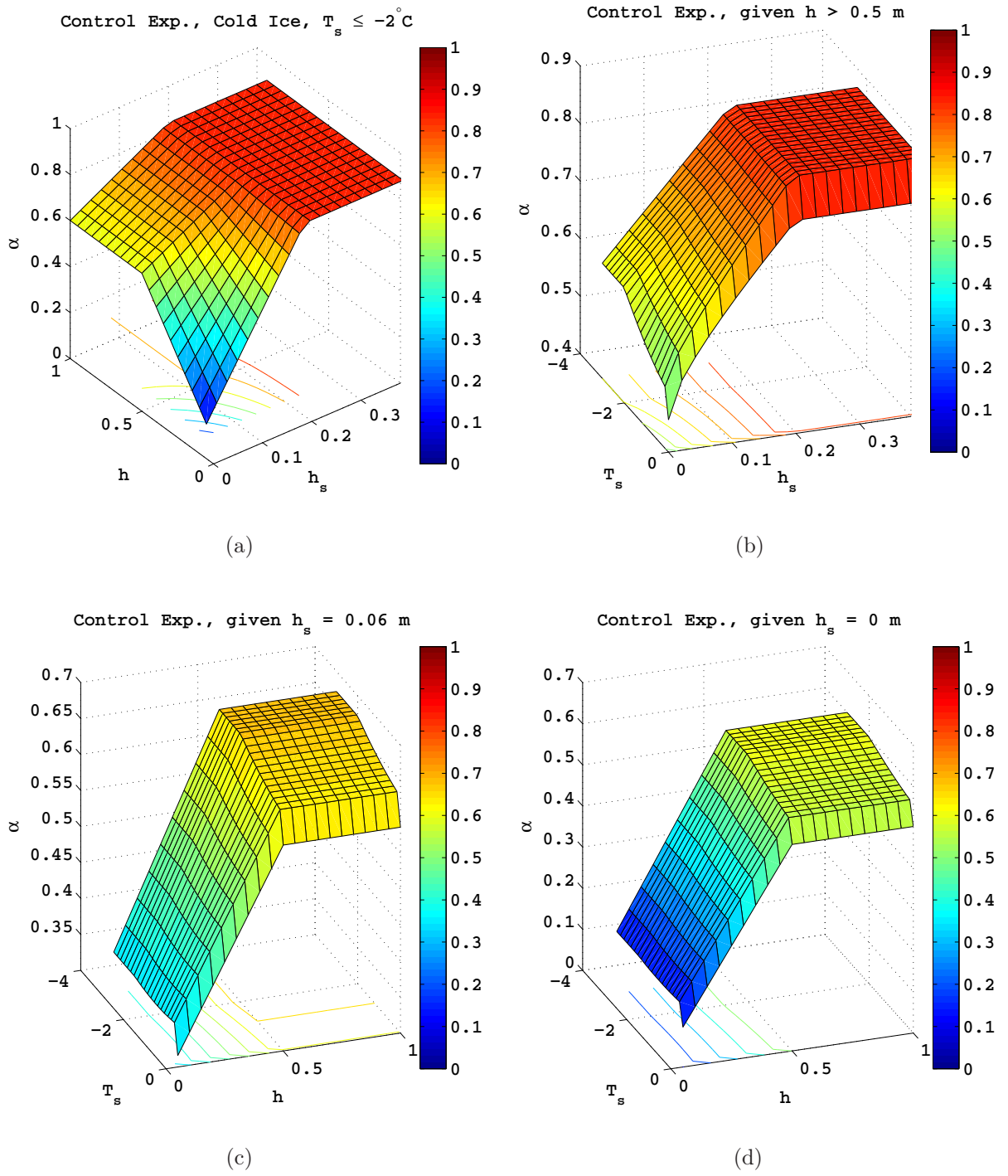

Figure 2.4: (a) shows the albedo of snow and ice as a function of ice thickness and snow thickness given that the interface temperature, T_s, is less than or equal to -2°C. (b) shows the albedo of snow and ice as a function of temperature and snow thickness, given that the ice is thicker than 0.5 m. (c) and (d) show the albedo as a function of the interface temperature and the ice thickness, (c) given a 6 cm mean snow thickness, and (d) given that the ice is bare ($h_s = 0$) .

strait is treated as a river with an influx of $1.1Sv$ with salinity and temperature retrieved from the SODA[5] reanalysis (*Carton et al.*, 2000). At the southern boundary (which is the

[5]Simple Ocean Data Assimilation

same as MI-IM's southern boundary) the version of MICOM used together with MI-IM gets its input from another version of MICOM that extends to 30°S. The latter version uses temperature and salinity specified by Levitus' climatology that is linearly interpolated between months and transferred to the model through a relaxation buffer zone at its open southern boundary. MI-IM receives salinity, sea surface temperature, and currents from MICOM.

2.4 Initialization and Forcing

MI-IM contains a flux module, a coupler, that ensure that the fluxes exchanged by the ocean, atmosphere and ice are conserved, including in ice-free areas. The model is run with atmospheric forcing constructed from ECMWF's reanalysis, ERA-40. ERA-40 is the ECMWF (European Center for Medium-Range Weather Forcasts) re-analysis, produced in collaboration with many institutions. It begins in September 1957, when the observing system had been enhanced in preparation for the International Geophysical Year, and runs until August 2002. The final version of ERA-40 was ready in 2003. For a detailed description of ERA-40 the reader is referred to *Uppala et al.* (2005). MI-IM receives the mean sea level pressure, 10 and 2 m wind velocity, the 2 m air and dew point temperature, the cloud coverage and precipitation every six hours from ERA-40.

From MICOM MI-IM receives salinity, sea surface temperature, sea level elevation and currents every hour. MI-IM exchanges fluxes with MICOM every hour. Because MICOM does not extend south of the Bering Strait, temperature, salinity and currents from the SODA climatology are used as input values for that area.

MI-IM was initialized with sea-ice values from December 1966. The ocean model is initialized from a six year run from 1960 to 1967. The atmosphere data from ERA-40 follows the dates in the model run, starting from January 1. 1980 ending December 31. 1990.

2.5 Hardware, Post-Processing, and Tools

The seven 11-year long experiments are executed on Njord, one of NOTUR - the Norwegian Center for Computational Science's high performance computing facilities. More information about the Notur facility can be found at `http://www.notur.no/`.

From each of the seven experiments monthly mean fields files have stored, as well as daily values of the following: total ice area, ice extent, total ice volume, total snow volume, mean snow thickness, and mean ice thickness. The latter were snapshots at noon. The total ice area and volume includes all of the sea-ice in the model. The ice extent is the area where the sea-ice concentration is more than 15%. This is chosen since the same number is used in the satellite products which are compared to the moodel results. The mean ice thickness and the mean snow thickness is the mean thickness in the sea-ice covered part of the model. The data is analyzed and visualized using Matlab and Diana.[6]

[6]Diana is an open source visualization and production tool for meteorological and oceanographical data developed by met.no, available for downloading at: `https://diana.wiki.met.no/doku.php`.

Chapter 3

Sensitivity Experiments

Table 3.1: An Overview of the Seven Experiments Performed

Group	Name	Description
Control	Control	Albedo scheme after *Køltzow* (2007), $h_0 = 0.50$ m
Albedo	Alb1	Simple albedo scheme (MK89)
	Alb2	Snow albedo not weighted towards the underlying ice
	Alb3	*tanh*-function for the snow cover fraction, f_s
OW Freezing	Freeze1	h_0 increased from 0.50 m to 1.00 m
	Freeze2	h_0 decreased from 0.50 m to 0.25 m
Forcing	Temp	For $-10°C \leq T_A < 0°C$: T_A increased with 10%.
		For $T_A < -10°C$: T_A increased with $1°C$.

To investigate which of the parametrizations that have the greatest influence on the modeled sea-ice variables, six sensitivity experiments are carried out in addition to a control experiment. The six experiments are split into three groups as listed in Table 3.1. The first group consists of three experiments in which the albedo parametrizations all differ from the control experiment. The second group, "OW (open water) Freezing Experiments" consists of two experiments where the value of the lead closing parameter h_0 differs from the control experiment. The third group, "Forcing Experiment", includes only one experiment in which the 2 m temperature is increased from its original value (from ERA-40).

3.1 Control Experiment

The control experiment is set up is as described in Chapter 2, including the standard albedo scheme of MI-IM which is based on *Køltzow* (2007) and described in Section 2.2. The lead closing parameter h_0 is set to 0.5 m.

3.2 Albedo Experiments

3.2.1 Alb1

Of the three albedo experiments, the first, Alb1, is the simplest. It completely replaces the original albedo scheme described in Section 2.2. It conforms to the albedo scheme used by *Mellor and Kantha* (1989) (here after MK89) which includes only three values for the albedo:

$$\alpha = \begin{cases} 0.82 & \text{; snow covered, no melting} \\ 0.73 & \text{; melting snow} \\ 0.64 & \text{; bare ice} \end{cases}$$

The albedo scheme is visualized in Figure 3.1(a). *Mellor and Kantha* (1989) based their albedo scheme on the values used in *Maykut and Untersteiner* (1971), who in turn used values suggested by *J. O. Fletcher* (1965). The values are based on the largest amount of observational data taken on perennial sea-ice available at the time.

3.2.2 Alb2

The second albedo experiment, Alb2, illuminates how sensitive the sea-ice variables are to weighing the snow albedo towards the albedo of the ice underneath it. If the mean snow thickness is less than 20 cm, the albedo is weighted by the local snow cover fraction, f_S, towards the albedo of the underlying ice, as given in (2.5) on page 7. As this is done in the present version of MI-IM (in the Control experiment), experiment Alb2 is to exclud the weighting, that is to remove (2.5) from the albedo scheme.

The resulting albedo can be seen in Figure 3.1(b) for surface temperatures below -2°C, with the albedo as a function of ice and snow thickness. Figure 3.1(c) shows the albedo given a mean ice thickness over 0.5 m, with the albedo as a function of the surface temperature and snow thickness, and Figure 3.1(d) depicts the albedo as a function of ice thickness and surface temperature, given a snow thickness of 6 cm.

The motivation for weighing the snow albedo towards the ice's albedo is to simulate the transparency of the snow cover when the snow cover is not optically thick (less than 20 cm thick). In an article by *Liu et al.* (2006) the correlation between the observed SHEBA[1] albedo and surface temperature, snow thickness and ice thickness was investigated. The albedo was found to be most correlated to the snow thickness. Even though this finding only applies for the given conditions at the site (on a multi-year floe), this result shows to that a good parametrization of the snow cover is very important in an albedo scheme.

[1]The Surface Heat Budget of the Arctic Ocean project, with observations from October 30, 1997 to October 10, 1998 from a MY ice floe drifting from 75°16.3'N 142° 41.2'W to 80°N 162°W during the year.

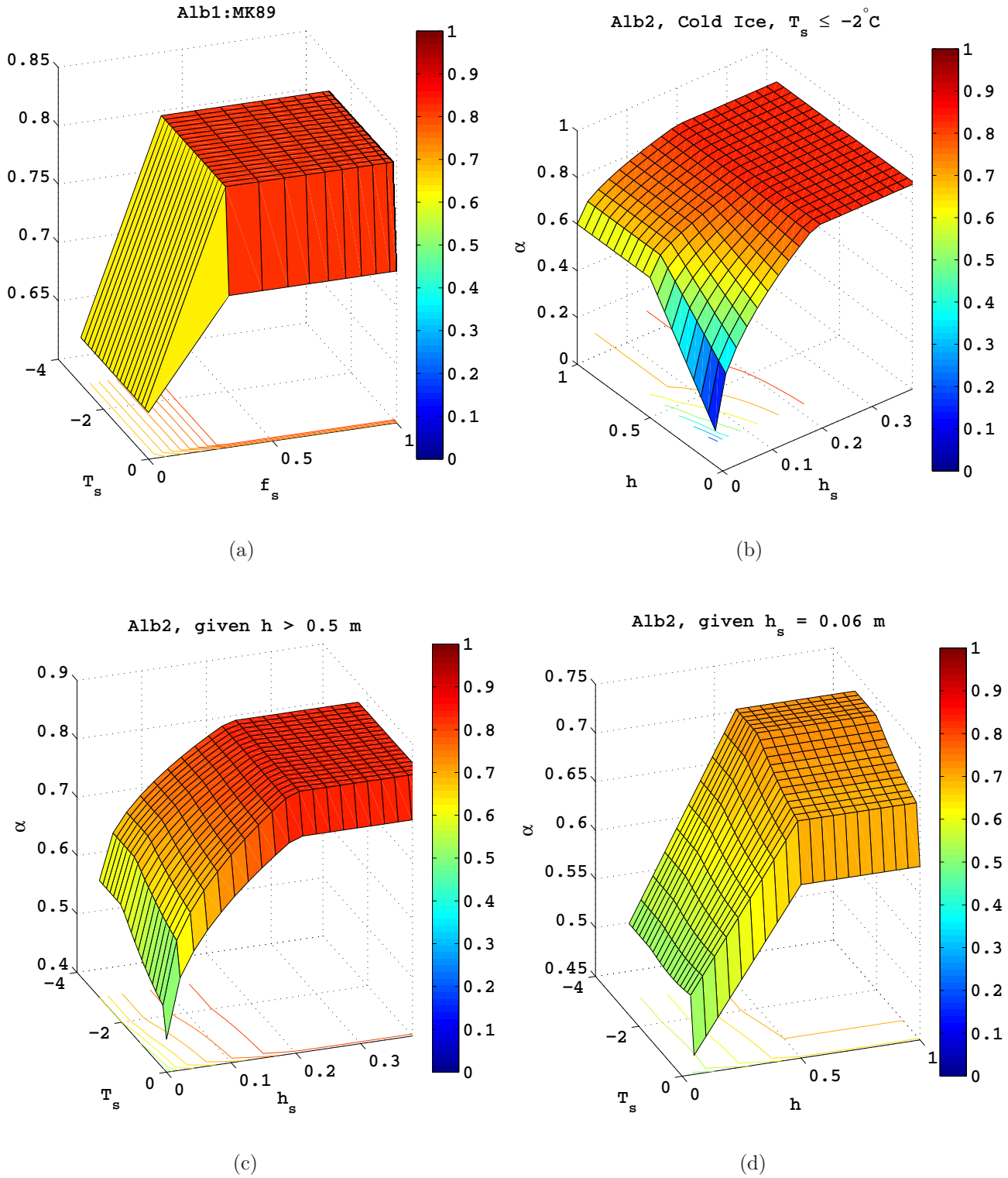

Figure 3.1: The figure depicts the two albedo schemes, Alb1 and Alb2. (a) shows the simple albedo scheme used in *Mellor and Kantha* (1989) and here in Alb1. (b) shows the albedo of snow and ice as a function of ice thickness and snow thickness given that the interface temperature, T_s, is less than or equal to -2°C. (c) shows the albedo of snow and ice as a function of temperature and snow thickness, given that the ice thickness is over 0.5 m. (d) shows the albedo as a function of the interface temperature and the ice thickness given a 6 cm mean snow thickness.

3.2.3 Alb3

In Alb3 a different parametrization for the snow cover fraction, f_S, is used. The snow cover fraction parametrization used in MI-IM and the Control experiment is substituted by the snow cover fraction parametrization proposed in *Yang et al.* (1997). Specifically, (2.4) on page 7 is substituted with:

$$f_S = \tanh(\frac{h_S}{2.5 z_0}) \tag{3.1}$$

where z_0, the roughness length is set to 0.02 m.

The snow cover fraction is an important part of the albedo scheme. Besides influencing how large the snow covered area of the sea-ice is trough (2.3) it also affects the fraction of melt ponds as displayed in (2.6), and it reduces the albedo for optically thin snow as shown by (2.5).

In flat areas such as on sea-ice the snow cover fraction should increase from zero to unity as the mean snow thickness increases. How quickly the snow cover fraction increases due to increasing snow thickness, and at what thickness the snow cover should reach its maximum should be reasonably parametrized. Figure 3.2 and Table 3.2 show some variations of snow cover fraction parametrizations used in some other models. For the models where the snow cover fraction is a function of snow water equivalent[2] (SWE), the conversion between SWE and snow thickness, h_S, has been using that $h_s/SWE = \rho_W/\rho_s$, and using a formula from *Verserghy* (1991):

$$\rho_S = 188.82 kgm^{-3} + 419.0 kgm^{-2} \cdot SWE$$

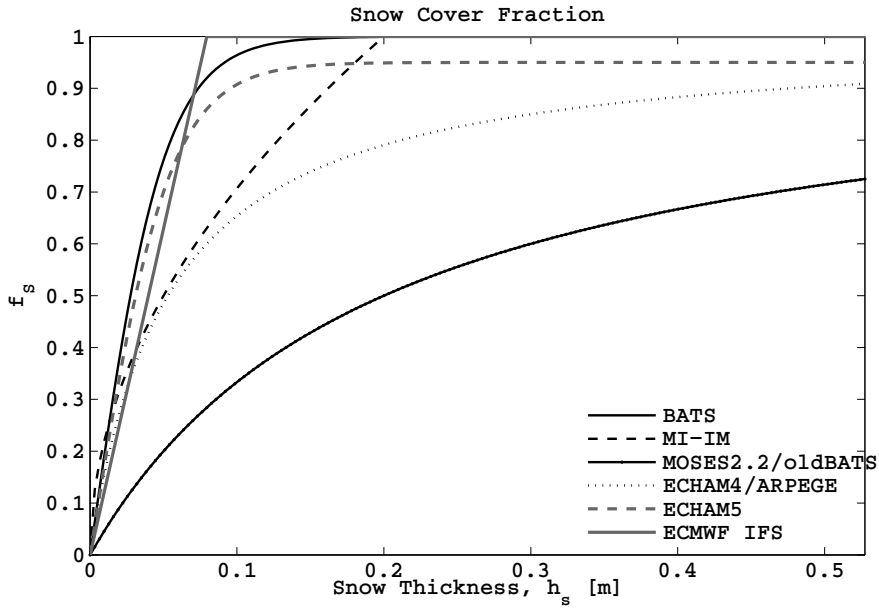

Figure 3.2: Various ways of describing the snow cover fraction, f_S, based on the mean snow thickness or snow water equivalent are shown. The models are listed in Appendix A.

[2]Snow water equivalent is the thickness the snow would have if it melted (was liquid).

Table 3.2: An overview of some different parametrizations of snow cover fraction. The models are listed in Appendix A. The snow cover parametrizations are visualized in Figure 3.2.

Model	Parametrization	Constants	Description in:
BATS	$f_S = \tanh(\frac{h_S}{2.5 \cdot z0})$	$z_0 = 0.02m$	*Yang et al.* (1997)
ECHAM4,ARPEGE	$f_S = \frac{\mathrm{SWE}}{\mathrm{SWE} + \mathrm{Sn}^*}$	Sn*=0.01	*Roesch et al.* (2001), *Douville et al.* (1995)
ECHAM5	$f_S = 0.95 \cdot \tanh(100 \cdot \mathrm{SWE})$		*Roesch et al.* (2001), *Roesch and Roeckner* (2006)
ECMWF IFS	$f_S = \min(1, \frac{\mathrm{SWE}}{\mathrm{Src}})$	Src=0.015	*ECMWF Research Department* (2003)
MI-IM	$f_S = \min(\sqrt{\frac{h_S}{0.2}}, 1)$		-
MOSES2.2,old BATS	$f_S = \frac{h_S}{h_S + 10 \cdot z0}$	$z_0 = 0.02$	*Essery et al.* (2001), *Yang et al.* (1997)

The ECMWF IFS is the only model with a snow cover parametrization which increases linearly. It also reaches its maximum snow cover when the mean snow thickness is around 8 cm (see Figure 3.2). The snow cover fractions of BATS, MI-IM, and ECHAM5 all approach their maxima at a mean snow thickness of 20 cm. The maximum snow fraction of BATS and MI-IM is unity, while for ECHAM5 it is 0.95.

The snow cover fraction of MOSES2.2 and the older version of BATS increases the slowest, and does not approach unity within the range of a realistic mean snow thickness for the Arctic. The snow cover fraction of ECHAM4 and ARPEGE increases at a faster rate than the snow cover fraction of MOSES2.2 and the old version of BATS, but slower than the rates of other models; and reaches a snow cover fraction of 0.95 when the mean snow thickness is around 1 m.

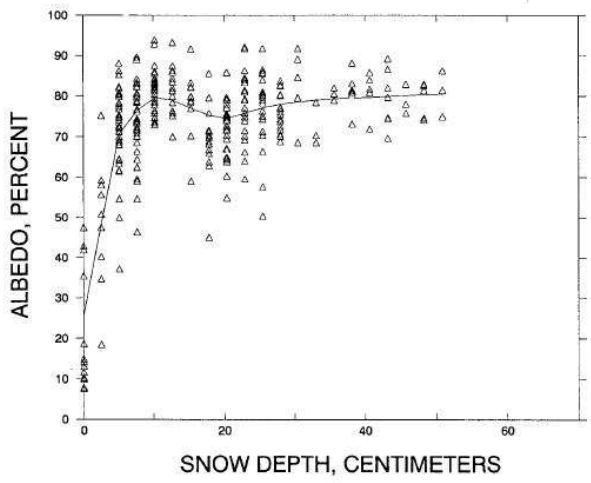

Figure 3.3: The relationship between the albedo and the snow thickness over vegetation free silt loam surface measured over 323 winter days at the St. Paul campus at the University of Minnesota (*Baker et al.*, 1991).

Yang et al. (1997) compares the former snow cover fraction parametrization of BATS (and

MOSES2.2) to observations (data from six stations in the former Soviet Union gathered between 1978-83). It is found that the snow cover fraction is underestimated in all cases. Consequently they suggested a new form for the snow cover parametrization given by (3.1). This new form of snow cover fraction parametrization is based on an article by *Baker et al.* (1991). In the article they compared observations of albedo to snow thickness and found that the albedo increased quickly as the snow depth increased, until the albedo reached 0.7-0.8 (70%-80%). At this point it more or less remained, even if the snow thickness increased further (see Figure 3.3). The *tanh*-function was found apropriate to replicate the albedo's relation to the snow thickness.

When a new snow cover fraction form was proposed for ECHAM4 (*Roesch et al.*, 2001), the *tanh*-function proposed by *Yang et al.* (1997) was found most suited. This was found after comparing satellite observations of snow cover fraction to ground-based observations of snow cover thickness. The *tanh*-function is included in ECHAM5.

Thus, the *tanh*-function proposed by *Yang et al.* (1997) (used by BATS in Figure 3.2) seems to be the most fitting parametrization of snow cover fraction. For snow thicknesses between 1.3 cm and 20 cm the *Yang*'s function produces a substantially higher snow cover fraction than the function used in MI-IM does; i.e. for 8 cm thick snow the BATS snow cover fraction is 0.92 while MI-IM's snow cover fraction is 0.63 (see Figure 3.2). The effect of the new snow cover fraction parametrization for the total albedo in sea-ice covered areas can be seen in the Figure 3.4(a)–(c).

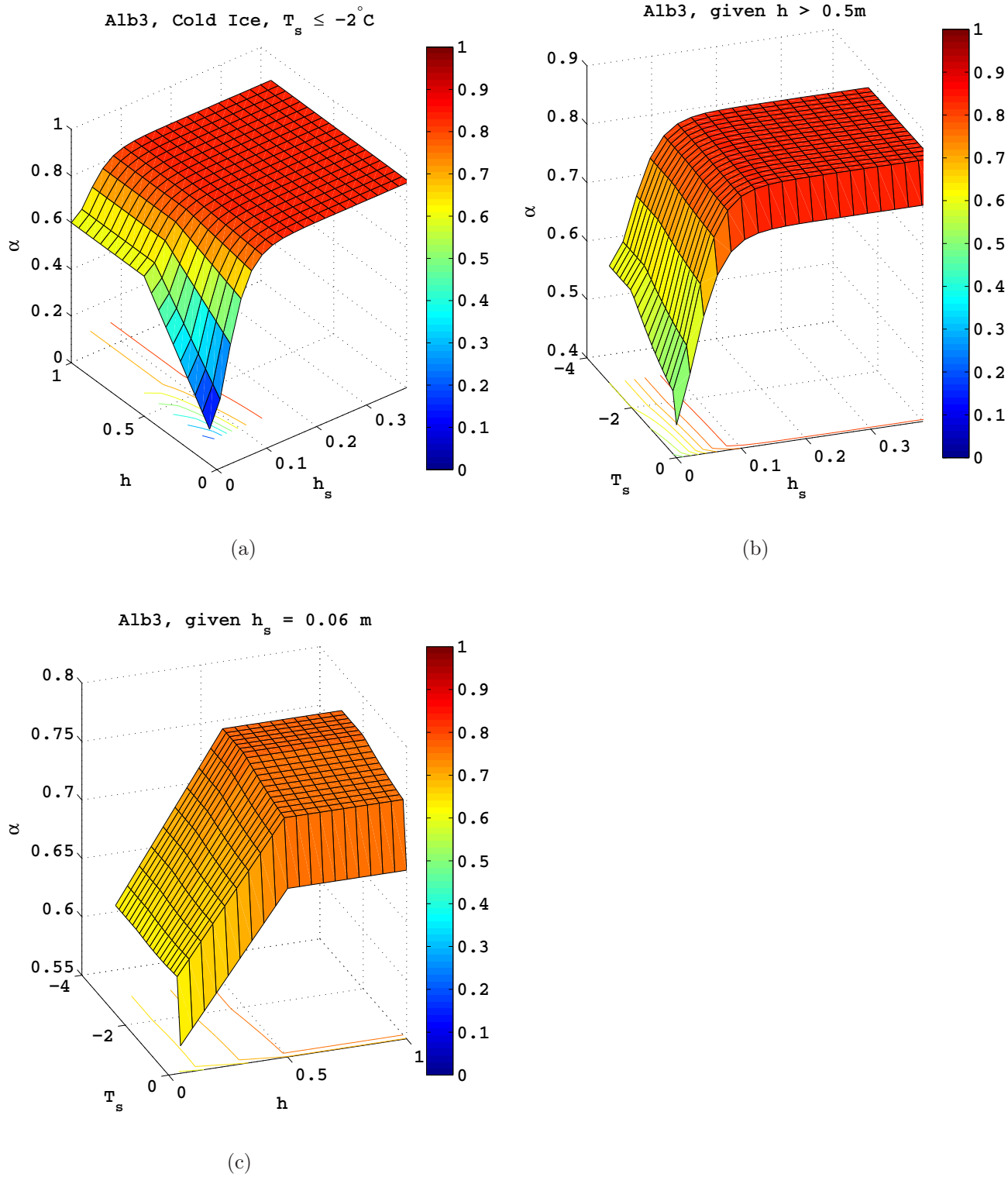

Figure 3.4: (a) shows the albedo of snow and ice as a function of ice thickness and snow thickness given that the interface temperature, T_s, is less than or equal to -2°C. (b) shows the albedo of snow and ice as a function of temperature and snow thickness, given that the ice thickness is over 0.5 m. (c) shows the albedo as a function of the interface temperature and the ice thickness given a 6 cm mean snow thickness.

3.3 OW Freezing Experiments

In order to improve our understanding of the modeled sea-ice variables' sensitivity to the albedo parametrization, a series of experiments changing other factors influencing the sea-ice variables was made; two experiments dealing with lateral freezing and the lead closing parameter h_0 which are described in the present section, and one experiment with increased atmospheric forcing (the ERA-40 2 m temperature) which will be discussed in the following section (Section 3.4).

Winter ice growth depends largely on the parametrization of lateral freezing, as the sea-ice extent doubles from September to March. How quickly the ice concentration grows horizontally and vertically affects the albedo in a unit area, the solar radiation penetrating the ice and the ocean, and the heat exchange between the ocean and the atmosphere. The equations controlling the ice mass and concentration are stated in Section 2.1.1. As mentioned before, the equation concerning the conservation of the sea-ice mass, (2.1), is an exact conservation equation, while (2.2) is an empirical equation.

The empirical lead closing parameter included in (2.2) was first included by *Hibler* (1979). It is also used and discussed in *Holland et al.* (1993), *Bjornsson et al.* (2003), and *Dorn et al.* (2007), and a variation of it is used and discussed in *Mellor and Kantha* (1989). In *Debernard and Køltzow* (2005) it is pointed out that the parameters affecting freezing and melting in MI-IM have to be tuned, and that this can be done without a fully coupled version of the model (ORCM).

The lead closing parameter controls how a new volume of ice formed in open water (as frazil ice in the water column, W_{fr}, and when the temperature in open water drops below the freezing point, W_{ao}) is distributed horizontally and vertically; over area and thickness. In MI-IM and in *Hibler*'s model the ice concentration increases with $1/h_0$ when ice formed in open water. The equation concerning the sea-ice's volume includes no such empirical coefficient. This means that if h_0 is larger than unity the increase in ice concentration, A, is relatively smaller than the increase in ice volume, Ah. Similarly, if h_0 is less than unity the increase in ice concentration is relatively larger than the increase in volume.

Setting $E = W_{io} = W_{ai} = 0$, multiplying (2.2) with h_0/h and subtracting (2.1) yields an equation for the ice thickness:

$$\frac{Dh}{dt} = \partial_t h + \mathbf{u} \cdot \nabla h = \frac{\rho_w}{A\rho_I}(1 - \frac{h}{h_0})[(1 - A)W_{ao} + W_{fr}] \tag{3.2}$$

From this equation it is obvious that if $h_0 = h$ the mean ice thickness remains the same, if $h_0 < h$ the mean ice thickness is reduced, and if $h_0 > h$ the mean ice thickness increases.

Several papers have discussed what may be the best value of h_0. In *Hibler* (1979) h_0 is set to 0.5 m, so when ice is produced in open water the ice concentration grows twice as fast as the ice volume (hA), resulting in a decrease in the mean ice thickness. In the paper the value of 0.5 m is argued to be the most fitting value of h_0, as the modeled growth rate of thin ice is closest to reality when h_0 is 0.5 m. It should be noted that this result is based on *Hibler*'s model which include predescribed growth rates for ice thickness, e.g. 12 cm/day for ice produced in open water. This growth rate is limited to specific geographical

areas and does not include feedback processes (*Mellor and Kantha*, 1989). Consequently the value of h_0 found to be most appropriate in *Hibler*'s model might not be the most appropriate value for MI-IM.

In *Mellor and Kantha* (1989) a similar empirical parameter to h_0, $\Phi = h/h_0$, is included. After a series of sensitivity studies with a decoupled, one-dimensional version of their ice model, they conclude that the parameter for freezing ice should be: $\Phi \geq 2$, that is $h_0 \leq h/2$. As h is a variable, it is difficult to draw a conclusion regarding a constant value for h_0. For example, consider a mean value of h oscillating between 2 and 3 m using a value for h_0 less than 1 m would suffice. But since h can be much smaller than 2 m in individual grid points, the criteria, $h_0 \leq h/2$ would not be met for these cases.

In *Holland et al.* (1993) the equation concerning the ice concentration include the coefficient C_f/h_0 acting on ice growing (both in open water and where there is ice already). In the paper they experiment with changing C_f while keeping h_0 constant at 0.5 m in a sea-ice model forced by oceanic and atmospheric climatological (seasonal) forcing. C_f is set to $1/2$ and 2 in two different runs. This is the same as doubling h_0 from 0.5 m to 1 m and to halve h_0 to 0.25 m. In the paper the experiment with $C_f = 1/2 \rightarrow h_0 = 1$ is considered most appropriate, i.e. $h_0 = 1$ m.

Bjornsson et al. (2003) state that an absolute lower bound on h_0 should be 0.1 m, as this is the typical thickness of pancake ice. In the paper they choose to use $h_0 = 0.3$ to retain reasonable ice concentrations within a polynya. They also state that for a large-scale model of the Arctic, h_0 should be 1 m for the ice cover to follow a reasonable seasonal cycle.

More recently *Dorn et al.* (2007) experiment with the lead closing parameter h_0 in a regional coupled atmosphere-ocean-ice model. In a quasi-stationary cyclic state of equilibrium an experiment with a simple albedo scheme and $h_0 = 0.5$ m oscillates around a volume of $10 \cdot 10^3$ km^3 while the a similar run with $h_0 = 1.2$ m oscillates around $20 \cdot 10^3$ km^3. Also experiments with the more complex albedo scheme following suggestion 2 of *Køltzow* (2007) and with values of $h_0 = 1.2$ m and 2.0 m are conducted. When comparing the sea-ice extent of the different runs with satellite data from the SSM/I in a time-series, all runs overestimate the winter ice extent. The run with the simple albedo scheme and $h_0 = 0.5$ m underestimates the sea-ice extent in the summertime. The same does the run with $h_0 = 2.0$ m and a more complex albedo scheme. The most fitting run in a time-series comparison with data from the SSM/I is the run with the more sophisticated albedo scheme and $h_0 = 2.0$ m.

When comparing the ice concentration from the different runs with the concentration from the SSM/I $h_0 = 0.5$ m gives the most realistic result in winter time, while using $h_0 = 2.0$ m gives too low ice concentrations in large areas. Also when the 2 m temperature of the different model runs are compared to the ERA-40 2 m temperature $h_0 = 0.5$ m gives the most realistic result. In the summertime the run with the standard albedo scheme and $h_0 = 1.2$ m gives the best result.

As no definite answer to which value of h_0 is the most appropriate, two experimental runs using two different values of h_0 are executed for MI-IM.

3.3.1 Freeze1

In Freeze1 h_0 is set to 1 m, a doubling from the value 0.5 m used in the control experiment. In our model this means that when new ice is formed the mean ice thickness increases if it initially is less than one and it decreases if it initially is greater than unity (see Equation (3.2)).

3.3.2 Freeze2

In Freeze2 h_0 is 0.25 m, half of h_0's value in the control experiment. This means that when new ice is formed the ice area increases four times faster (see Equation (3.2)) than it did in the previous experiment, Freeze1, and twice as feast as it did in the control experiment.

3.4 Forcing Experiment

3.4.1 Temp

In this experiment an increment was added to the ERA-40 2 m temperature for temperatures below 0°C.

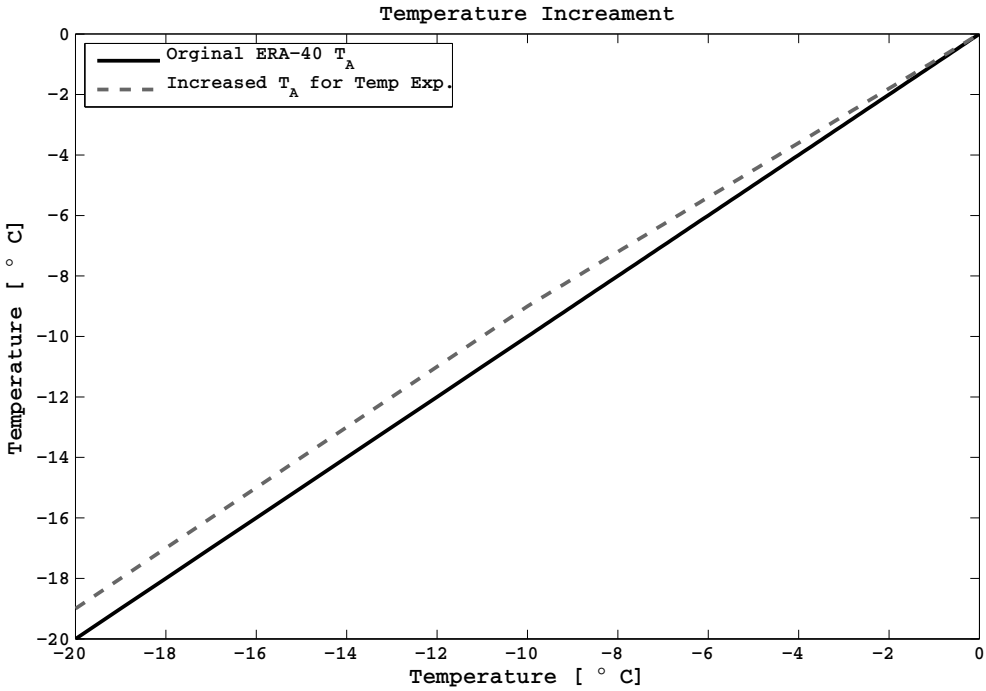

Figure 3.5: The solid line shows the normal ERA-40 2 m temperature. The dashed line shows the ERA-40 2 m temperature after an increment is added to it, as it is used in experiment Temp.

For temperatures equal to or larger than $-10°C$, but less than $0°C$ 10% of the orignal temperature was added to T_A. For $T_A < -10°C$ the temperature was increased by $1°C$

(see Figure 3.5). Changing T_A directly influences the downward longwave radiation, the latent and sensible heat flux from open water, and the sensible heat flux from the ice/snow-atmosphere. These in turn changes the atmospheric heat flux from the ice- and ocean covered areas which influence the production rates of ice. The change in T_A does not influence whether the precipitation from ERA-40 is treated as rain or snow, as the treshold for this is 1 $°C$. The wind and precipitation included in MI-IM are not influenced by the change in T_A; they are left as they are in ERA-40. Also the dew point temperature is unchanged as it is calculated from ERA-40 specific humidity and temperature before the temperature increament is added. This is unrealistic because in reality or in a fully coupled model subjected to an increased 2 m temperature the change in temperature would alter the atmospheric humidity and wind, cloud, and precipitation pattern.

The motivation for the experiment is to see how the model reacts to an increase in the 2 m temperature, and specifically how this change influences the sea-ice concentration and ice and snow thickness. The experiment results give insight into how the model responds to a slight warming in the surface temperature. This is especially interesting in the light of an Arctic (and global) surface temperature increase since pre-industrial time (the global average surface temperature has increased with 0.76 °C ±0.19 °C from 1850-1899 to 2001-2005 and the temperature in the Arctic has increased at almost twice the rate of the global temperature in the last 100 years (*Solomon et al.*, 2007).

The small temperature increment can also reflect the uncertainty in the ERA-40 Arctic surface temperature due to a lack of synoptic and radiosonde observations north of 75°N (leaving only temperatures derived from satellite measurements). Initially the experiment was also conducted in order to rectify a cold bias identified by *Bromwich et al.* (2001). The cold bias was later found to be caused by the assimilation of HIRS radiances [3] to ERA-40. In the last production stream of ERA-40, the version of ERA-40 presently used together with MI-IM, changes had been made that virtually eliminated the cold bias.

In contrast to the cold bias found in the earlier versions of ERA-40, a later paper by *Bromwich and Wang* (2005) finds that the ERA-40 surface temperature is somewhat higher (a root-mean-square error of 1.7 °C) than observations from CAREX[4]. Also in *Graversen et al.* (2008) the Arctic surface temperature in ERA-40 is found to be warmer than observations (see Figure 3.6).[5]

The lack of synoptic and radiosonde observations in the Arctic makes the satellite observations especially important. The satellite observations that are used to compare with the experimental runs are described in following chapter.

[3] From the TIROS Operational Vertical Sounder (TOVS)

[4] Coordinated Eastern Arctic Research Experiment conducted over the Norwegian Sea from Sept. 1988 to May 1989

[5] From the Historical Arctic Rawinsonde Archive, from 1979 to 1996

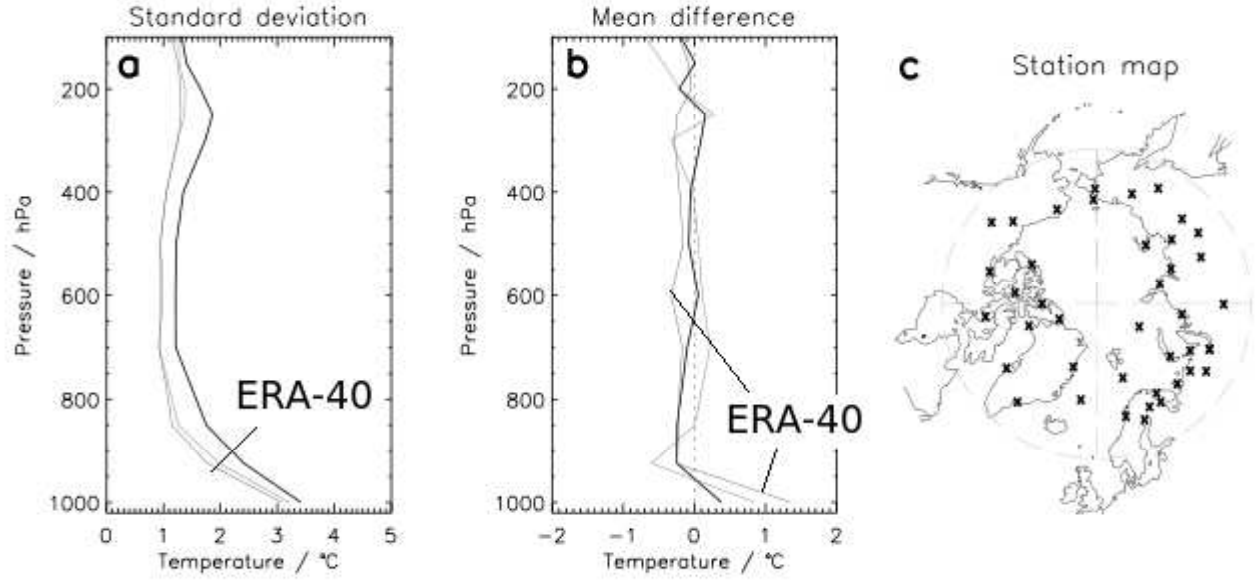

Figure 3.6: Comparison of temperature for three reanalyses with soundings from the HARA-archive for the period 1979-1996. The ERA-40 line is marked. (a) shows the total root-mean-square deviation and (b)shows biases, and (c) shows the location of the observations. Note that there are few observations in the central part of the Arctic. (*Graversen et al.*, 2008). According to *Bromwich and Wang* (2005) most of the HARA data are assimilated into ERA-40, so ERA-40's temperature is not independent of HARA's.

Chapter 4

Observations

To analyse the effect of the various sensitivity experiments we have used observations derived from satellite imagery, specifically the NSIDC[1] Sea Ice Index (Section 4.3) and the OSI SAF[2] Global Sea Ice Concentration Reanalysis Product (Section 4.4). The NSIDC Sea Ice Index is derived from satellite imagery from the SMMR and the SSM/I (Section 4.1), while the OSI SAF product used only include data from the SSM/I (Section 4.2).

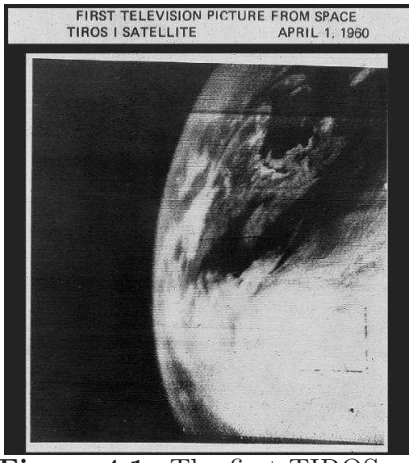

Figure 4.1: The first TIROS TV image, planet earth from TIROS-1 (*TIROS Program/NASA*, 2000)

The field of numerical weather prediction is quite young, starting in the 1950s. Using satellites imagery to obtain knowledge about the earth is also a quite new innovation; the first successful satellite pictures came from the TIROS (Television Infrared Observation Satellite) launched by NASA in 1960.

A series of satellites called the Nimbus series was launched by NASA in 1964. The Nimbus series was dedicated to research and development experiments. The Nimbus-5 launched in 1972 included an Electrically Scanning Microwave Radiometer (ESMR) which measured the brightness temperature of the surface and the atmosphere. It operated at a wavelength of 1.55 cm and with a spatial resolution of 30 km. NASA planned to use this satellite information to collect global observations of how much and where it rained, but only months following its launch mapping sea-ice concentration became a new priority (*Lindsey*, 2005). In *Parkinson and Cavalieri* (1989) the algorithms for calculating the sea-ice concentration (C) using the measured brightness temperature are described. Given constant emissivities for water, $\epsilon_W = 0.44$, and ice, $\epsilon_I = 0.94$, the ice concentration follows:

$$C = \frac{T_B - \epsilon_W T_W}{\epsilon_I T_I - \epsilon_W T_W} \tag{4.1}$$

[1]National Snow and Ice Data Center

[2]Ocean and Sea Ice Satellite Application Facility, a project under the European Organisation for the Exploitation of Meteorological Satellites

T_B is the observed brightness temperature[3], T_I the ice temperature and T_W the water temperature. The emissivity of ice is complicated as it depends on the age of the ice and the surface conditions of the ice. Multi-year ice (MYI) has a lower emissivity (∼0.84) than first-year ice (FYI) (∼0.92), therefore the concentration data from the ESMR is only valid in the grid squares containing open water and FYI.

4.1 SMMR

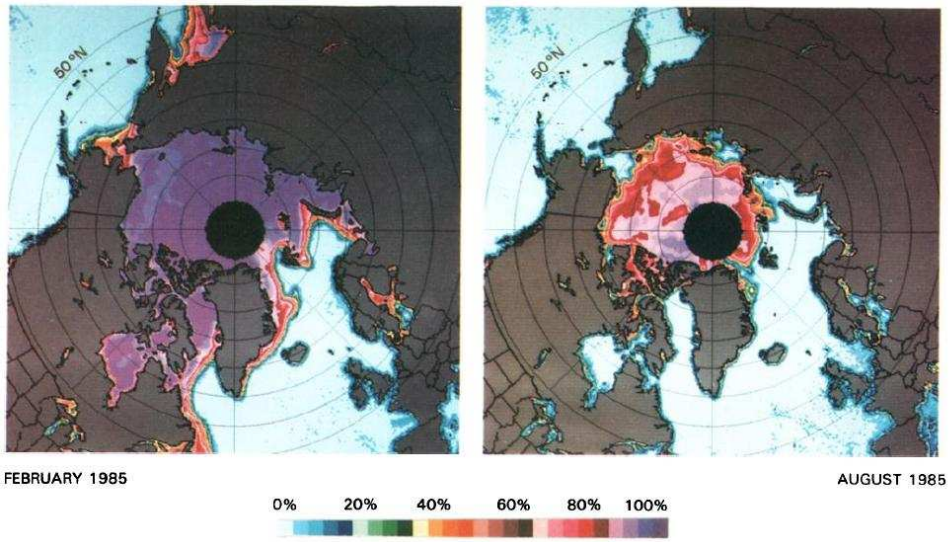

Figure 4.2: Mean monthly sea-ice concentration for February and August 1985 derived from the SMMR on Nimbus-7. (*Parkinson and Cavalieri*, 1989)

This problem of separating MYI from FYI was reduced with the multi-channel microwave radiometer (SMMR) included on the Nimbus-7. The SMMR was operational from October 1978 to August 1987. Nimbus-7's near polar orbit prevented it from retrieving data poleward of 84° latitude. The SMMR recorded data from five wavelengths, 0.81, 1.4, 1.7, 2.8 and 4.6 cm, with both horizontal and vertical polarization. The footprint size[4] for the 0.81 cm and 1.7 cm wavelength is respectively 27×18 km and 55×41 km.

The contrasting vertically and horizontally polarized brightness temperatures of open water, FYI and MYI at wavelengths of 0.81 and 1.7cm, were used to calculate the fraction of multi-year ice and the ice concentration, using an algorithm described by *Cavalieri et al.* (1984)[5]. Included in the algorithm is ratio of polarization (PR), which is used to distinguish water from ice, and the ratio of the spectral gradient (GR), used to distinguish MYI from FYI. (The later NASA Team Sea Ice Algorithm is functionally the same algorithm.)

[3]The apparent temperature of the surface assuming a surface emissivity of 1.0 (black body radiation).
[4]effective field view
[5]The Oceans and Ice Branch, Laboratory for Hydrospheric Processes at NASA Goddard Space Flight Center.

4.2 SSM/I

The subsequent microwave radiometer was the Special Sensor Microwave/Imager (SSM/I), launched July 1987 by the United States Air Force DMSP[6] on a F-8 platform in a near polar, sun-synchronous orbit. The satellite's orbit and inclination makes data available up to 87.2° latitude. It made 14.1 orbits a day. The purpose of the SSM/I was to provide night and day measurements of ocean surface wind speed, area and intensity of precipitation, cloud water content, land surface moisture, ice coverage and ice age.

The SSM/I operates with four wavelengths, 0.35, 0.81, 1.35 and 1.55 cm, and with horizontal and vertical polarization for three of the wavelengths (thus, a total of seven channels). The footprint size of the channels used to estimate the sea-ice concentration are 38×30 km, 60×40 km, and 70×45 km, respectively for the 0.81, 1.35 and 1.55 cm wavelengths. Because of inadequate thermal shielding the instrument was turned off from December 2, 1987 to January 12, 1988. All data from December 1987 and January 1988 are therefore omitted from the analysis in following chapters.

The SSM/I was operational on the F8 until it was decommissioned in August 1991. The SSM/I is still operational, presently flown on the F-14, -15 and -17 satellites of the DMSP (as of April, 2010).(*NASA web page, NSSDC*, 2010)

4.3 NSIDC Sea Ice Index

The National Snow and Ice Data Center (NSIDC) have sea-ice concentration data generated from brightness temperatures from the Nimbus-7 SMMR and the DMSP SSM/I with a grid cell size of 25×25 km in the polar stereographic projection. The data is generated using the revised NASA Team algorithm[7] (*Cavalieri et al.*) and improved brightness temperatures[8]. As the product is designed to provide consistent sea-ice data, the sea-ice algorithm coefficients (the tie-points) are changed to reduce differences in sea-ice extent and area, as estimated by the SMMR and SSM/I sensors (with data from the SSM/I starting from July 1987). Also, improvements have been made to the data set to minimize the coastal and open ocean influences that causes inaccurate sea-ice concentrations, and by removing sea-ice from areas where the monthly averaged SST is more than 278K.[9] Missing data has been filled through interpolation, except for the period between December 2, 1987 to January 12, 1988.

The monthly averaged sea-ice concentration in the form of a time series of the sea-ice extent for the northern hemisphere between 1980 through 1990 is used (*Fetterer et al.*, 2002, updated 2009) to compare with the modeled sea-ice extent. The sea-ice extent is obtained by summing the area covered by all pixels that have 15% or greater ice concentration. Both the SSMR and the SSM/I have gaps over the pole due to the orbits of their satellites. This

[6] Defense Meteorological Satellite Program

[7] Including a new weather filtering technique using brightness temperatures of 1.35 cm wavelength, and different tie-points than the original NASA Team algorithm.

[8] see *NSIDC: Sea Ice Conc.* (2010)

[9] 275 K in the SH.

area is assumed to have an ice concentration of more than 15% (*NSIDC: Sea Ice Index*, 2008).

4.4 OSI SAF Global Sea Ice Concentration Reanalysis Product

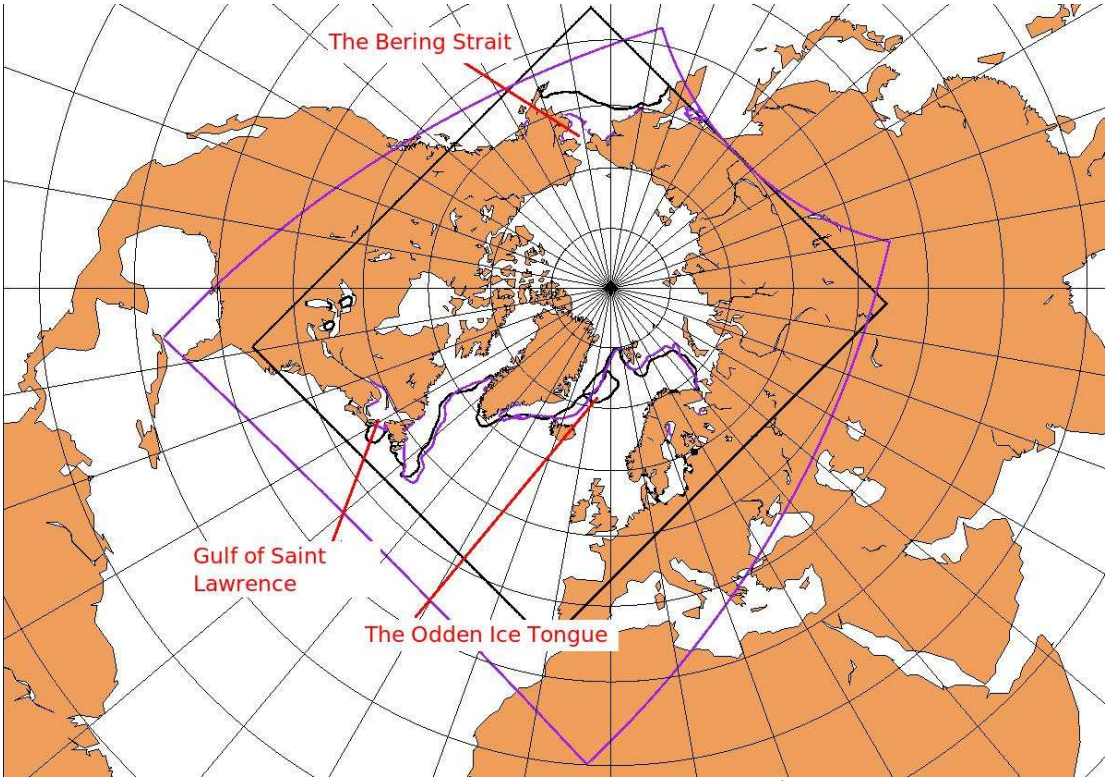

Figure 4.3: The 1990 March sea-ice extent derived from MI-IM (the Control experiment)(purple) and from OSI SAF(black). MI-IM's domain is marked in a purple color while OSI SAF's is marked in black. Regions where the ice extent differs are marked.

The Ocean and Sea Ice Satellite Application Facility (OSI SAF) is an EUMETSAT[10] project started in 1997. The OSI SAF uses brightness temperatures from the SMMR and antenna temperatures from the SSM/I as input data. The SSM/I antenna temperatures are converted to brightness temperatures and corrected for atmospheric emissions and absorption by using a fast atmospheric radiative transfer model and model fields from ERA-40. For calculating the ice concentrations a combination of the Bootstrap and Bristol algorithm is used.[11]

The OSI SAF uses dynamical tie-points. The tie-points are derived using a first guess of the sea-ice concentration from the NASA Team sea-ice algorithm and by using the

[10]The European Organisation for the Exploitation of Meteorological Satellites

[11]Over open water the Bootstrap algorithm in frequency mode is chosen, as it is shown to have the lowest sensitivity to atmospheric noise over open water. The Bristol algorithm is chosen over ice as it is showed to have the lowest sensitivity to ice surface emissivity variability. At ice concentrations up to 40% an average between the two algorithms is made by wheighing them according to the ice concentration.

mean brightness temperature of the data points from where the NASA Team algorithm gives concentrations above 95%. This way, varying surface and atmospheric conditions as well as climatic trends are taken into account. Before the product is finished the OSI SAF processing includes coastal and climatological corrections, marking data points as questionable where the ice concentration is unconsistent with the ERA-40 2 m temperature interpolated to the same grid point, and filling gaps of missing data by interpolation (this includes the polar observation holes). The data has a resolution of 10×10 km in the polar stereographic projection. (*Eastwood et al.*, 2010)

The OSI SAF data that will be used is the monthly average sea-ice extent derived from the SSM/I antenna temperatures from July 1987 to December 1990 (*OSI SAF*, 2010), where the coastal areas and the area in the polar observational hole are included. Data from December 1987 and January 1988 are omitted. When a regional comparison of the modeled sea-ice extent and the observed sea-ice extent is made, the OSI-SAF sea-ice concentration is used in its original form. The data have also been interpolated to the ORCM grid and MI-IM's land mask has been applied, to remove sea-ice from areas treated as land in MI-IM. A time series of the total sea-ice extent derived from the modified OSI SAF sea-ice concentration is used to make a comparison with the modeled sea-ice total extent. Also a version of the sea-ice extent where sea-ice outside the Bering Strait is disregarded is used, to make a fairer comparison with MI-IM, as MI-IM has problems representing sea-ice in that area. The modifications done to the OSI SAF data set (the interpolation and the application of MI-IM's land mask) and the calculation of both types of total sea-ice extent have been performed by Yvonne Gusdal at met.no.

4.5 Error Sources

The sea-ice observations from passive microwave radiation from the SSMR and the SSM/I are not without errors. The assumption that has to be made about the radiative properties of the atmosphere, sea-ice and ocean, which are not true in all areas and at all times. Instrument noise also contributes to the errors. Another source of error is the low resolution/large footprint size of the microwave images (>27 km), which is too large to resolve individual floes, leads and small polynyas. The signal received from a large area is interpreted through an algorithm to be a result of a distinct mixture of surface types. In reality the same signal could come from a variety of mixtures of surface types (*Meier*, 2005). The large footprint size also limits the resolution of the ice edge. In addition, the uncertainty of the represented data increases when the ice concentration data is represented on a finer grid than the sensor resolution (27-70 km) (*Eastwood et al.*, 2010). The NSIDC products grid size is 25×25 km, while OSI SAF's is 10×10km.

Given that the error of each algorithm with its chosen tie-points, the large footprint size, and the weather noise are unknown, an estimate has to be made by comparing these sea-ice concentration products to other sea-ice concentration products. It is important to keep in mind that none of the products are error free, so the error estimate will be relative to the product which it is compared to.

On the web site for the NSIDC Sea Ice Index the errors in the data set are discussed (*NSIDC: Sea Ice Index*, 2008). They compare the ice concentration retrieved from pass-

ive microwave radiances to ice concentrations retrieved from charts from operational ice centers. The advantage of the ice charts is that they gather information from a variety of sources: satellites,[12] ships, planes, weather forecasts, their own previous ice charts as well as ice charts and aerial maps provided by other countries. The disadvantage of the ice charts is that they are subjective and the types of observations used to produce them is not consistent. This makes the accuracy of the ice charts hard to estimate as it varies with the level of skill of the analyst who interpreted the data and the accuracy of the sources he chooses to use. In an article by *Partington et al.* (2003) the U.S. National Ice Center's (NIC) estimates the uncertainty of the ice concentration in their charts to be between ±5% and ±10%, while in *OSI SAF Global Sea Ice Concentration Reprocessing Validation Report* the uncertainty is evaluted to be about 20% (*Tonboe and Nielsen*, 2010).

4.5.1 Summer Underestimation of the Sea-Ice Concentration

sea-ice concentration from passive microwave ice retrievals based on the NASA Team algorithm have been compared to NIC charts (between 1972-1994) and charts from Canadian Ice Service (CIS) (between 1979-1996). The NIC charts report ∼4% more ice per unit area than the passive microwave retrievals until June when the difference increases to ∼23%. After June the difference decreases again. The difference in sea-ice concentration between the Canadian charts charts and the passive microwave retrievals is as much as 30 to 40% between spring melt and fall freeze-up. The larger difference between the satellite products in comparison to the Canadian charts than the NIC charts is probably caused by the fact that the CIS rarely use passive microwave data, while the NIC uses passive microwave data when other data are not available. Thus the SSM/I imagery and the NIC charts are not independent.

In *Meier* (2005) the sea-ice concentration computed from the SSM/I is compared to concentrations computed from an AVHRR.[13] When using the NASA Team algorithm[14] the error relative to the AVHRR is -8.4% in the winter time, and -10.5% during the Arctic summer. *Comiso and Kwok* (1996) compared the SSM/I sea-ice concetration calculated using the Bootstrap algorithm to sea-ice concentration measured by a synthetic aperature radar (SAR) with a resolution of 30 m (100 times higher than the passive microwave images). They find that the SSM/I ice concetrations are as much as 30% less than the SAR concentrations in some places during the summer.

The greater inaccuracy throughout the Arctic summer is caused by wet snow, melting ice and melt ponds which alter the emissivity of the ice surface. Because the tie-points used in most algorithms are constant, and for sea-ice retrieved from the brightness temperature of cold, thick ice with no melt ponds, the ice concentration is underestimated in the summer time when the surface properties of sea-ice have changed (melt ponds have the radiative signature of open water). In the winter time the problem is that most of the algorithms cannot distinguish thin ice between leads from open water, and the ice concentration is consequently underestimated.

[12]The VHRR, AVHRR, ESMR, SSM/I, and later on the synthetic aperature radar (SAR) (the acronyms are listed in Appendix A).

[13]Advanced Very High Resolution Radiometer

[14]The algorithm included the weather filter used in NSIDC Sea-Ice Index (using the GR of the 0.81 and 1.55cm, and the 0.81 and 1.35cm wavelengths (*Cavalieri et al.*)

In the OSI SAF sea-ice concentration validation report (*Tonboe and Nielsen*, 2010) the OSI SAF sea-ice concentration reanalysis product is compared to ice charts from NIC. The difference between the OSI SAF products and the NIC charts (OSI SAF concentration - NIC concentration) is presented in Figure 4.4.

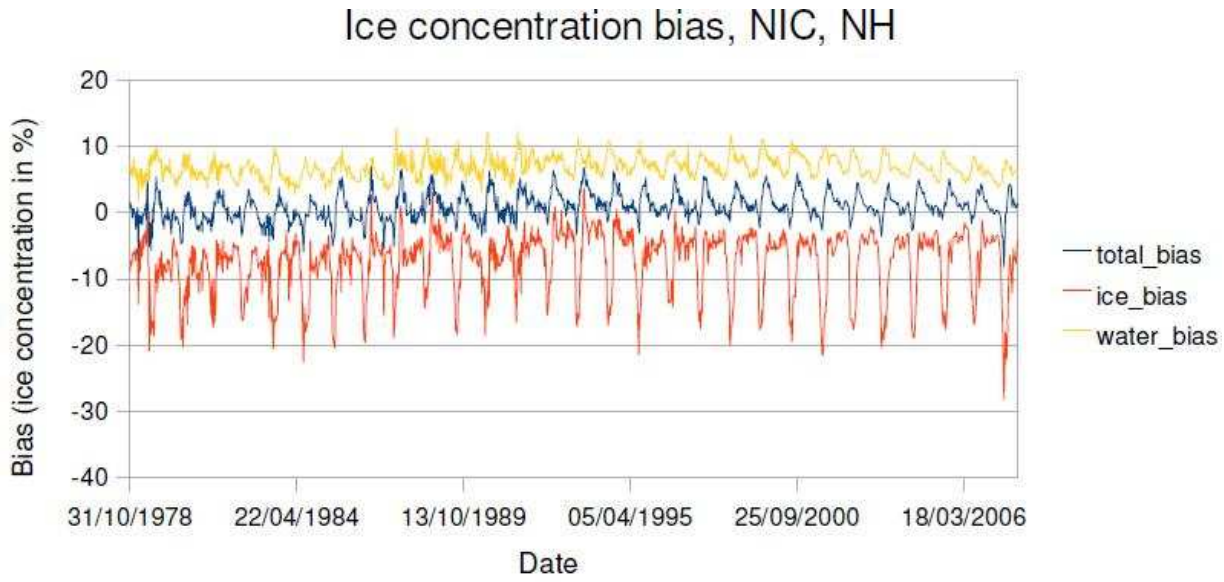

Figure 4.4: Comparison between the National Ice Center charts' and the OSI SAF reanalysis' sea-ice concentration for the Northern Hemisphere. The total difference between the OSI SAF reanalysis and the NIC charts are shown by the blue line. The OSI SAF ice concentration over areas marked by NIC charts as open water is marked with yellow and the difference in ice concentration between OSI SAF and NIC ice charts in ice covered regions is marked by the red curve. This figure is from the *OSI SAF Global Sea Ice Concentration Reprocessing Validation Report* (*Tonboe and Nielsen*, 2010).

Figure 4.4 shows that the OSI SAF product estimates sea-ice concentrations where the ice charts only have open water (the yellow line on Figure 4.4). In the report this is explained as atmospheric noise affecting the radiometers (of the SSMR and the SSM/I). In Figure 4.4 there is a discontinuity in the yellow line between June and July 1987. This is when the SMMR radiances was replaced by the SSM/I radiances. The SSMR was less affected by atmospheric noise than the SSM/I because the SSMR read radiances on a wavelength less influenced by water vapor. The difference in ice concentration over ice (the blue line on Figure 4.4) has a similar pattern to that observed between the NSIDC product and the NIC charts; a seasonal cycle with larger underestimations of the sea-ice concentration in the summer than in the winter.

Chapter 5

Results

In this chapter an overview of ice extent, mean ice thickness, ice volume, and mean snow thickness produced from the experiments is given. Section 5.1 presents the results from the Control experiment and the albedo experiments. The results of the remaining experiments are presented in Section 5.2. In Section 5.3 the mean snow thickness and average number of snow free days of each experiment are presented. The section also includes a statistical comparison of the variables. The last section compares the modeled sea-ice extent to satellite observations (from the NSIDC and the OSI SAF) of the sea-ice extent.

5.1 Albedo Experiments

As indicated by Table 5.1 and Figure 5.1 and 5.2 the ice thickness, extent and volume in all the experiments increased or remained unchanged from the Control experiment. The effect each albedo experiment had on the ice thickness, ice extent, and ice volume is summarized in Table 5.1.

It is clear that the mean sea-ice thickness of the Alb1 experiment diverges the most from the Control experiment as it increases substantially from 1980 to 1985 (Figure 5.1). The sea-ice thickness of Alb1 in January 1980 is around 2.3 m, while in January 1985 the thickness is closer to 2.9 m.

Figure 5.2 depict the 1985-1990 average monthly mean ice thickness. From this and Table 5.1 it can be seen that from 1985 to 1990 the Alb1 mean sea-ice thickness oscillates around a thickness 0.6 m higher than the Control experiment does. Experiment Alb2 had almost no effect on the mean sea-ice thickness, while experiment Alb3 had a small effect, with a monthly average sea-ice thickness around 10 cm greater than the Control experiment.

The effect on the ice extent can be seen from Figure 5.3. The difference in the 1985-1990 average monthly mean sea-ice extent is much greater during the summer than during the winter. As for ice thickness, experiment Alb1 has a much larger effect on the ice extent than Alb2 and Alb3. The average minimum ice extent for Alb1 is $1.7{\cdot}10^6$ km^2 greater than the average minimum ice extent for the Control experiment. The average minimum ice extent of experiment Alb2 and Alb3 is also greater than the Control experiment, respectivly $1 \cdot 10^5$ km^2 and $2{\cdot}10^5$ km^2 (Table 5.1).

The difference in response is also reflected in the ice volume. Again Alb1 has the largest effect, with a mean ice volume between 1985 and 1990 around 7600 km^3 greater than the Control experiment (see Figure 5.4 and Table 5.1). In comparison, Alb2 results in an average ice volume around 300 km^3 greater than the Control experiment, and Alb3 in an ice volume around 1100 km^3 greater than the Control experiment.

Table 5.1: Maximum, minimum and mean values of ice thickness, extent and volume from the 1985-1990 average monthly mean values for the albedo experiments listed in Table 3.1.

		Control	Alb1	Alb2	Alb3
Ice Thickness [m]	Max	3.1	3.6	3.1	3.2
	Min	2.3	2.9	2.3	2.4
	Mean	2.7	3.3	2.7	2.8
Ice Extent [$10^6 km^2$]	Max	13.4	13.5	13.4	13.4
	Min	7.5	9.2	7.6	7.7
	Mean	11.0	11.7	11.0	11.1
Ice Volume [$10^3 km^3$]	Max	35.1	41.0	35.4	36.1
	Min	18.4	27.7	18.8	19.7
	Mean	26.6	34.2	26.9	27.7

5.2 Remaining Sensitivity Experiments

The effect each OW freezing experiment had on the ice thickness, ice extent, and ice volume is summarized in Table 5.1. As indicated by Table 5.2 the Freeze1 experiment has lower mean values of ice thickness, extent and volume than the Control experiment, while the Freeze2 and Temp experiments have higher mean values than the Control experiment.

The 1985 to 1990 mean ice thickness for Freeze1 is 20 cm more than it is for the Control experiment (Table 5.2 and Figure 5.5 and 5.6). Freeze1 has the smallest seasonal variation in ice thickness (the smallest difference between the average minimum and maximum ice thickness). Freeze2 and Temp have mean ice thicknesses thinner than the Control experiment, respectivly 10 and 20 cm. While experiment Freeze2 and Temp have comparable effects on the mean ice thickness it is visible that the seasonal cycles of their mean ice thickness differ, as the mean ice thickness grows slower with Freeze2 than Temp, but melts quicker for Temp than for Freeze2. For the Temp experiment the second ice thickness maximum has almost disappeared (Figure 5.6).

None of the experiments have a large effect on the sea-ice extent (Figure 5.7). Freeze2 had the smallest effect, with the 1985-1990 average minimum sea-ice extent $1{\cdot}10^5$ km^2 smaller than the Control experiment. The seasonal variation of sea-ice extent is smaller in Freeze1 than it is in Control experiment, while Freeze2 and Temp have a larger variation in sea-ice extent during a year than the Control experiment. The 1985-1990 average minimum sea-ice extent for Freeze1 is substantially larger than for the Control experiment, $3{\cdot}10^5$ km^2, while it is substantially smaller for the Temp experiment, around $4{\cdot}10^5$ km^2.

Finally, Freeze1 gives a substantially larger volume than the Control experiment, with a mean volume around 2100 km^3 larger than the Control experiment (Table 5.2 and Figure

5.8). Freeze2 and Temp give mean volumes somewhat smaller than than the Control experiment, both around 1100 km^3 smaller.

Table 5.2: Maximum, mean and minimum values of ice thickness, extent and volume from 1985-1990 monthly mean values for the experiments Freeze1, Freeze2, and Temp, listed in Table 3.1.

		Control	Freeze1	Freeze2	Temp
Ice Thickness [m]	Max	3.1	3.3	2.9	3.0
	Min	2.3	2.6	2.1	2.1
	Mean	2.7	2.9	2.6	2.5
Ice Extent $[10^6 km^2]$	Max	13.4	13.3	13.4	13.1
	Min	7.5	7.8	7.4	7.1
	Mean	11.0	11.1	11.0	10.7
Ice Volume $[10^3 km^3]$	Max	35.1	37.8	33.8	34.0
	Min	18.4	19.8	17.7	15.7
	Mean	26.6	28.7	25.5	25.5

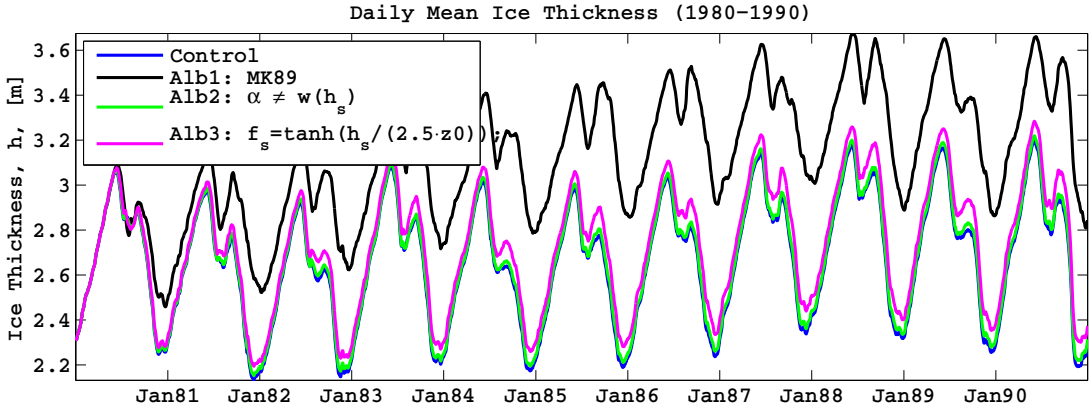

Figure 5.1: Daily mean ice thickness for the Control exp. and the albedo exp. from 1980 to 1990.

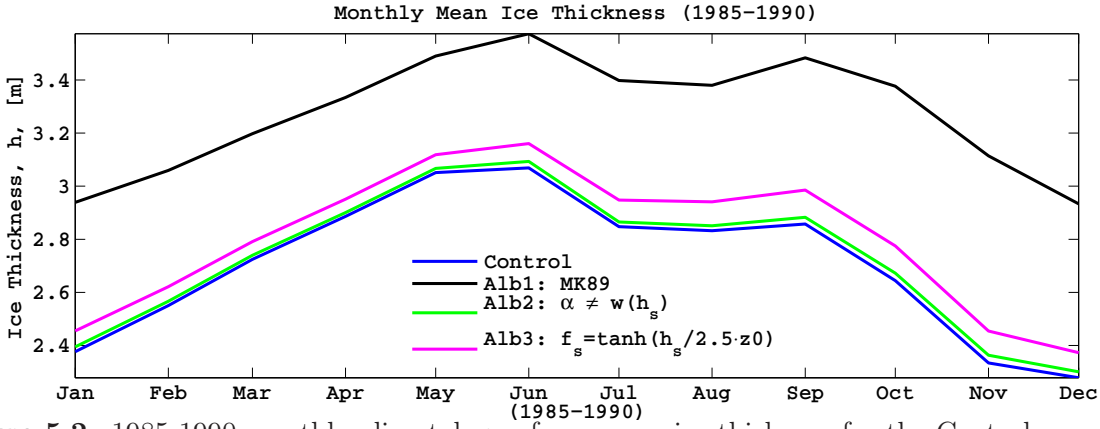

Figure 5.2: 1985-1990 monthly climatology of mean sea-ice thickness for the Control exp. and the albedo exp..

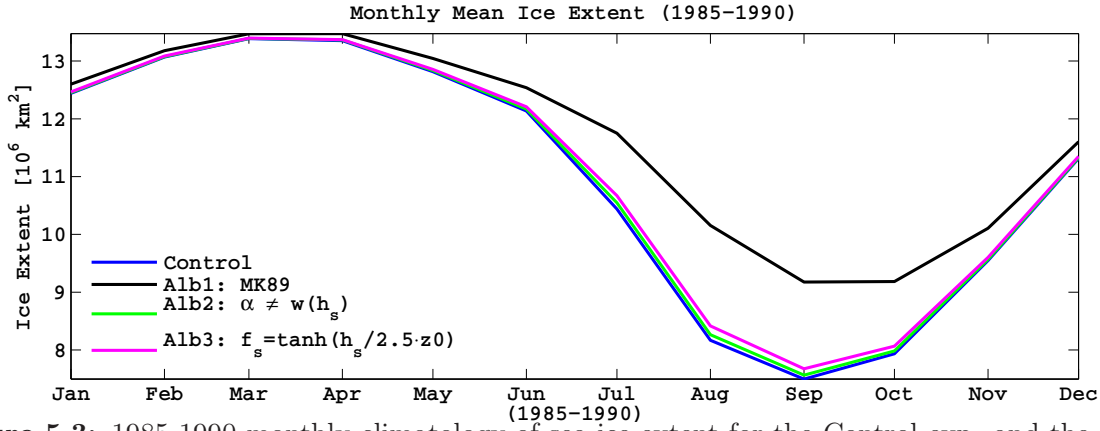

Figure 5.3: 1985-1990 monthly climatology of sea-ice extent for the Control exp. and the albedo exp..

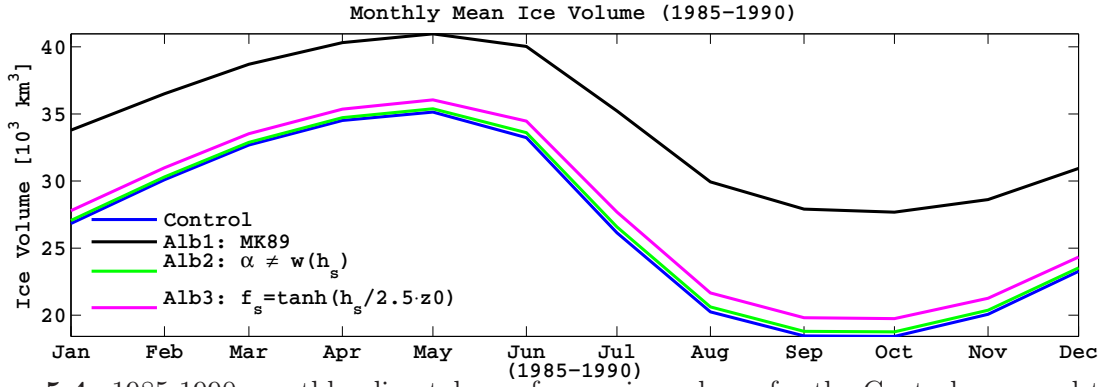

Figure 5.4: 1985-1990 monthly climatology of mean ice volume for the Control exp. and the albedo exp..

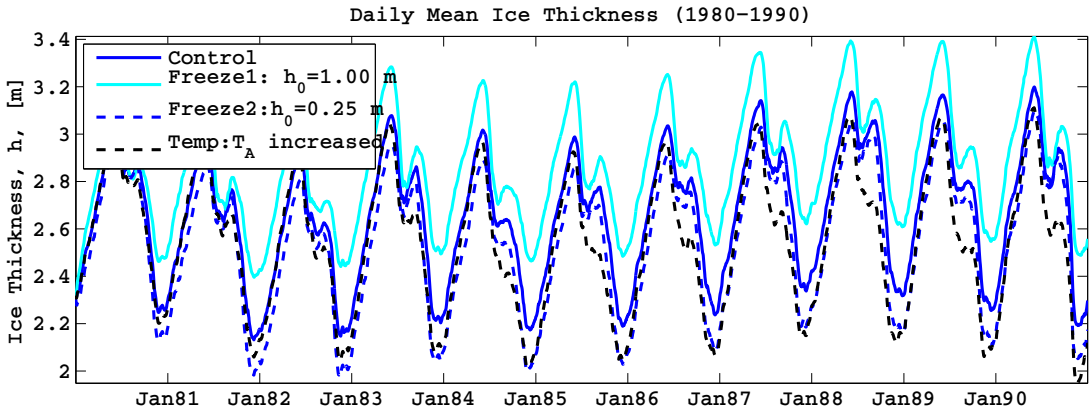

Figure 5.5: Daily mean ice thickness for the Control, OW freezing and forcing experiments from 1980 to 1990.

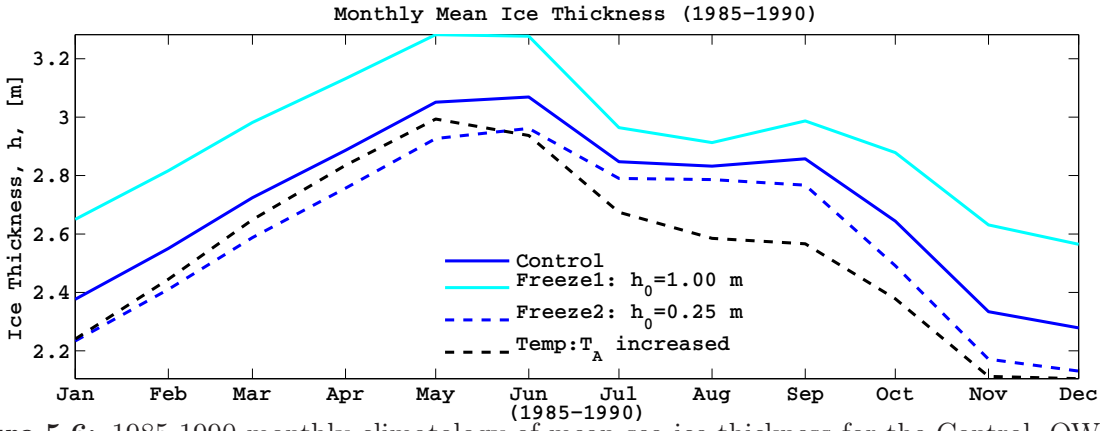

Figure 5.6: 1985-1990 monthly climatology of mean sea-ice thickness for the Control, OW freezing, and forcing experiments.

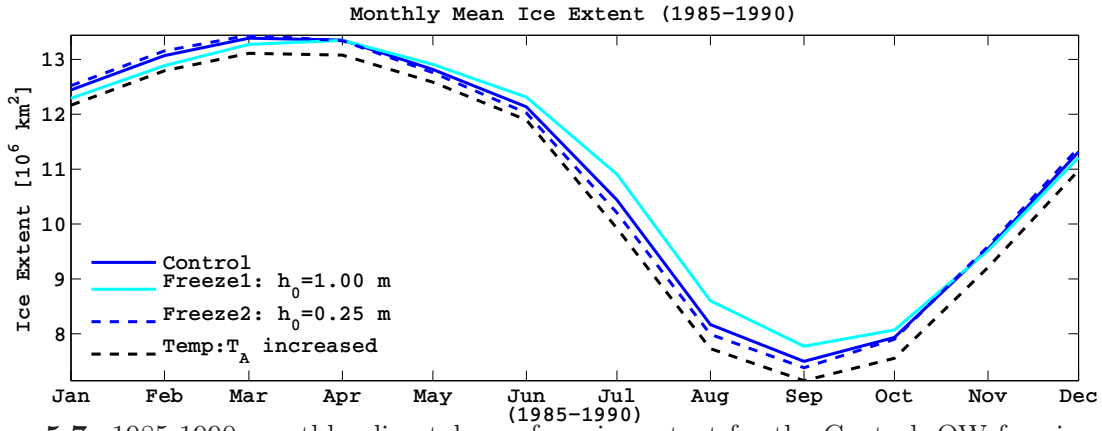

Figure 5.7: 1985-1990 monthly climatology of sea-ice extent for the Control, OW freezing, and forcing experiments.

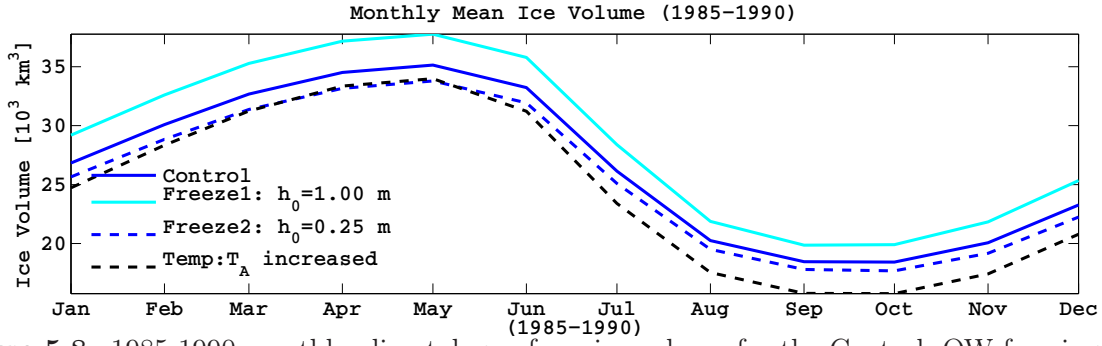

Figure 5.8: 1985-1990 monthly climatology of sea-ice volume for the Control, OW freezing, and forcing experiments.

5.3 All Experiments

Table 5.3: Bias and root mean square error (in brackets) of the sensitivity experiments when compared to the Control experiment (1985-1990). Values displaying a large change a marked with **bold numbers**, and small changes are marked with *slanted numbers*

	Alb1	Alb2	Alb3	Freeze1	Freeze2	Temp
h_s [cm]	1.28 (1.58)	0.18 (0.22)	0.33 (0.50)	0.07 (0.16)	*-0.04 (0.10)*	**-5.62 (6.77)**
h [cm]	**56.9 (57.9)**	*2.0 (2.1)*	9.3 (9.6)	21.9 (23.0)	-12.0 (12.6)	-16.1 (18.0)
Extent [10^3 km^2]	**681 (951)**	37 (*51*)	88 (122)	83 (231)	*-34* (111)	-328 (342)

5.3.1 Snow Thickness

Table 5.4: Snow Free Period and Mean Value of h_s from Daily Climatology (1985-1990) (see Figure 5.9). The experiments which led to the largest change in mean snow thickness and snow free days are marked with bold letters and numbers.

	Control	**Alb1**	Alb2	Alb3	Freeze1	Freeze2	**Temp**
Snow Free Period [days] ($h_s < 1.5$ mm)	34	**29**	34	33	35	34	**49**
Mean [cm]	10.4	**11.7**	10.6	10.7	10.5	10.4	**4.8**

The 1985-1990 average mean daily snow thickness and the mean length of the period[1] when the ice is snow free in the same period are presented in Table 5.4. It is noted that the Temp experiment has the greatest effect on the mean snow thickness. The average mean snow thickness of the Temp experiment between 1985 and 1990 is less than half of the average mean snow thickness of the Control experiment. It has an average 49 snow free days, while the Control experiment on average has 34 snow free days. From Figure 5.10 it is observed that the Temp experiment has the lowest correlation coefficient (0.95) and the highest bias (-6 cm) of all the sensitivity experiments when compared to the Control experiment. Also, from Figure 5.13, showing the average snow thickness of the Temp experiment in May 1990, it is observed that the Temp experiment has much thinner snow and more snow free areas than all the other experiments.

Experiment Alb1 has a positive effect on the mean snow thickness, with a five days shorter snow free period and a mean snow thickness about 1 cm higher than the Control experiment. From Figure 5.13 it is observed that in May 1990 the Alb1 snow is thicker than in the Control experiment around Baffin Island/Baffin Bay and near the Chukchi Sea, while it seems thinner than in the Control experiment in the central part of the Arctic Ocean.

Alb3 also has a small effect on the snow thickness, as can be seen in Figure 5.9 and 5.10, with a mean snow thickness 3 mm higher than the Control experiment. This can also bee seen in Figure 5.13.

The remaining experiments have little effects on the snow thickness.

[1]Defined as the 1985-1990 average continuous number of days when the mean snow thickness is below 1.5 mm (the red stapled line in Figure 5.9)

5.3.2 Ice Thickness

Figure 5.11 shows the correlation coefficient and bias of the monthly mean ice thickness of the sensitivity experiments compared to the Control experiment from 1985 to 1990. The Alb1 experiment has the lowest correlation coefficient and the highest bias (almost 60 cm) of the sensitivity experiments. Freeze1 has the second largest bias (+22 cm) compared to the Control experiment. The Temp experiment has a bias of -16 cm and also has the second lowest correlation coefficient of the experiments.

Freeze2 has a bias of -12 cm and Alb3 a bias of +9 cm. Both have correlation coefficients close to unity. Alb2 has almost no effect on the mean ice thickness, with a bias of only +2 cm and a correlation coefficient very close to unity.

The geographical variation of the mean ice thickness of the various experiments in March 1990 is displayed in Figure 5.14. Alb1, Alb3 and Freeze1 all have thicker ice than the contorol experiment in the Arctic Ocean, especially near the Canadian Archipelago, Alb1 more than the others. Alb1 also has more and thicker ice between Svalbard and Franz Joseph Land. Freeze1 has thicker ice further south than the Control experiment, notably in the Hudson Bay, the Baffin Bay and the Davis Strait, in the Gulf of Saint Lawrence, the Chukchi Sea and the Bering Sea, and in the Sea of Okhotsk.

Freeze2 and Temp has thinner ice than the Control experiment. Freeze2 has thinner ice in all regions, while Temp has thinner ice most visibly in the Gulf of Saint Lawrence, the Hudson Bay, and in the Arctic Sea, especially near the Canadian Archipelago. This is consistent with the fact that the average mean sea-ice thickness is thinner for the Freeze2 experiment than the Temp experiment in March (see Figure 5.6).

In Figure 5.15 the 1990 September ice thickness of the various experiments are visualized. Alb1 has much thicker ice than the Control experiment in the areas that are ice covered in the Control experiment: the Arctic Ocean, the Canadian Archipelago, the Kara and Barents Sea, and the Greenland sea, as well as ice where the Control experiment has none. Alb3 and Freeze1 has somewhat thicker ice in the Arctic Ocean than the Control experiment. Freeze1 also has thicker ice in the Canadian Archipelago and ice extending further south into the Greenland Sea than the Control experiment.

The Freeze2 and the Temp experiments both have thinner ice than the Control experiment in the Arctic Sea, especially near the Canadian Archipelago; the Temp experiment more so than the Freeze2 experiment. They both have less ice in the Laptev Sea than the Control experiment. The Temp experiment also has less ice around the Canadian Archipelago and thinner ice extending into the Greenland Sea than the Control experiment. This is consistent with Figure 5.6 showing that the Temp experiment has substantially thinner sea-ice in September than the Freeze2 experiment.

5.3.3 Sea-Ice Extent

The average bias and correlation coefficient of the monthly sea-ice extent between 1985 and 1990 for the individual experiments and the Control experiment are displayed in Figure 5.12. In Table 5.5 the correlation coefficient, RMSE and bias of each experiment's sea-ice extent is compared to the Control experiment.

Table 5.5: Correlation coefficient, RMSE and bias of each experiment's sea-ice extent in relation to the Control experiment. Values displaying a large change a marked as `typewriter numbers`, and small changes are marked with *slanted numbers*.

	Alb1	Alb2	Alb3	Freeze1	Freeze2	Temp
Correlation Coefficient	`0.981`	*1.000*	*1.000*	`0.996`	0.999	0.999
RMSE [10^6 km^2]	`0.95`	*0.05*	0.12	0.23	0.11	`0.34`
Bias [10^6 km^2]	`0.68`	*0.04*	0.09	0.08	*-0.04*	`-0.33`

Clearly the radical albedo experiment, Alb1, has the largest effect on the sea-ice extent as it has the lowest correlation coefficient with the Control experiment and the largest bias (around $7 \cdot 10^5$ km^2) and root mean square error (around $9.5 \cdot 10^5$ km^2). The Temp experiment that has the second most influence on the sea-ice extent, whith has a bias and a difference in mean sea-ice extent to the Control experiment of around -3·10^5 km^2. Alb3 and Freeze1 both have biases to the Control experiment around 1·10^5 km^2. Alb2 and Freeze2 have the smallest biases, around $\pm 0.4 \cdot 10^5$ km^2. The OW freezing experiments have average root mean square errors over twice as large as their average biases.

The sea-ice extent of the various experiments will be further discussed in the next section where they are compared to satellite observations.

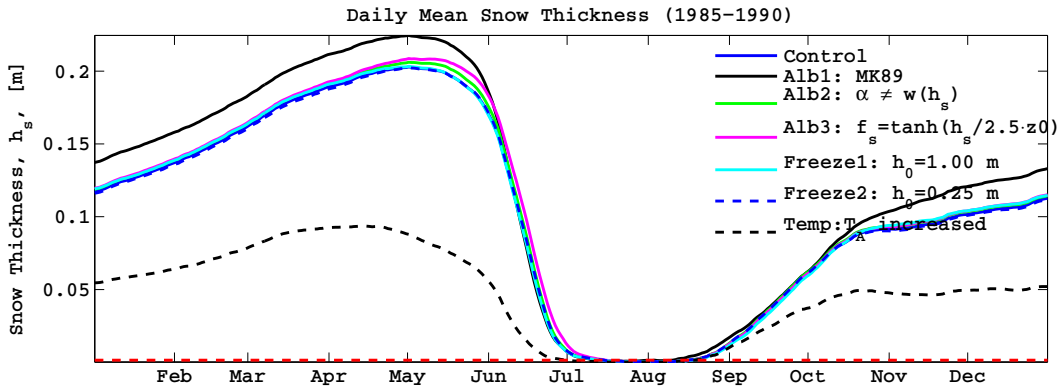

Figure 5.9: Climatology of daily mean snow thickness between 1985 and 1990 for all experiments. The red, stapled line shows $h_s = 1.5$ mm, the melt season criteria.

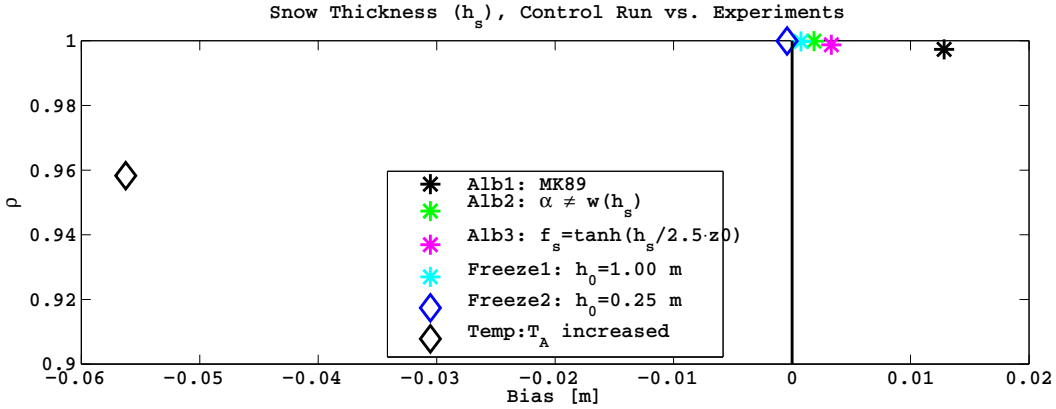

Figure 5.10: Bias (x-axis) and correlation coefficient, ρ, (y-axis) for monthly values of mean snow thickness between 1985-1990 for each sensitivity experiment compared to the Control experiment.

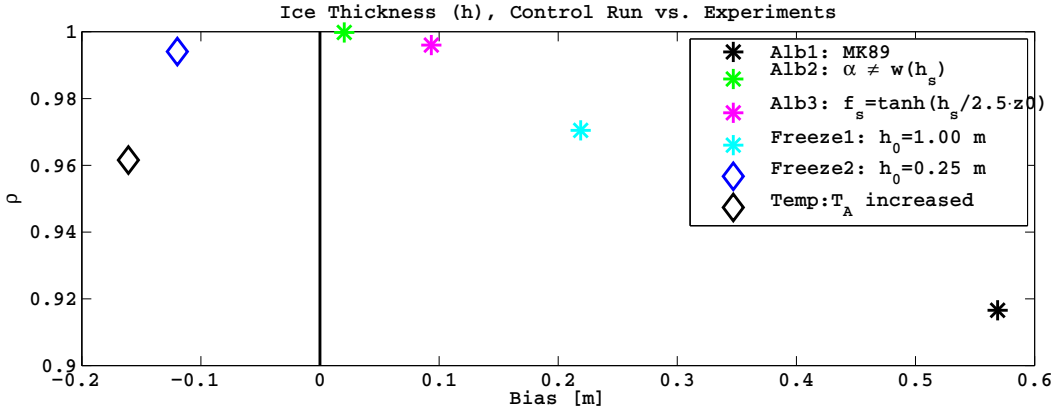

Figure 5.11: As in Figure 5.10, but for the mean ice thickness.

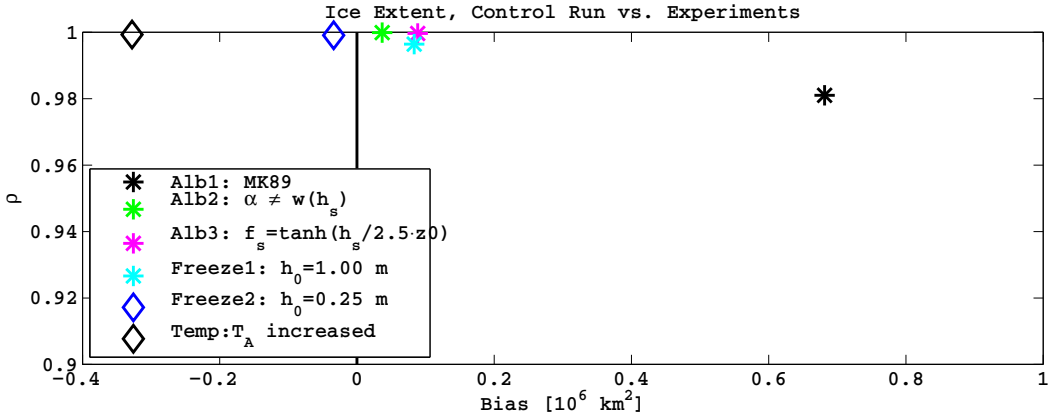

Figure 5.12: As in Figure 5.10, but for the sea-ice extent.

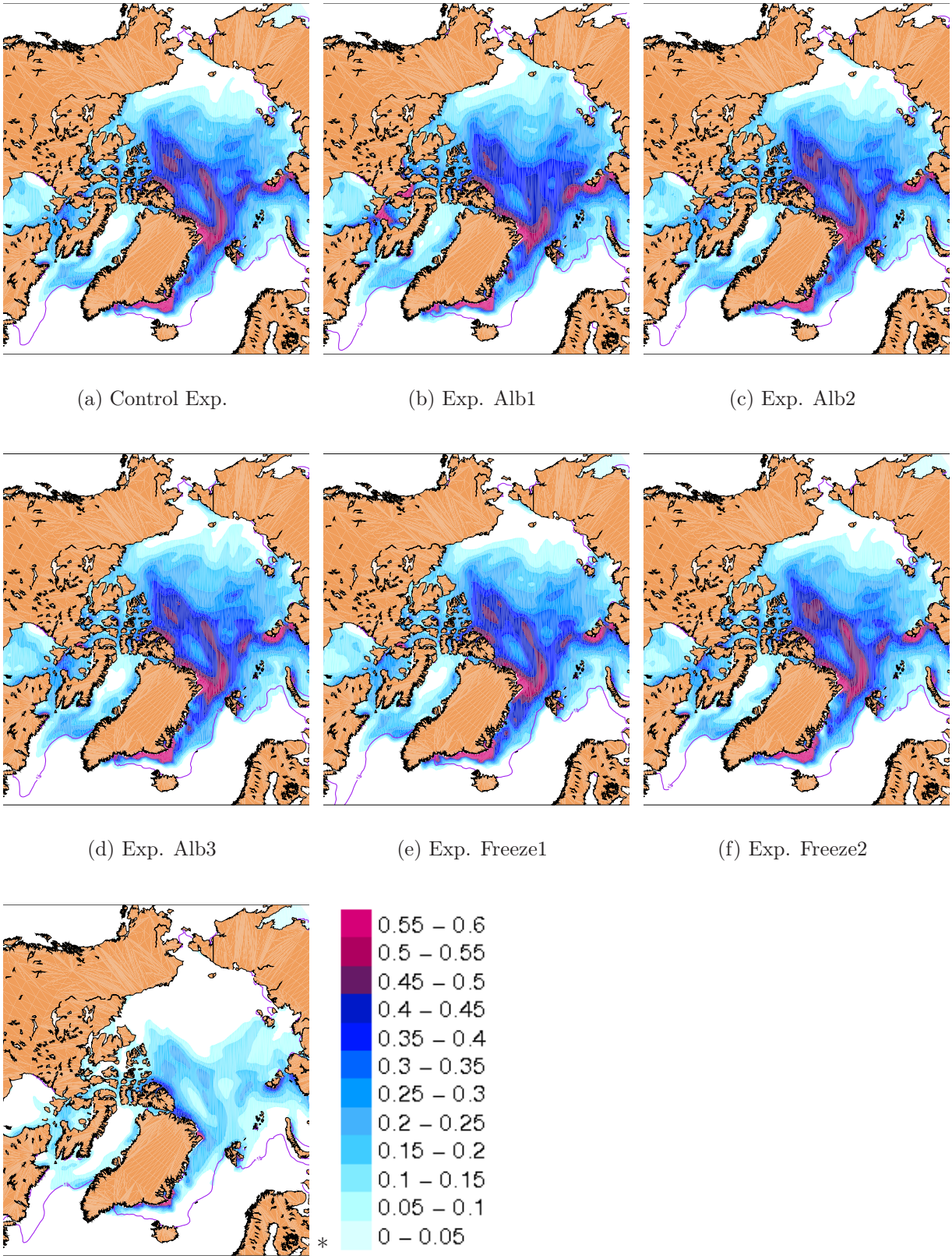

(a) Control Exp. (b) Exp. Alb1 (c) Exp. Alb2

(d) Exp. Alb3 (e) Exp. Freeze1 (f) Exp. Freeze2

(g) Exp. Temp

Figure 5.13: Snow thickness in May 1990 for the Control and sensitivity experiments. A purple line marks the modeled sea-ice extent for the respective experiment.

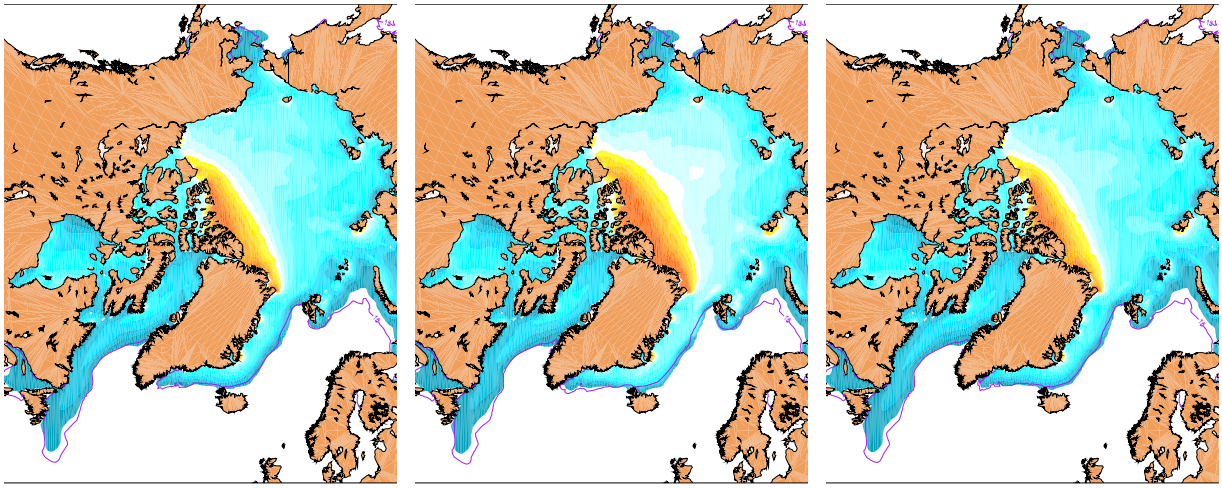

(a) Control Exp. (b) Exp. Alb1 (c) Exp. Alb2

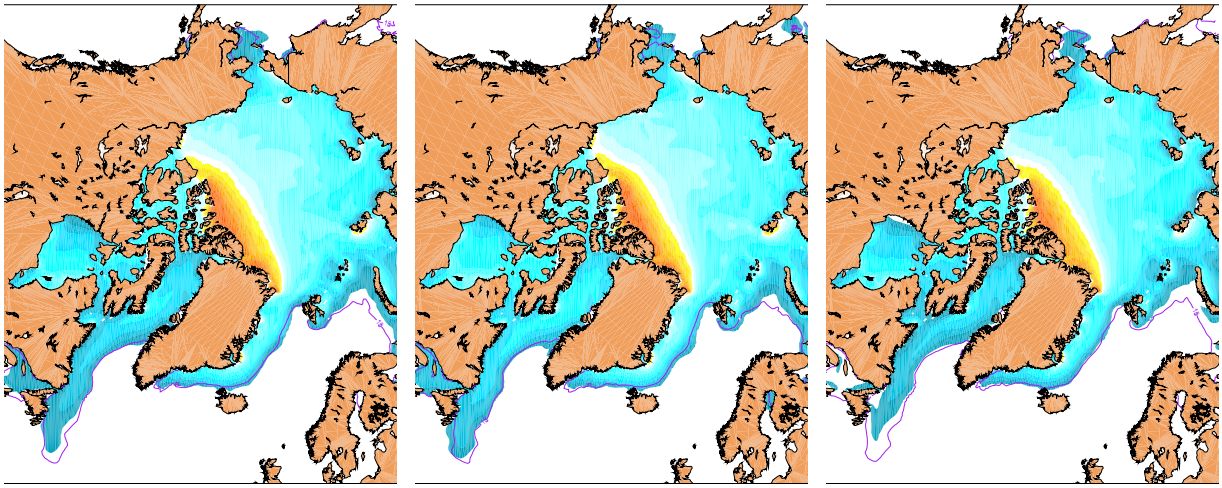

(d) Exp. Alb3 (e) Exp. Freeze1 (f) Exp. Freeze2

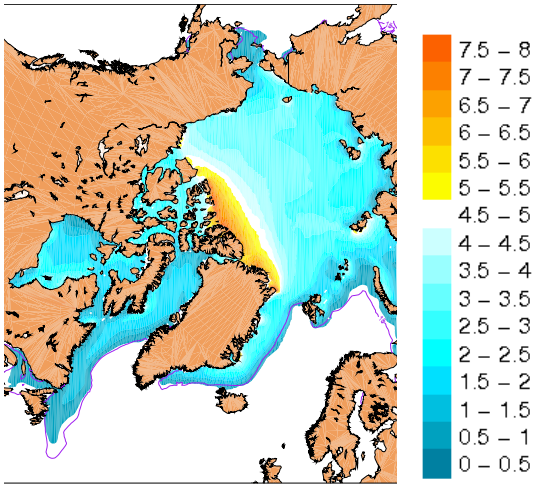

(g) Exp. Temp

Figure 5.14: sea-ice thickness in March 1990 for the Control and sensitivity experiments. The sea-ice extent of each experiment is marked with a purple line.

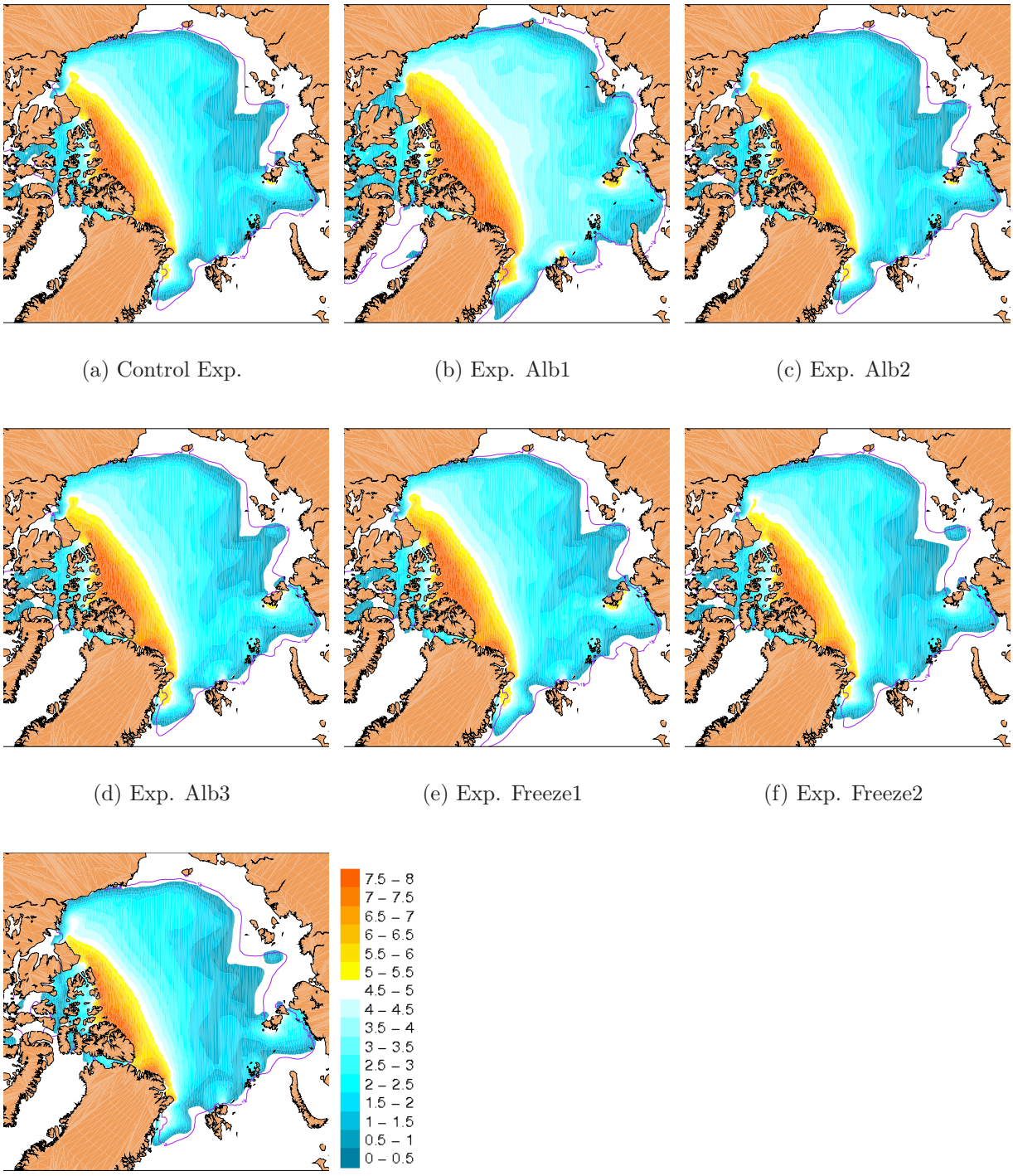

(a) Control Exp. (b) Exp. Alb1 (c) Exp. Alb2

(d) Exp. Alb3 (e) Exp. Freeze1 (f) Exp. Freeze2

(g) Exp. Temp

Figure 5.15: sea-ice thickness in September 1990 for the Control and sensitivity experiments. The sea-ice extent of each experiment is marked with a purple line.

5.4 Sea-Ice Extent in Comparison to Satellite Observations

To compare with our model results the sea-ice extent from the NSIDC is used for the entire Northern Hemisphere (N.H.), while the OSI SAF sea-ice extent used is manipulated to only include sea-ice which is within MI-IM's domain. MI-IM's domain is not large enough to cover the whole area of sea-ice in the North Pacific (Figure 4.3 on page 26). A version of the OSI SAF sea-ice extent that disregards sea-ice south of the Bering Strait has also been constructed. This is to make a fairer comparison with MI-IM, which produces too little ice south of the Bering Strait during winter (Figure 4.3 on page 26).

The reason MI-IM has problems representing the sea-ice extent south of the Bering Strait is probably that MI-IM relies on sea surface temperature and salinity from the SODA climatology and not from MICOM in this area, as MICOM's domain ends at the Bering Strait, see Section 2.3. Here after the OSI SAF sea-ice extent that is interpolated to MI-IM's domain is referred to as OSI-SAFv1, and the version which is interpolated to MI-IM's domain, but excludes data south of the Bering Strait is referred to as OSI-SAFv2. sea-ice concentration data from December 1987 and January 1988 are omitted from all observations due to a malfunction in the SSM/I during these months.

The regional distribution of sea-ice concentration for each experiment together with the sea-ice extent derived from OSI SAF concentrations (for the entire Northern Hemisphere) are presented in Figure 5.20 for September 1990. The sea-ice extent of the experiments that differs mostly in geographical distribution from the Control experiment is also presented in Figure 5.21 for July and October 1990 together with the OSI SAF sea-ice extent.

To get insight into how each experiment performs throughout the year the correlation coefficient, root mean square error and bias between the sea-ice extent of each experiment and OSI-SAFv2 have been calculated for different seasons. Figure 5.19(c) shows the root mean square error and correlation coefficient for January, February and March. Figure 5.19(d) shows the same for April, May, and June, Figure 5.19(e) for July, August, and September, and Figure 5.19(f) for October, November, and December. Table 5.6 gives an overview of the correlation coefficients, root mean square error and biases of each experiment in each season. Values indicating an especially good match between the experiment and the observation are marked with bold numbers, while values indicating a bad match are marked in italics.

Table 5.6: Correlation coefficient, root mean square error and bias of each experiment's sea-ice extent in comparison to the OSI-SAFv2 sea-ice extent. The top values are typed in **bold letters**, while the worst values are typed in *italics*. The unit of the RMSE and bias is 10^6 km^2.

	Winter			Melt Season			Summer			Freeze Up		
	ρ	RMSE	Bias	ρ	RMSE	Bias	ρ	RMSE	Bias	ρ	RMSE	Bias
Control	0.843	0.89	**0.05**	0.962	0.48	0.61	0.978	0.43	0.34	0.983	1.34	-1.10
Alb1	0.845	**0.78**	0.16	0.961	*0.68*	*0.83*	*0.958*	*2.03*	*2.00*	*0.952*	**0.78**	**-0.34**
Alb2	0.844	0.88	0.06	0.963	0.49	0.63	0.977	0.50	0.43	0.983	1.31	-1.07
Alb3	0.841	0.87	0.07	0.963	0.51	0.65	0.976	0.62	0.56	0.983	1.26	-1.02
Freeze1	*0.840*	1.02	-0.08	*0.941*	0.58	0.70	0.977	0.77	0.72	0.980	1.34	-1.09
Freeze2	**0.852**	0.83	0.11	**0.966**	**0.41**	0.54	0.978	0.32	**0.17**	**0.985**	1.31	-1.07
Temp	0.845	*1.15*	*-0.22*	0.958	0.45	**0.38**	**0.982**	**0.28**	-0.24	0.983	*1.70*	*-1.46*

From Figure 5.16, 5.17, 5.18 and 5.19(c) it is clear that in January, February and March the variation in the modeled sea-ice extent of the experiments is very small. There is also little variability between the experiments in the regional distribution of the March 1990 sea-ice extent (see Figure 5.14 in the previous section).

In Figure 4.3 on page 26 the regional distribution of the March 1990 modeled and observed (OSI SAF) sea-ice extent was presented. As mentioned above MI-IM produces too little ice south of the Bering Strait (compare OSI-SAFv2 to the modeled extent in Figure 5.16 and 5.17). From figure 4.3 it was also visible that MI-IM lacks ice outside the Gulf of Saint Lawrence and where the Odden ice tongue is. The modeled sea-ice extent in March 1990 corresponds well to the observed sea-ice extent, except in the mentioned areas.

In January the observed sea-ice extent is somewhat higher than the modeled sea-ice extent, while in March it is somewhat lower. This is because MI-IM's sea-ice extent grows slower than the observed sea-ice extent during freeze-up, and thus is smaller than the observed sea-ice extent in January, but has some ice south of the Bering Strait in the winter months, making the sea-ice extent larger than the OSI-SAFv2 sea-ice extent. The correlation coefficients for the winter period are therefore lower than in the other seasons. For the same reason the bias is the lowest compared to the other seasons, and much smaller than the root mean square error in the period. The Temp experiment has the highest root mean square error, 1 150 000 km^2, and the highest bias in magnitude, underestimating the sea-ice extent with 220 000 km^2. The Alb1 experiment has the lowest root mean square error in the period. The Freeze1 experiment has the lowest correlation coefficient of the experiments, while Freeze2 has the highest.

In conclusion, in wintertime, the modeled and OSI-SAFv2 hemispheric sea-ice extent correspond well (see Figure 5.16, 5.17, 5.18 and, 5.19(c)). Apart from MI-IM having problems representing sea-ice south of the Bering Strait, the Odden ice tongue, and the observed sea-ice outside the Gulf of Saint Lawrenc (Figure 4.3), the sea-ice edge fits well with the observed sea-ice edge. The misfit in the mentioned areas does not show when comparing the total/integrated sea-ice extent of MI-IM with OSI-SAFv2, because MI-IM has some ice south of the Bering Strait (which is not included when calculating the sea-ice extent in OSI-SAFv2), making up for what it is lacking.

In April, May and June the magnitude of the sea-ice extents of the experiments are also quite similar (see Figure 5.16, 5.17, 5.18 and, 5.19(d)). In May 1990 the regional distribution of sea-ice in the experiments are also similar, see Figure 5.13.

When compared to OSI-SAFv2 the modeled sea-ice extent of all the experiments are too large. In April this can be caused by the fact that there still is some ice outside the Bering Strait in MI-IM (see Figure 5.13). In May and June the sea-ice extent of the MI-IM experiments are larger than OSI-SAFv1 and OSI-SAFv2. As OSI-SAFv1 includes all the sea-ice within MI-IM's domain this shows that the sea extent in MI-IM retreats too slowly, the sea-ice in MI-IM melts too slowly. Looking at the regional distribution of sea-ice in these months there is visibly too much ice in the Greenland and Labrador Sea in MI-IM (not shown). The Temp and Freeze2 sea-ice extents are more similar to OSI-SAFv2 than the other experiments in these months (see Figure 5.19(d)). Temp has the smallest bias in the period, while Freeze2 has the smallest root mean square error and the highest correlation coefficient in the period (see Table 5.6). Experiment Alb1 has the highest root means square error and the highest bias in the melt season.

In July, August and September the sea-ice extent of the experiments varies more (see Figure 5.16, 5.17, 5.18 and, 5.19(e)). Especially the sea-ice extent of the Alb1 experiment diverges from the other experiments. From Figure 5.18 you can see that all of the experiments, except for the Temp experiment, have ice extents of larger magnitudes than OSI-SAFv1. From Figure 5.16 and 5.17 it is apparent that all the experiments except the Temp experiment has a higher sea-ice extent than OSI-SAFv1, OSI-SAFv2 and the NSIDC Sea-Ice index. After the Temp experiment, which has the smallest bias and highest root mean square error in the period, the Freeze2 experiment has compares best with the observations (see Table 5.6).

In Figure 5.21 the July 1990 regional distribution of the sea-ice extents of the Control, Alb1, Freeze1, Freeze2 and Temp experiments and the OSI SAF observations are visualized. The Alb2 and Alb3 experiments are not included as their regional distributions of sea-ice are more similar to the Control experiment in this period. It is clear that in this month the Alb1 and Freeze1 experiments' ice extent extends too far south in all areas except around Greenland's southern tip. The Control, Freeze2 and Temp experiments' sea-ice extent are more similar to the observations than Alb1 and Freeze1, especially in the Labrador Sea.

September 1990 sea-ice concentrations (the concentration is marked from 15 to 100%, making the edge of the marked area corresponds to the ice edge) for each experiment are displayed in Figure 5.20 together with the OSI SAF sea-ice extent. In the Arctic Ocean all experiments overestimate the sea-ice extent, the Alb1 does so especially much. The Alb1 experiment also has sea-ice in the Hudson Bay, Davis Strait and the Baffin Bay where none is observed. On the other hand all the experiments except Alb1 and Freeze1 underestimates how far south into the Greenland Sea the sea-ice extends. The Control, Freeze2 and Temp experiment underestimate the amount of ice east of Severnaya Zemlya and north of New Seberian Islands.

In October, November and December the experiments underestimate the sea-ice extent (see Figure 5.16, 5.17, and 5.18), the Temp experiment does so especially much. From Figure 5.19(f) and Table 5.6 it is obvious that the Temp experiment has the largest root mean square error and bias, around -1 460 000 km^2, in this period. The Alb1 experiment has the lowest root mean square error and bias, but also clearly a much lower correlation coefficient than the other experiments. The Freeze2 experiment has the highest correlation coefficient of the experiments.

In Figure 5.21 the October 1990 sea-ice extent is displayed for the Control, Alb1, Freeze1, Freeze2 and Temp experiments, and OSI SAF. All of the experiments, but to a lesser degree Alb1, have too little ice around Baffin Island and in the East Siberian, Laptev and Kara Sea. The Control experiment, Freeze2 and Temp experiments also have too little ice in the Greenland Sea.

Statistical comparisons of each experiment's sea-ice extent and the OSI-SAFv2 sea-ice extent (between July 1987 and December 1990) are displayed in Figure 5.19 and in Table 5.7. The average monthly bias and correlation coefficients for the same period of the monthly averaged sea-ice extent for each experiment and OSI-SAFv2 are shown in Figure 5.19(b). Figure 5.19(a) shows the correlation coefficients and the average root mean square error of the monthly averaged sea-ice extent for each experiment and OSI-SAFv2 in the period.

Looking at Figure 5.19(a) and 5.19(b) and Table 5.7 it is clear that compared to observations from OSI-SAF (OSI-SAFv2) all experiments except experiment Alb1 have correlation coefficients higher than 0.90. Experiment Freeze2 has the highest correlation coefficient, 0.955, while Alb1 has the lowest one, 0.879 and a high root mean square error to the observations, $1.28 \cdot 10^6$ km^2. The Temp experiment also has a high root mean square error to the observations, $1.06 \cdot 10^6$ km^2. Experiment Freeze2 has the lowest root mean square error, $0.82 \cdot 10^6$ km^2. The Control experiment has a similar results to experiment Alb2 and Alb3, a root mean square error of $0.87 \cdot 10^6$ km^2 and a correlation coefficient of $0.94 \cdot 10^6$ km^2.

Table 5.7: Root mean square error (RMSE) and correlation coefficient (ρ) of modeled and observed sea-ice extent from July 1987 to December 1990 (see Figure 5.19(b)). The top values are typed in **bold letters**, while the worst values are typed in *italics*.

	Control	Alb1	Alb2	Alb3	Freeze1	Freeze2	Temp
RMSE [10^6 km^2]	0.87	*1.28*	0.87	0.87	0.98	**0.82**	*1.06*
ρ	0.944	*0.879*	0.941	0.937	0.918	**0.955**	0.946

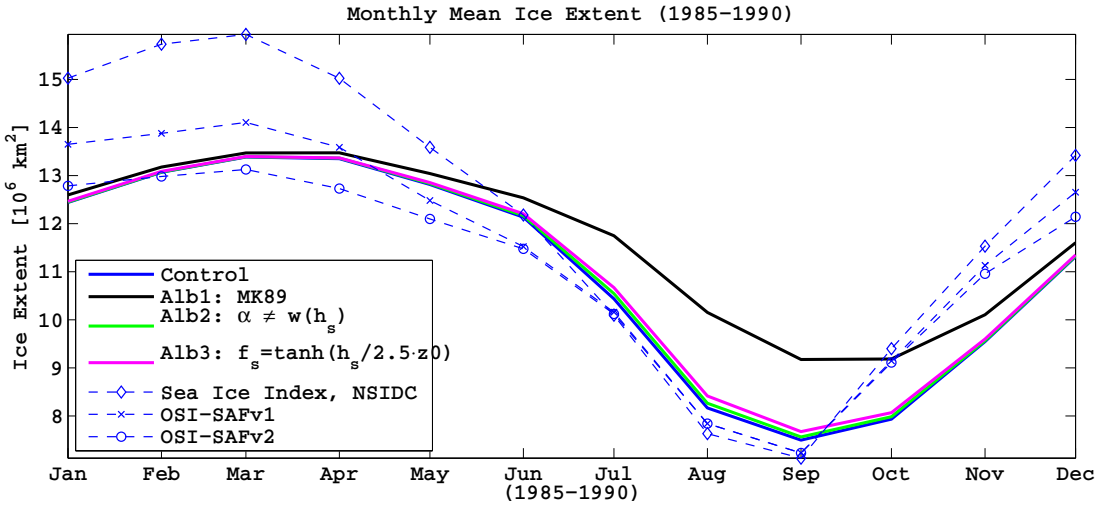

Figure 5.16: 1985*-1990 monthly climatology of sea-ice extent for the Control and albedo experiments and from satellite observations from the NSIDC, and OSI SAF. The NSIDC extent is for the entire N.H., while the OSI SAF extent is derived from data interpolated to MI-IM's domain (OSI-SAFv1). The OSI SAF sea-ice extent is also calculated excluding data south of the Bering Strait (OSI-SAFv2). *The OSI SAF data starts 07/87.

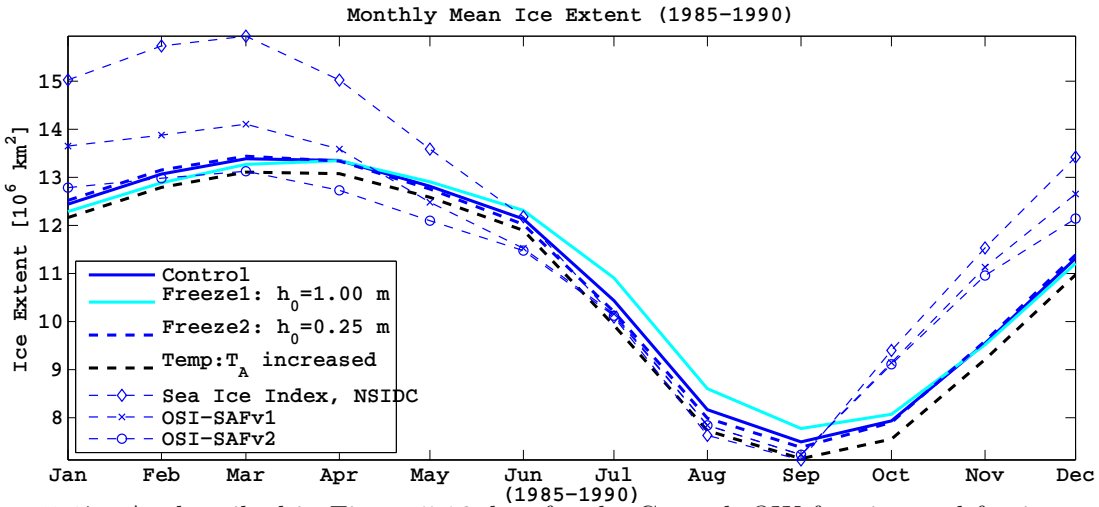

Figure 5.17: As described in Figure 5.16, but for the Control, OW freezing and forcing experiments.

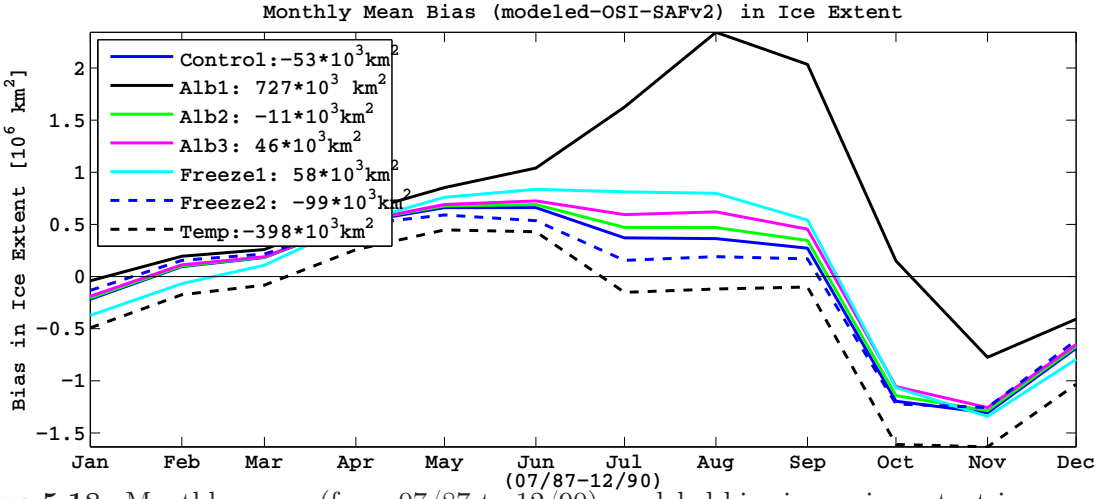

Figure 5.18: Monthly mean (from 07/87 to 12/90) modeled bias in sea-ice extent in comparison to the OSI SAF sea-ice extent excluding ice from the area outside the Bering Strait (OSI-SAFv2).

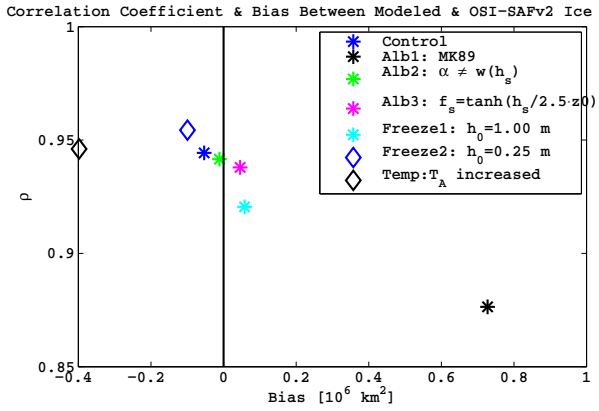

(a)

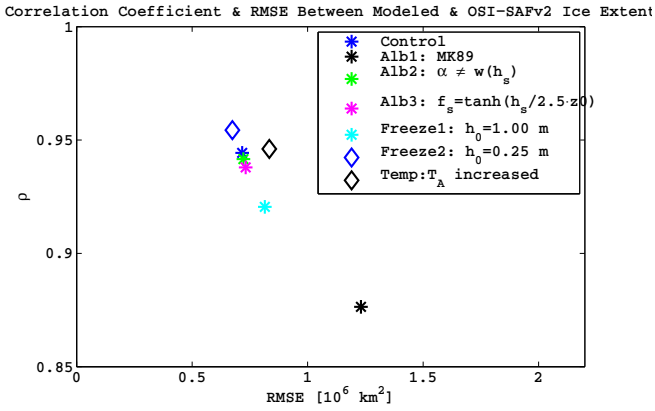

(b)

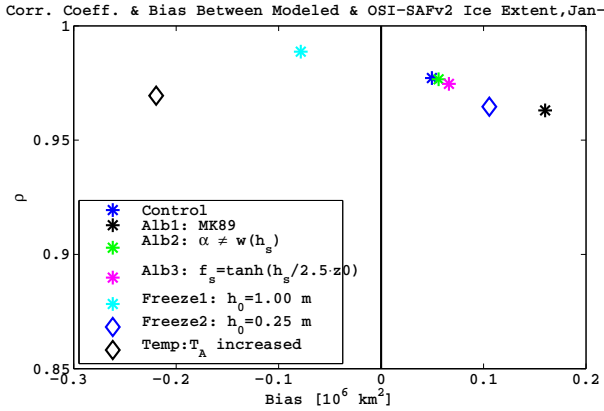

(c)

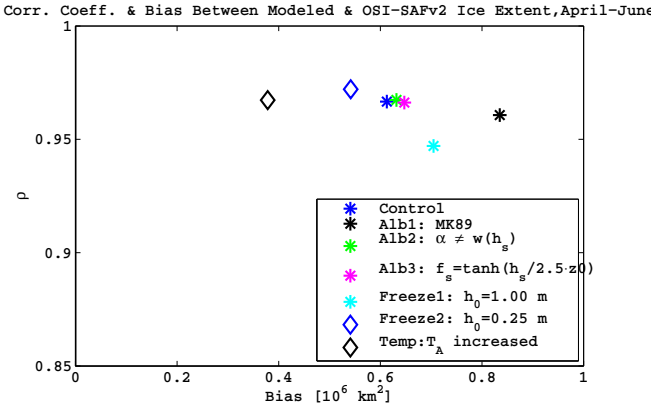

(d)

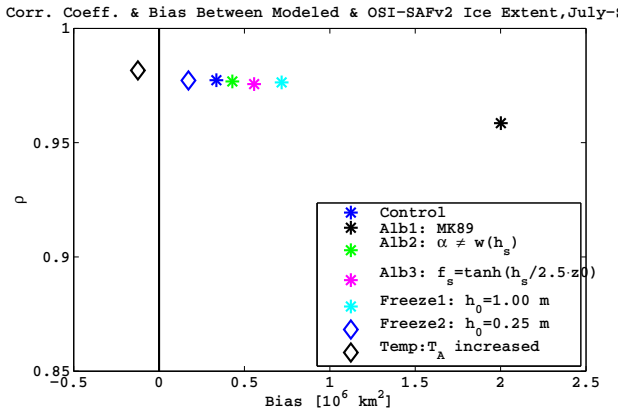

(e)

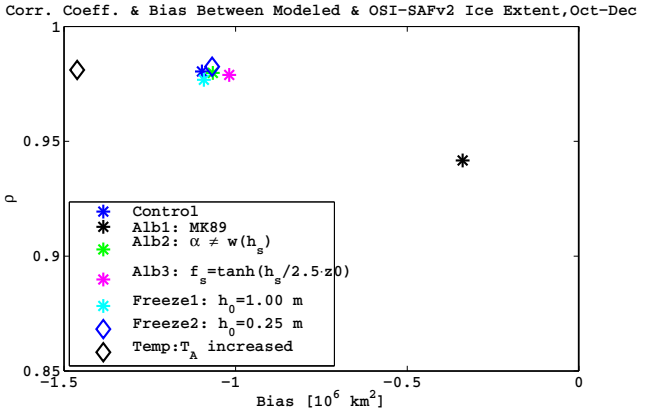

(f)

Figure 5.19: Figure 5.19(a) shows the bias and correlation coefficient (ρ) of monthly mean sea-ice extent from July 1987 to December 1990 between model experiments and satellite observations, OSI-SAFv2. Figure (b) shows the root mean square error and correlation coefficient in the period. Figure (c), (d) (e) (f) are as figure (b), but respectively for January through March, April through June, July through September, and October through December.

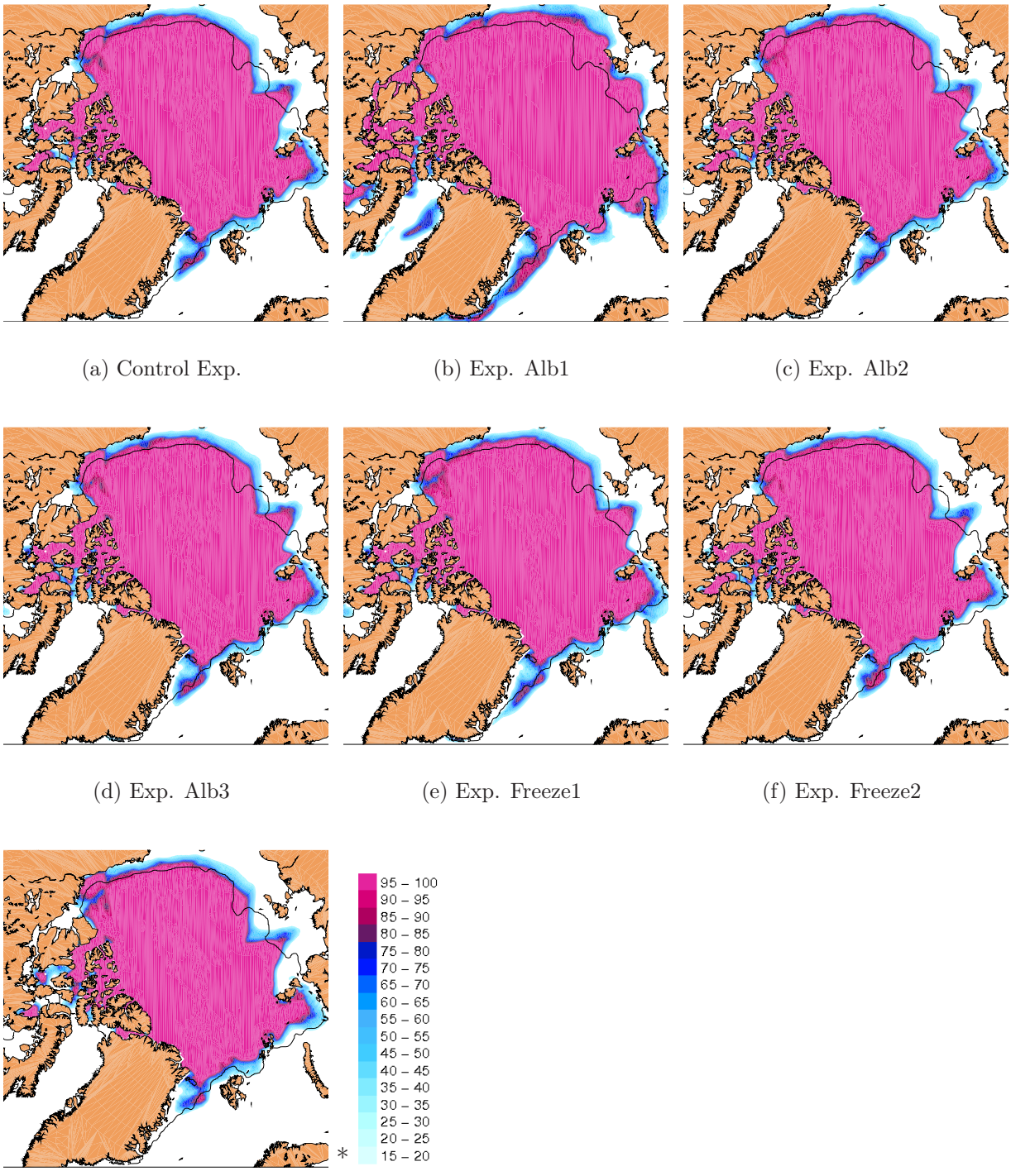

(a) Control Exp. (b) Exp. Alb1 (c) Exp. Alb2

(d) Exp. Alb3 (e) Exp. Freeze1 (f) Exp. Freeze2

(g) Exp. Temp

Figure 5.20: sea-ice concentrations in September 1990 for the Control and sensitivity experiments. The concentration is marked from 15% and upwards, making the outer edge equivalent to the sea-ice extent of the experiment. The OSI SAF sea-ice extent is also marked with a black line.

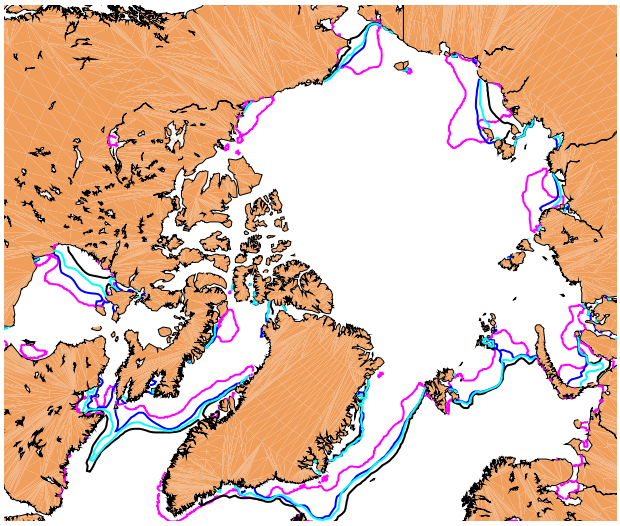

(a) July Extent: Control, Alb1, Freeze1, and OSI SAF

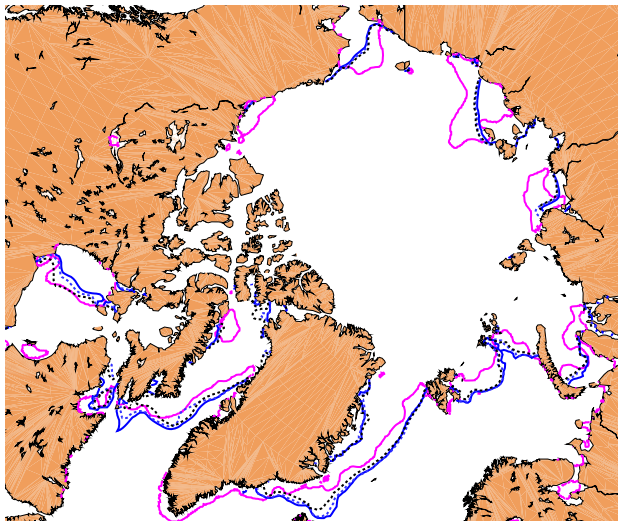

(b) July Extent: Control, Freeze2, Temp, and OSI SAF

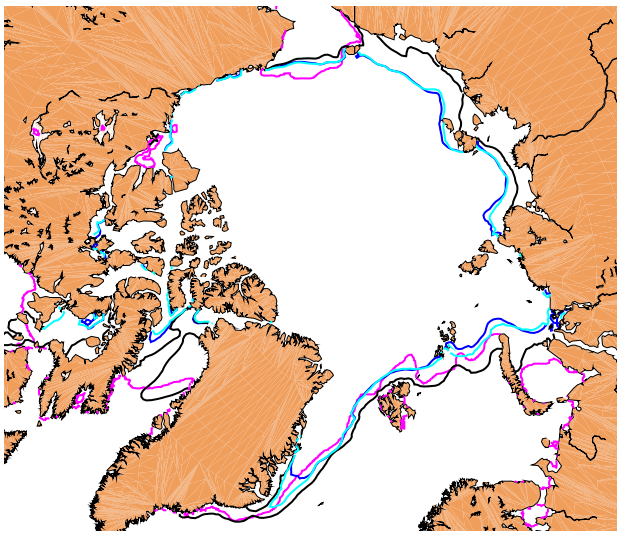

(c) October Extent: Control, Alb1, Freeze1, and OSI SAF

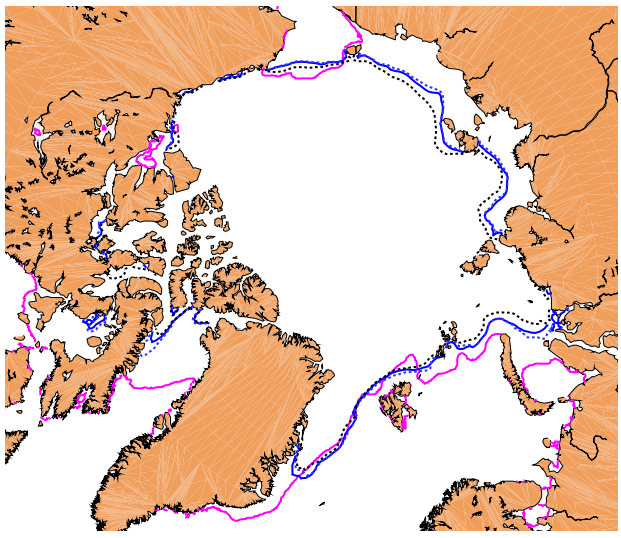

(d) October Extent: Control, Freeze2, Temp, and OSI SAF

Figure 5.21: sea-ice extent in July and October 1990 for the Control, Alb1, OW freezing and forcing experiments and from sea-ice concentrations from OSI SAF. The OSI SAF sea-ice extent is marked with a pink line. The experiments are marked with colors consistent with those previously used. The Control experiment is marked with a blue line, the Alb1 experiment with a black line; the Freeze1 experiment with a turquoise line. The sea-ice extent of the Freeze2 experiment is marked with a blue dotted line, and the sea-ice extent of the Temp experiment is marked with a black dotted line.

Chapter 6

Analysis

The first section of this chapter aims to answer questions identified in Chapter 1.

6.1 How does the Sensitivity Experiments Compare the Control Experiment and to Observations?

Table 6.1: The change in % cuased by the experiment on the mean snow and ice thickness and mean and minimum ice extent (Change in % $=(\bar{E}/\bar{C}-1)\cdot 100$), where $\bar{C}$ is the 1985-1990 mean/minimum value of the variable for the Control experiment, while $\bar{E}$ is the 1985-1990 mean/minimum value of the variable for the experiment. The mean values can be found in Table 5.1, 5.2 and 5.4.

	Alb1	Alb2	Alb3	Freeze1	Freeze2	Temp
Ice thickness [%]	22.2	0.0	3.7	7.4	-3.7	-7.4
Ice Extent [%]	6.4	0.0	0.9	0.9	0.9	-2.7
Min. Ice Extent [%]	22.7	1.3	2.7	4.0	-1.3	-5.3
Snow Thickness [%]	12.5	1.9	2.9	1.0	0.0	-59.0
|total|	|63.8|	|3.2|	|10.2|	|13.3|	|5.9|	|69.2|

Table 6.2: (The difference in % between the observed (OSI SAF) and modeled minimum ice extent. Difference in % $=(\bar{E}/\bar{O}-1)\cdot 100$), where $\bar{O}$ is the mean minimum ice extent from 1987-1990, while $\bar{E}$ is the 1987-1990 modeled mean minimum ice extent in the same period

	Control	Alb1	Alb2	Alb3	Freeze1	Freeze2	Temp
Min. Ice Extent [%]	3.76	28.08	4.78	6.29	7.50	2.34	-1.38

6.1.1 Alb1

From Figure 5.11 and 5.12 it is easy to see that the radical albedo experiment, Alb1, by far had the greatest effect on the ice thickness and extent of all the sensitivity experiments. Alb1 increased the mean ice thickness between 1985 and 1990 by 22.2%, from 2.7 m to

3.3 m. The average minimum sea-ice extent increased by $1.7{\cdot}10^6$ km^2, 22.7%, in the same period.

Alb1 had the second largest effect of the experiments on the snow thickness. This experiment led to a mean snow thickness between 1985 and 1990 that was 12.5% than in the Control experiment, and decreased the average number of snow free days with five days.

Compared to satellite observations, the sea-ice extent of Alb1 has the lowest correlation coefficient, and the highest bias and root mean square error of all the experiments (see Figure 5.19). Using Alb1 as the albedo scheme of MI-IM resulted in an unrealistically large sea-ice extent during summer and freeze-up.

As can be seen in Section 3.2, the albedo scheme of *Mellor and Kantha* (1989), which is used in Alb1, has a sea-ice albedo varying between 0.64 (for bare ice) and 0.82 (for snow covered ice). The albedo in the original scheme varies from 0.84 (for ice covered with snow thicker than 20 cm) to 0.09 (for 5 cm thin ice which is melting). The original albedo scheme allows for a much lower albedo than Alb1.

The thicker ice and snow and the larger ice extent is a result of the ice-albedo feedback mechanism. The higher ice and snow albedo allows less short wave radiation to penetrate into the snow or ice and the ocean underneath it and this decreases the surface temperature. As a result, the ice becomes thicker and more extensive. The snow cover also becomes thicker as less heat is conducted from the ocean through the thicker ice to melt the snow. The albedo also increases with a vaster snow cover and fewer snow free days. The short wave radiation allowed to penetrate from the snow into the ice also decreases with increasing snow thickness (in MI-IM, if the snow thickness is 20 cm or more, no short wave radiation is allowed to penetrate into the ice). The thicker the ice is lets less short wave radiation penetrate into the ocean (in MI-IM the short wave radiation allowed to penetrate into the ocean decreases exponentially with ice thickness). The cooler ocean produces more/melts less ice, and the albedo increases.

In *Laxon et al.* (2003) the authors found that the interannual variability of Arctic sea-ice (derived from satellite observations) were highly correlated to the length of the melt season. The large change Alb1 brought to the albedo scheme decreased the 1985-1990 average number of snow free days by five days. This experiment had the largest effect on the sea-ice thickness, which is consistent with the findings of *Laxon et al.* (2003).

As mentioned in Section 3.2 *Mellor and Kantha* (1989) based their albedo scheme on the values used in *Maykut and Untersteiner* (1971). In the paper by *Maykut and Untersteiner* (1971) it is acknowledged that the albedo during melting season is highly complex and fluctuating due to melt ponds, snow patches and bare ice, which have different radiative properties and can coexist in a relative small area. The authors conclude that "*It is obviously impractical to attempt to duplicate such random fluctuations and horizontal variations in a one-dimensional model, so some realistic average must be used.*". After a long discussion, they choose not to take the effect of melt ponds into account, and the albedo of melting ice is set to 0.64. In the end of the article, when they have taken into account their model results, it is stated that the albedo in the melt season should be lower than 0.64. This means that using a minimum albedo of 0.64 for sea-ice is previously acknowledged to be to high.

6.1.2 Alb2

Alb2 had the smallest effect on the ice thickness of the sensitivity experiments; a 1985-1990 mean bias and a root mean square error to the Control experiment of 2 cm (see Table 5.3). The sea-ice extent of Alb2 also had the smallest root mean square error, 51 000 km^2, and second smallest bias, 37 000 km^2, to the Control experiment. It had the smallest effect of the albedo experiments on the snow thickness, but a larger effect than the OW freezing experiments. (See also Figure 5.11, 5.12, and 5.10.)

The change made to the albedo scheme can be seen by comparing Figure 3.1 in Section 3.2 with Figure 2.4 in Section 2.2. The albedo increases faster with snow thickness in Alb2 than in the Control experiment. This is not a dramatic change in the sea-ice albedo scheme of MI-IM. That the Alb2 experiment only led to minor changes in the sea-ice reflects this.

Compared to satellite observations of sea-ice extent Alb2 compares quite equally to the Control experiment, as Alb2 did not lead to a large change in the sea-ice extent. Studying Figure 5.19 you can see that Alb2 has a slightly larger bias than the Control experiment in each season. Coincidentally the bias of Alb2 from July 1987 to December 1990 adds up to the smallest bias of the experiments (see Figure 5.18 and 5.19(a)). It has a root mean square error to the observations in the same period similar to the Control and Alb3 experiments, around 870 000 km^2 (see Figure 5.19(b)).

The Alb2 experiment did not weight the snow towards the underlying ice if the snow was thinner than 20 cm. In the original albedo scheme the snow albedo *is* weighted towards the albedo of the underlying ice. Given that the snow/ice atmosphere interface temperature is -2$^\circ C$ or less, combining (2.5) and (2.3) on 7 yields an expression for the total snow/ice albedo:

$$\alpha = f_S^2 \cdot \alpha_s + (1 - f_S^2)\alpha_i$$

In experiment Alb2, which does not include Equation (2.5) the total snow/ice albedo in the same case ($T_s \leq -2^\circ C$) is :

$$\alpha = f_S \cdot \alpha_s + (1 - f_S)\alpha_i$$

Given that:

$$f_S = \min(\sqrt{\frac{h_S}{0.2}}, 1)$$

in the Control experiment, and f_S has become f_S^2 and the expression for the total snow/ice albedo in the Control experiment is:

$$\alpha = \min(\frac{h_S}{0.2}, 1) \cdot \alpha_s + (1 - \min(\frac{h_S}{0.2}, 1))\alpha_i$$

This new "snow cover fraction" is a linear function[1] instead of a non-linear, parabolic expression (see Figure 6.1, or compare Figure 2.4 to Figure 2.5).

[1]Like the ECMWF IFS snow cover parametrization, except for that the ECMWF IFS parametrization increases much faster.

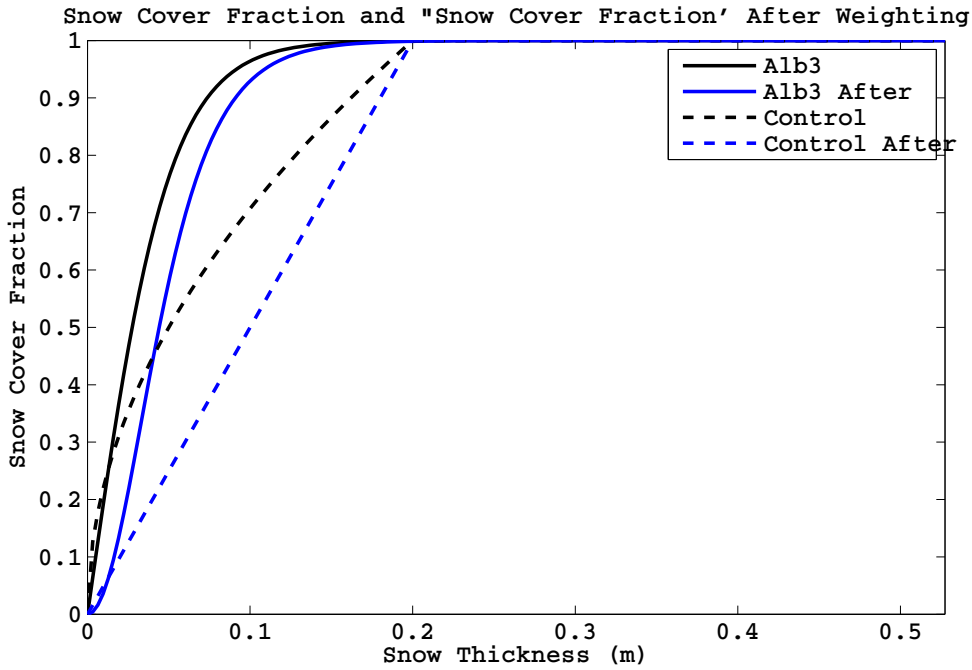

Figure 6.1: The snow cover fraction and the similar expression resulting from weighing the snows albedo towards the underlying snow, in the case where no melt ponds or melting is present ($T_S \leq -2°C$) for both the snow cover fraction parametrization used in the Control experiment and for the parametrization used in Alb3.

6.1.3 Alb3

Changing the parametrization of the snow cover fraction to a *tanh*-function led to larger changes in the snow and ice thickness and ice extent than experiment Alb2. Compared to the Control experiment's snow thickness it had the third largest bias (3.3 mm) and root mean square error (5.0 mm) of the sensitivity experiments. It had a larger bias to the Control experiment's ice extent than Alb2 and Freeze2, 88 000 km^2 (but a smaller root mean square error than Freeze2). On the ice thickness the experiment only had a larger effect than Alb2 (a bias and RMSE around 9 cm).

Compared to satellite observations Alb3, as Alb2, has similar results to the Control experiment, with a positive bias in all months except for the period October through December. In all seasons Alb3 has a bias somewhat larger than the Control and Alb2 experiment. (See Figure 5.19(c)–(f)). Also, in Figure 5.20 it is visible that the Alb2 experiment produces more sea-ice than the Control experiment, e.g. east of Severnaya Zemlya.

When comparing Figure 3.4 and 3.1 in Section 3.2 with Figure 2.4 in Section 2.2, it is appearent that the albedo in Alb3 increases faster with increasing snow thickness than the albedo in Alb2 and in the Control experiment. This can also be seen in Figure 6.1 by comparing the graph of MI-IM and BATS.

In conclusion, Alb3 had a larger effect on the sea-ice extent and ice and snow thickness than Alb2. This is consistent with the fact that the Alb3 experiment made the snow and ice albedo increase more from what it was in the Control experiment than Alb2 did. Compared to the effect of Alb1, neither Alb2 or Alb3 had large effects on the sea-ice and

snow thickness and ice extent.

6.1.4 Freeze1

The Freeze1 experiment, that consisted of doubling the value of the lead closing parameter h_0 from from 0.5 m to 1 m, effected the ice thickness more than the sea-ice extent and the snow thickness. After experiment Alb1 it contributed to the largest change in the ice thickness of the experiments (see Figure 5.11), with an average bias and RMSE in the mean ice thickness between 1985 and 1990 of around 22 cm (Table 5.3). The correlation coefficient of the Control experiment's and Freeze1's mean ice thickness was substantially lower than the correlation coefficients of Alb2, Alb3 and Freeze2 (Table 5.6).

Freeze1's thick ice made its sea-ice extent retract more slowly than the other experiments in the melting season (Figure 5.20, 5.21(a), and 5.21(c)). Subsequently, Freeze1 has a larger sea-ice extent on average than the Control, Alb2 and Alb3, Freeze2 and Temp experiments during the melt season and the summer.

Because of its changed physics, with a greater part of a new volume of sea-ice distributed vertically than horizontally, the sea-ice extent in Freeze1 grows more slowly than the other experiments during freeze-up and winter. Freeze1 leads to both a slower growing and a slower decreasing sea-ice extent. This means that increasing h_0 makes the seasonal cycle of sea-ice extent less pronounced. The same result was found in *Holland et al.* (1993) when they decreased their coefficient of freezing, C_f, from 1 to 0.5 (equivalent of doubling h_0 from 0.5 m to 1m, see Section 3.3). Freeze1's bias to the Control experiment's ice extent is less than half of its root mean square error (Table 5.5). This is a result of Freeze1 underestimating the winter sea-ice extent, and overastimating the summer sea-ice extent; a consequence of its less pronounced seasonal cycle.

Figure 5.8 shows that the ice volume is substantially larger for the Freeze1 experiment than the Control experiment. This is because the ice concentration grows slower during freeze-up and more heat is allowed to escape from the open water to the atmosphere, further cooling the mixed layer of the ocean and allowing more ice to be produced. The ice is produced slower, but thicker. As MI-IM is not coupled to an atmosphere model, but forced with data from ERA-40, the heat escaping from the open water is probably larger than it would be as the atmosphere above does not become warmer as a result of the escaping heat.

The Freeze1 experiment had only a very small positive effect on the mean snow thickness (Figure 5.10). Even though the thicker sea-ice of Freeze1 more effectively isolates the snow from the ocean, the albedo still melts it equally effective as in the Control experiment in the springtime (Figure 5.9).

As mentioned above Freeze1 has the second largest sea-ice extent in summer of all experiments. Compared to observations the sea-ice extent is already overestimated by MI-IM in summertime. As can be seen in Figure 5.21(a) and 5.20 Freeze1 has a substantially larger sea-ice extent in July and September than what is observed. The sea-ice in MI-IM refreezes too slow during the fall (Figure 5.16 and 5.17). Freeze1's September sea-ice extent was larger than the other experiments' (except Alb1's). This made the October sea-ice extent

of Freeze1 fit better with observations than the experiments which had a lower minimum sea-ice extent (Figure 5.21(c)).

Despite this it has on average the second largest root mean square error and bias, and the second lowest correlation coefficient compared to observations, after experiment Alb1, in October, November and December (Table 5.5 and Figure 5.19(f)). Freeze1 has the second largest root mean square error during winter, the melt season, summer and freeze-up, and the second highest bias in all seasons, except winter. It also has the lowest correlation coefficient in the wintertime and in the melt season.

Though it is argued that Freeze1 contains the most appropriate value for h_0, 1 m, (*Holland et al.*, 1993; *Bjornsson et al.*, 2003) (see Section 3.3) it does not compare well with observations in the present version of MI-IM.

6.1.5 Freeze2

Freeze2 did not lead to a large change in the mean ice thickness. The average bias between the Freeze2 and Control experiments' sea-ice thickness is -13 cm. Doubling h_0, Freeze1, led to a bias of almost twice the magnitude resulting from halving h_0 (+23 cm). As h_0 originally was 0.5 m this makes sense, because in Freeze1 50 % of its value was added to it, while in Freeze2 only 25 % of its value was subtracted from it.

The smaller change in the mean ice thickness resulting from Freeze2, and no change in the albedo scheme from the Control experiment, implies that Freeze2 has the smallest effect on the mean snow thickness of the sensitivity experiments.

Compared to the Control experiment's sea-ice extent Freeze2 had the smallest bias of all the sensitivity experiments (see Table 5.3). It did not have the smallest root mean square error, though, this was higher than the root mean square error of Alb2. As Freeze1, the root mean square error of Freeze2's sea-ice extent was over twice as large as its bias. The change in h_0 makes the sea-ice concentration grow and decrease faster than in the Control experiment. It thus has a negative bias to the Control experiment in the melting season and summer, and a positive bias during freeze-up and winter. This is consistent with the findings of *Holland et al.* (1993), where a similar change accentuated the seasonal cycle of the sea-ice coverage. The thinner and vaster ice produced makes the sea-ice area increase quicker, and also melt quicker, as it has little thermal inertia.

Compared to satellite observation MI-IM's sea-ice melts and freezes up too slowly. MI-IM also has a smaller ice extent in September than the observed ice extent. Freeze2 accentuated seasonal cycle thus improves MI-IM's match with observations of sea-ice extent. Looking at Table 5.6 Freeze2 stands out as the experiment which compares best to the OSI-SAFv2 sea-ice extent. Looking at Figure 5.21 it is visible that the regional sea-ice extent of Freeze2 also compares well with observations in July 1990 (the melting season).

In the present version of MI-IM it seems that setting h_0 to 0.25 m improves the match of the model's sea-ice extent with satellite observations.

6.1.6 Temp

After increasing the surface temperature in the Arctic one would expect to find thinner ice, a smaller ice extent and thinner snow. All of this was found. The Temp experiment had the largest effect on the sea-ice extent, after Alb1. While Alb1 led to a much larger sea-ice extent, Temp led to a smaller one; it has a bias of -328 000 km^2 to the Control experiment.

The Temp experiment had the third largest effect on the sea-ice thickness, after Alb1 and Freeze1. Adding an increment to the 2 m temperature (T_A) increasing linearly from zero for $T_A = 0°C$ to one degree Celsius for $T_A \leq -1°C$ led to a bias in the ice thickness to the Control experiment of -16 cm.

The experiment had by far the largest effect on the snow thickness of all the sensitivity experiments. It reduced the 1985-1990 average mean snow thickness with almost 60 %, from 11.7 cm to 4.8 cm. It also increased the number of snow free days with 15 days (see Table 5.4 and Figure 5.9 and 5.13).[2]

Changing T_A directly influences the downward longwave radiation, the latent and sensible heat flux from open water and the sensible heat flux from the ice/snow-atmosphere. As the ocean surface mostly is warmer than the air, the latent and sensible heat flux from the ocean surface to the air would decrease with an increase in the 2 m temperature, as the vertical temperature gradient (the difference between the ocean surface temperature and the 2 m temperature) is reduced. Also the incoming longwave radiation increases if the 2 m temperature is increased (as it is parametrized in MI-IM). Apart from that the outgoing longwave and the sensible and latent heat flux will act to minimize the increased vertical temperature gradient, the increased ocean temperature will lead to less sea-ice (less produced and more melted). The change in the latent and sensible heat fluxes from the ocean does not influence the air temperature, which this is fixed in these experiments.

The mean snow thickness is calculated over the ice covered area, so the decrease in the ice extent would not be connected with a thinner mean snow thickness. The decrease in the sea-ice thickness seems not to be the major reason for the radical decrease in the snow thickness, as the change in snow thickness following Freeze2, which reduced the ice thickness with 80 % of what the Temp experiment did, was minimal. (It had the smallest effect of all the experiments on the ice thickness, with a bias of -0.3 mm.)

This means that the decrease in snow thickness must be mostly a result of the change in downward longwave radiation and in the sensible heat flux over a grid cell containing sea-ice. In MI-IM the downward longwave radiation depends in part on the difference between the surface and the 2 m temperature. The downward longwave radiation increases if the 2 m temperature increases and the surface temperature does not increase equally much (the vertical temperature gradient becomes larger).

According to *Overland et al.* (2000) the sensible heat flux over thick floes is mostly directed

[2]In a fully coupled ocean-ice-atmosphere model the effect of an increased air temperature would most likely not be a dramatic decrease in the mean snow thickness. The increased air temperature would lead to more evaporation over the ocean. More moisture would reach higher latitudes because the warmer air holds more moisture than cold air. Thus precipitation would most likely increase in the Arctic and maybe lead to more snow than before.

from the atmosphere to the surface (the snow/ice surface is usually colder than the 2 m temperature). With an increment added to the 2 m temperature the sensible heat flux from the atmosphere to the surface would intensify. Because the 2 m temperature does not interact with the surface this effect is probably intensified. *Overland et al.* (2000) also state that the Arctic in wintertime has a radiative boundary layer so that the 2 m temperature cannot be considered independent from the surface temperature. In a fully coupled model the 2 m temperature would approach equilibrium with the surface temperature through the flux of sensible heat exchanged between the media.

Experiments increasing the atmospheric forcing to a sea-ice model have been conducted before, though with temperature increments of different magnitudes and with sea-ice models of different types. An experiment increasing the atmospheric temperature with 2°C, conducted by *Semtner Jr* (1987) on a ice-ocean model of the Arctic Ocean and Greenland Sea during a two year long run, made the sea-ice disappear in late summer. In *Semtner Jr* (1987) it is argued that since the Control simulation of the model had an unrealistically thin sea-ice, the disappearance of sea-ice in late summer would perhaps only occur in a model with a realistic sea-ice thickness after an increase in the atmospheric temperature of 4°C. That a higher temperature increment would be needed to make the September sea-ice disappear may be more consistent with the results of the Temp experiment.

Holland et al. (1993) experiment with increasing the atmosphere temperatures with 5°C in an uncoupled dynamic thermodynamic sea-ice model of the Arctic. Their sea-ice model did not contain snow, as MI-IM does. The temperature change led to a decrease in the ice thickness of 50 cm. The sea-ice did not disappear during any time of the seasonal cycle. As our experiment only increased the atmospheric temperature with one degree it is hard to say how *Holland et al.*'s findings fit with ours.

6.2 How does MI-IM's Sea-Ice Extent Compare to Observations?

It is already established that MI-IM has problems representing sea-ice south of the Bering Strait. In that area MI-IM relies on sea surface temperature and salinity from the SODA climatology and not from MICOM, because MICOM's domain ends at the Bering Strait, see Section 2.3. Compared to observations interpolated to MI-IM's domain excluding sea-ice outside the Bering Strait (OSI-SAFv2) MI-IM's sea-ice extent compares pretty well. The total sea-ice extent has a correlation coefficient of 0.944, and a root mean square error of $0.87 \cdot 10^6$ km^2 to OSI-SAFv2 (Table 5.7 and page 47-50). The average bias of the Control experiment, $-0.05 \cdot 10^6$ km^2, is much lower than its root mean square error probably because MI-IM simulates a somewhat higher sea-ice extent in the melt season and summer than the observations (the biases are respectively $0.61 \cdot 10^6$ km^2 and $0.34 \cdot 10^6$ km^2), but a lower one during freeze-up (with a bias to the observations of $-1.10 \cdot 10^6$ km^2). The positive bias is a result of MI-IM's sea-ice melting too slowly in spring and summer, while the negative bias is mostly a result of sea-ice produced too slowly during freeze-up (Figure 5.16 and 5.17). The Odden ice tongue is also not present in the Control experiment (or any of the sensitivity experiments) in the winters that it has been observed between 1980 and 1990.

The sea-ice extent as it is modeled in MI-IM diverges the most from the satellite observa-

tions from October through December, where MI-IM has a negative bias of $1.10{\cdot}10^6\ km^2$. If the MI-IM summer sea-ice concentration was too small, allowing too much short wave radiation to heat the ocean, this would explain the slowed down freeze-up. Looking at Figure 5.20 this seems not to be the case (unless too much energy is allowed to be stored in the upper ocean in MI-IM), as the sea-ice extent in MI-IM is larger than the observed sea-ice extent in September, and in most parts over 95%. The delayed freeze-up can also be an effect of the bulk mixed layer in MICOM beeing to thick, making the upper ocean temperature increase slower and allowing too much heat to be absorbed in the layer.

The inclusion of brine pockets can delay freeze-up, because heat accumulated during the melt season and summer is stored in these pockets. In *Holland et al.* (1993) an experiment where brine pockets were included in the sea-ice model delayed fall freeze-up with around six weeks. As brine pockets in the sea-ice are now included in MI-IM, this could have something to do with the delayed freeze-up in the model. However, the problem of MI-IM producing to little ice during freeze-up has been addressed before brine pockets were included in the model (*Debernard and Køltzow*, 2005).

6.3 Observation Uncertainty

MI-IM's positive bias to the NSIDC and OSI-SAF sea-ice extent during the melt season and the summer may be caused by the fact that the sea-ice concentration derived from satellites observations tend to be underestimated during summer (see 4.5.1). If the ice edge is sharp (it the sea-ice concentration rapidly decreases) the sea-ice extent may be little influenced by the underestimation of the sea-ice concentration. If the sea-ice edge is less sharp the observed sea-ice extent may be underestimated.

In *Kattsov et al.* the uncertainty of sea-ice concentration derived from satellite passive microwave sensors are addressed. The authors estimate the uncertainty of the sea-ice extent to be of the order of 20%, the same as the difference is sea-ice extent between different satellite products can be. In the text an example is given where a minimum September ice extent of $5.1{\cdot}10^6\ km^2$ on 12 September is reported by NSIDC, while a sea-ice product from Arctic ROOS[3] report a minimum of $6.0{\cdot}10^6\ km^2$ the same day, over 17% more.

Looking at Table 6.2 shows how the difference in percent of the modeled and the observed sea-ice extent. All the experiments overestimate the minimum sea-ice extent except experiment Temp. If the observations tend to underestimate the sea-ice extent the Temp experiment further underestimates it. It also has the closest average minimum sea-ice extent to OSI SAF. Alb1 overestimates the sea-ice extent with over 28%. The Freeze2 experiment has the second smallest difference to the observed minimum sea-ice extent, 2.34%, and the Control experiment the thrid smallest, 3.76%. Not knowing if the OSI SAF observed sea-ice extent is correct or ±20% (most likely 0-+20%) makes it hard to evaluate the modeld sea-ice extent against it. Even if it is clear from Figure 5.16 and 5.17 that the average minima observed sea-ice extent from NSIDC and OSI SAF are closer than the modeled and the observed minima, the satellite derived sea-ice extent may be underestim-

[3]the Arctic Regional Ocean Observing System

ated due to the fact that it has problems distinguishing melt ponds from leads during the melt season and summer.

6.4 A Summary of Each Sensitivity Experiment's Results

Experiment Alb1, using the albedo scheme of *Mellor and Kantha* (1989), had by far the greatest effect on the ice. Both the 1985-1990 average mean ice thickness and minimum ice extent increased with about 22%. The scheme did however lead to an unrealistically large sea-ice extent during the melt season, summer and freeze-up, which did not compare well to observations. The scheme was aknowledged in 1971 to include a too high minimum sea-ice albedo (*Maykut and Untersteiner*, 1971). Alb1 compares the worst to observations, with an average minimum ice extent between 1987 and 1990 28% larger than the observed sea-ice extent, the lowest correlation cofficient to OSI-SAFv2, 0.88, and with the highest root mean square error, $1.28{\cdot}10^6\ km^2$.

Alb2, not weighting the snow albedo towards the albedo of the underlying ice, had the smallest effect of all the experiments on the sea-ice (the only effect it had was in increase of 1.3 % in the minimum sea-ice extent). On the snow thickness it had the smallest effect of the albedo experiments, but a larger effect than the open water experiments had. It should be made clear if the show cover fraction should paramatize the transparancy of thin snow or the fraction of a unit are which is snow covered given a mean snow thickness in the unit area. Compared to satellite observations of sea-ice extent Alb2 compares quite equally to the Control experiment, as Alb2 did not lead to a large change in the sea-ice extent from the Control experiment. It has a slightly larger bias than the Control experiment in each season, and a correlation coefficent during the whole period slightly lower than the Control experiment.

Alb3, changing the snow cover fraction to a *tanh*-function, increased the mean ice thickness with around 4 %, and the minimum ice extent and mean snow thickness with around 3%. It had a larger effect on the sea-ice than Freeze2 and Alb2, and a larger effect on the snow thickness than both OW freezing experiments and the Alb2 experiment had. That experiment Alb3 caused greater changes in the sea-ice and snow than experiment Alb2 is consistent with the fact that Alb3 made the albedo increase faster with increasing snow thickness than Alb2. Compared to observations Alb3 has a slightly larger positive bias than the Control and Alb2 experiment.

Experiment Freeze1, changing the lead closing parameter, h_0, from 0.5 m to 1.0 m led to the second largest change in the ice thickness after Alb1. It had a larger net effect on the sea-ice extent than Alb1 and 2 and Freeze2, leading to a 4 % increase in the minimum sea-ice extent. The thicker sea-ice of Alb1 made, as expected, the seasonal cycle of sea-ice extent less pronounced. As MI-IM overestimates the sea-ice in summertime and underestimates the sea-ice in wintertime, Freeze1 did not compare better to observations than the Control experiment. It had a higher root mean square error and a lower correlation coefficient than the Control experiment to the observations. Even though 1 m is argued to be the most apropriate value of h_0 (*Holland et al.*, 1993; *Bjornsson et al.*, 2003), a h_0 value of 1 m dose not make MI-IM compare better with observations, but worse.

In experiment Freeze2 h_0 was decreased with 25% from the Control experiment, from 0.5 m to 0.25 m. In Freeze1 h_0 was doubled from the Control experiment. Appropriately Freeze2 had only about half the effect on the ice thickness Freeze1 had, decreasing the mean ice thickness with 13 cm. On the sea-ice extent it had only a larger effect than the Alb2 experiment. It increased the seasonal cycle of the sea-ice extent, making a fairer comparison with observations than the Control experiment (a higher correlation coefficient and lower root mean square error to the observations).

The Temp experiment had an equally large effect on the sea-ice thickness as Freeze1. Where Freeze1 increased the ice thickness with 7.5%, Temp decreased it with the same percentage. It had the second largest effect on the sea-ice extent after Alb1, decreasing the minimum sea-ice extent almost 3%, making it compare better than the other experiments to observations during summertime, but worse during freeze-up and winter. Increasing the 2 m temperature for temperatures below zero degrees had a dramatic effect on the snow thickness. It decreased the 1985-1990 mean snow thickness with almost 60%. The decrease is probaly mostly a result of a change in the sensible heat and downward longwave radiation which are directly affected by the temperature increase. Because the model is not coupled to an atmosphere model and the surface does not interact with the atmosphere, the extreme decrease in snow thickness is not likely a realistic result of an increased temperature in the Arctic. It does show that the snow cover is sensitive to the the parametrization of sensible heat and longwave radiation.

Chapter 7

Summary and Key Findings

Considered are to which extent it is possible to reproduce the seasonal and inter-annual variations in the Arctic sea ice extent; and the effects changing crucial parameters in the sea-ice model have on the ice extent, ice thickness and snow thickness. To this end six six sensitivity experiments in addition to a control experiment are conducted using a coupled ice-ocean model, namely MI-IM (*Røed and Debernard*, 2004) coupled with MICOM (*Bleck et al.*, 1992). The coupled model is forced by atmospheric input from the ERA-40 (*Uppala et al.*, 2005). Three of the sensitivity experiments change how the snow/ice-albedo is parametrized in MI-IM. Two experiments alter the lead closing parameter, h_0, controlling the thickness of ice formed in open water. In the final sensitivity experiment is to add an increment to the 2 m temperature, after it is derived from ERA-40.

The model domain covers the Arctic Ocean and the Atlantic Ocean, from the southern tip of Florida in the west to Morocco in the east, and is projected on a rotated spherical grid with a mesh size of 0.25×0.25 degrees. The albedo scheme in MI-IM is based on the work of *Køltzow* (2007), where the surface is divided into three types: bare ice, snow, and melt ponds; where snow and melt ponds covers fractions of the total ice area. The snow/ice-albedo is dependent on the snow thickness, ice thickness, and the surface temperature. The albedo has a wide range, from 0.84, for completely snow covered ice, to 0.16, for thin, bare, melting ice.

MI-IM was initialized with sea-ice values from December 1966. The ocean model is initialized from a six year run from 1960 to 1967. The atmosphere data from ERA-40 follows the dates in the model run, starting from January 1. 1980 ending the 31. of December 1990.

The experiments are summarised in Table 3.1. In Chapter 1 three key questions were identified, namely "1) How sensitive are the ice thickness, the minimum ice extent, and the snow thickness to the various parametrizations and to a change in the atmospheric forcing?", "2) How well is the seasonal and inter-annual variation in the Arctic sea-ice extent reproduced in the model?", and "3) Which parameters are most important to determine?".

1. How sensitive are the ice thickness, the minimum ice extent, and the snow thickness to the various parametrizations and to a change in the atmospheric forcing?

The sea-ice thickness is most sensitivite to the use of the entirely different albedo scheme (Alb1). Using this albedo scheme changed the mean ice thickness with more than 22%. It is second most sensitive to the Temp and Freeze1 experiments. The Temp experiment decreased the mean ice thickness while Freeze1 increased it, both with around 7%. The Alb3 and Freeze2 had the third larges effect on the mean sea-ice thickness, with the Alb2 experiment increasing it with 3.7% and the Freeze2 decreasing it with 3.7%. The Alb2 experiment had virtually no effect on the mean sea-ice thickness, changing it with less than 0.8%.

Regarding the sea-ice extent it is most sensitivity to the Alb1 experiment, increasing the minimum sea-ice extent with about 22%. The minimum sea-ice extent showed the second most sensitivity to the Temp experiment, which decreases the minimum sea-ice extent with more than 5%. The Freeze1 experiment increased the minimum sea-ice extent with 4%. The Alb3 increased the minimum sea-ice extent with 2.7%, the Alb2 with 1.3%, while the Freeze2 decreased the sea-ice extent with 1.3%

The snow thickness showed the most sensitivity to the Temp experiment, which reduced the mean snow thickness with almost 60%. Furthermore the Alb1 experiment had a positive effect, increasing the snow thickness with 12.5%. Finally it is observed that the remaining experiments (Alb2, Alb3, Freeze1 and Freeze2) had a very small or no effect on the mean snow thickness.

2. How well is the seasonal and inter-annual variation in the Arctic sea-ice extent reproduced in the model?

First it should be observed that in the Bering Strait the model is uncoupled, because MI-IM relies on input from the SODA climatology and not from MICOM in this area. Thus it does not *exchange* fluxes with the atmosphere or the ocean in that area. Regarding the Arctic Ocean proper the standard model (the Control experiment) simulates a somewhat higher sea-ice extent in the melt season and summer than the observations, by respectively $0.61 \cdot 10^6$ km^2 and $0.34 \cdot 10^6$ km^2. The average minimum sea-ice extent between 1987 and 1990 is 3.8% larger than the sea ice extent observed by OSI SAF. The observed sea-ice extent can however be underestimated, as the passive microwave sensor derived sea-ice concentration can be up to 30% lower during the melt season and summer than other types of sea-ice concentration observations. For instance, ice charts (from the Canadian Ice Service and the U.S. National Ice Center), and products derived from synthetic aperature radars or the AVHRR show sea-ice concentrations 10%-30% higher than the sea-ice concentration derived from passive microwave images (see Chapter 4).

Ice is however produced too slowly during freeze-up. Between 1987 and 1990 it has an average negative bias in October, November, and December of $1.10 \cdot 10^6$ km^2. Despite the delayed freeze-up the coupled ice-ocean model reproduces the seasonal and inter-annual variations in the Arctic sea-ice extent fairly well. From July 1987 to December 1990 the

root mean square error compared to OSI-SAF observations excluding sea-ice south of the Bering Strait is $0.87{\cdot}10^6$ km^2. The correlation coefficient is 0.944.

Freeze2 compares better with observations than all of the other experiments; it has the highest correlation coefficient and the lowest root mean square error to the observations. The sea-ice model has problems with the sea-ice area increasing too slowly during freeze-up and decreasing too slowly during the melt season and summer. As the sea-ice area in Freeze2 increases and decreases faster than in the other experiments, Freeze2 compares better with observations of the sea-ice extent.

The experiment which compares the worst to observations is Alb1, with an average minimum ice extent between 1987 and 1990 28% larger than the observed average minimum, the lowest correlation cofficient, 0.88, and the highest root mean square error, $1.28{\cdot}10^6$ km^2. The Temp experiment had the sea-ice extent which compared best to the observed average minimum sea-ice extent, only 1.4% lower. This is because the sea-ice in Temp melted quicker than in the other experiments. It also increased slower than the other exeriments, making it underestimate the sea-ice extent during freeze-up and winter more than the other experiments. Consequently it had the second highest root mean square error of the experiments ($1.06{\cdot}10^6$ km^2).

Freeze1 overestimates the minimum sea-ice extent with almost twice the amount of the Control experiment. It also has a lower correlation coefficient and a higher root mean square error than the Control experiment. The Alb2 and Alb3 experiments are comparable to the Control experiment, as only negligibly more ice is produced.

3. Which parameters are most important to determine?

It should be emphasized that the Alb1 experiment shows the lowest correlation coefficient (0.88) and the highest RMSE ($1.28{\cdot}10^6$ km^2). This suggest that to realistically reproduce the sea ice extent a complex albedo parametrization is needed, to take into account, e.g. melt ponds. The small changes to the models albedo scheme, Alb2 and Alb3, did not have a large effect on the model, especially the change made in experiment Alb2 had a small effect on the model's ice and snow thickness and ice extent.

It is also noted that the lead closing parameters have a substantial effect on the ice thickness and therefore the seasonal cycle of the sea-ice extent. Changing these could be used to tune the model into having a seasonal cycle which fits closer to observations.

Finally it is evident that increasing the 2 m atmospheric temperature with $1°C$, or less, had a drastic effect on the snow cover. As the 2 m temperature directly effects the latent heat from the ocean, the sensible heat from the sea-ice and the ocean and the longwave radiation to the surface, it could be valuable to conduct more experiments changing the parametrizations of these.

7.1 Future Work

As the Temp experiment has such a large effect on the mean snow thickness, the snow thickness seems very sensitive to the sensible heat flux and incoming longwave radiation. It could be interesting to experiment with the models sensitivity to coefficients included in these parametrizations or to a differently parametrized incoming longwave radiation.

Experiments combining an albedo experiment with an OW experiment would also be interesting to conduct, e.g., combining the experiment changing the snow cover fraction and the experiment setting h_0 to 0.25 m. In *Dorn et al.* (2007) changing severeal parametrizations in one experiment proved useful.

Conducting a coupled sea-ice-ocean experiment from 1990 to 2000 would give insight in the model's ability to simulate the decrease in ice extent observed during the 90s. More observations available from this period would give information on how well the modeled variability of the ice thickness compares to observations (*Laxon et al.*, 2003).

Conducting the albedo experiments and the OW freezing experiments on a fully coupled ice-ocean-atmosphere model is necessary to see the effects of the experiments when atmospheric feedback effects are included.

More research should be conducted to find out why the freeze-up in MI-IM occurs later than in the observations.

Appendix A

Acronyms

ARPEGE	Action de Recherche Petite Echelle Grande Echelle
AVHRR	Advanced Very High Resolution Radiometer
BATS	Biosphere-Atmosphere Transfer Scheme
CAREX	Coordinated Eastern Arctic Research Experiment
CIS	Canadian Ice Service
DSMP	Defense Meteorological Satellite Program
ECHAM4	4^{th} Generation Global Climate Model developed by MPI-M (Hamburg)
ECHAM5	5^{th} Generation Global Climate Model developed by MPI-M (Hamburg)
ECMWF	European Center for Medium-Range Weather Forcasts
ECMWF IFS	ECMWF Integrated Forecast System
ESMR	Electrically Scanning Microwave Radiometer
ERA	ECMWF Re-Analysis
ERA-15	A 15 year ERA starting from 1979
ERA-40	A 40 year ERA from Sept. 1957 to Aug. 2002
EVP	Elastic-Viscous-Plastic
FYI	First-Year Ice
HARA	Historical Arctic Rawinsonde Archive
HIRS	High-Resolution Infrared Spectrometer
IGY	International Polar Year
met.no	Norwegian Meteorological Institute
MICOM	Miami Isopycnic Coordinate Model
MI-IM	Norwegian Meteorological Institute's Ice Model
MOSES2.2	Met Office Surface Exchange Scheme Version 2.2
MPDATA	Multidimensional Positive Definite Advection Transport Algorithm
MPI-M	Max Planck Institute for Meteorology
MSU	Microwave Sounding Unit
MYI	Multi-Year Ice
NASA	National Aeronautics and Space Administration
NCAR	National Center for Atmospheric Research
NIC	U.S. National Ice Center
NSIDC	National Snow and Ice Data Center
NTNU	Norwegian University of Science and Technology
RCN	Research Council of Norway
RMS	Root Mean Square
SAR	Synthetic Aperature Radar
SHEBA	Surface Heat Budget of the Arctic Ocean
SMMR	Scanning Multichannel Microwave Radiometer
SODA	Simple Ocean Data Assimilation
SSM/I	Special Sensor Microwave Imager
SSU	Stratospheric Sounding Unit
SWE	Snow Water Equivalent
TOVS	TIROS Operational Vertical Sounder
VTPR	Vertical Temperature Profile Radiometer
UiB	University of Bergen
UiO	University of Oslo
UiT	University of Tromsø

Appendix B

Variables in MI-IM

Symbol	Description	Unit
A	the fraction of sea ice in a unit area $\epsilon[0,1]$	
β	lateral melting rate of sea ice, always negative or equal to zero	
E	Heat Content	J/m^2
Ev	Evaporation rate over ice	m/s
g	the gravitational acceleration= 9.806 m/s^2	m/s^2
h	ice thickness	m
h_0	lead closing parameter=0.5 m	m
h_s	snow thickness	m
$\mathcal{R}$	2-D stress tensor	kg/s^2
ρ_f	Reference density of fresh water=1000 kg/m^3	kg/m^3
ρ_I	Reference density of sea ice=900 kg/m^3	kg/m^3
ρ_S	Reference density of snow=300 kg/m^3	kg/m^3
ρ_w	Reference density of sea water=1026 kg/m^3	kg/m^3
T_A	2 m temperature of the atmosphere	$^\circ C$
T_{ai}	temperature at the atmosphere-ice interface	$^\circ C$
T_{ao}	temperature at the atmosphere-ocean interface	$^\circ C$
T_f	freezing temperature of sea water at a given salinity	$^\circ C$
T_{as}	temperature at the atmosphere-snow interface	$^\circ C$
T_I	interior ice temperature	$^\circ C$
T_{io}	temperature at the ice-ocean interface ($\equiv T_f$)	$^\circ C$
T_{is}	temperature at the ice-snow interface	$^\circ C$
T_O	upper ocean mixed layer temperature	$^\circ C$
$\mathbf{u}$	sea ice velocity	m/s
Q_A^{ai}	heat flux from the atm.-ice interface to the atm.	W/m^2
Q_A^{ao}	heat flux from the atm.-ocean interface to the atm.	W/m^2
Q_A^{as}	heat flux from the atm.- snow interface to the atm.	W/m^2
Q_I^{ai}	heat flux to the atm.- ice interface from the ice	W/m^2
Q_I^{io}	heat flux from the ice-ocean interface into the ice	W/m^2
Q_I^{is}	heat flux to the ice-snow interface from the ice	W/m^2
Q_O^{ao}	heat flux to the ocean-atm. interface from the ocean	W/m^2
Q_O^{io}	heat flux to the ice-ocean interface from the ocean	W/m^2
Q_S^{as}	heat flux to the ice-ocean interface from the snow	W/m^2
Q_S^{is}	heat flux from the ice-snow interface to the snow	W/m^2
W_{ai}	ice production rate at the atm.-ice interface	m/s
W_{ao}	ice production rate at the atm.-ocean interface	m/s
W_{as}	the melting rate of snow	m/s
W_{io}	ice production rate at the ice-ocean interface	m/s
W_{fr}	frazil ice production in the water column	m/s
W_S	snow production due to frozen precipation minus evaporation	m/s

Bibliography

Baker, D., R. Skaggs, and D. Ruschy (1991), Snow depth required to mask the underlying surface, *J. Appl. Meteor*, *30*, 387–392.

Bjornsson, H., A. Willmott, and M. LA MYSAK (2003), Polynyas in a high-resolution dynamic–thermodynamic sea ice model and their parameterization using flux models, *Tellus A*, *53*(2), 245–265.

Bleck, R., C. Rooth, D. Hu, and L. Smith (1992), Salinity-driven thermocline transients in a wind-and thermohaline-forced isopycnic coordinate model of the North Atlantic, *Journal of Physical Oceanography*, *22*(12), 1486–1505.

Bromwich, D., and S. Wang (2005), Evaluation of the NCEP–NCAR and ECMWF 15-and 40-yr reanalyses using rawinsonde data from two independent Arctic field experiments, *Monthly Weather Review*, *133*(12), 3562–3578.

Bromwich, D., S. Wang, A. Monaghan, and O. Columbus (2001), ERA-40 representation of the Arctic atmospheric moisture budget.

Carton, J., G. Chepurin, and X. Cao (2000), A simple ocean data assimilation analysis of the global upper ocean 1950–95. Part II: Results, *Journal of Physical Oceanography*, *30*(2).

Cavalieri, D., P. Gloersen, and W. Campbell (1984), Determination of sea ice parameters with the Nimbus 7 SMMR, *Journal of Geophysical Research*, *89*(D4), 5355–5369.

Cavalieri, D. J., C. L. Parkinson, P. Gloersen, and H. J. Zwally (), Arctic and Antarctic Sea Ice Concentrations from Multichannel Passive-Microwave Satellite Data Sets: October 1978 - September 1995 - User's Guide NASA Technical Memorandum 104647, [Online; accessed 23-April-2010], `http://nsidc.org/data/docs/daac/nsidc0051_gsfc_seaice/TM104647.html`.

Comiso, J., and R. Kwok (1996), Surface and radiative characteristics of the summer Arctic sea ice cover from multisensor satellite observations, *Journal of Geophysical Research*, *101*(C12), 28,397.

Debernard, J., and M. Ø. Køltzow (2005), Technical documentation of the Oslo Regional Climate Model, Version 1.0, *RegClim, General Technical Report No. 8*, *8*, 51–68.

Dorn, W., K. Dethloff, A. Rinke, S. Frickenhaus, R. Gerdes, M. Karcher, and F. Kauker (2007), Sensitivities and uncertainties in a coupled regional atmosphere-ocean-ice model with respect to the simulation of Arctic sea ice, *Journal of Geophysical Research*, *112*(D10), D10,118.

Douville, H., J. Royer, and J. Mahfouf (1995), A new snow parameterization for the Meteo-France climate model, *Climate Dynamics*, *12*(1), 21–35.

Eastwood, S., K. R. Larsen, T. Lavergne, E. Nielsen, and R. Tonboe (2010), Global Sea Ice Concentration Reprocessing, Product User Manual, Version 1.1, *Tech. rep.*, met.no/DMI.

ECMWF Research Department (2003), *IFS Documentation Cycle CY23r4, Part IV: PHYSICAL PROCESSES(CY23R4), chapter 7*.

Essery, R., M. Best, and P. Cox (2001), MOSES 2.2 Technical Documentation, *Tech. Rep. Hadly Center technical note 30*, Hadly Center, Met Office.

Fetterer, F., K. Knowles, W. Meier, and M. Savoie (2002, updated 2009), Sea Ice Index, Boulder, Colorado USA: National Snow and Ice Data Center. Digital media., `http://nsidc.org/data/g02135.html`.

Graversen, R., T. Mauritsen, M. Tjernström, E. Källén, and G. Svensson (2008), Vertical structure of recent Arctic warming, *Nature*, *451*(7174), 53–56.

Hartmann, D. (1994), *Global physical climatology*, Academic Pr.

Hibler, W. D. (1979), A dynamic thermodynamic sea ice model, *Journal of Physical Oceanography*, *9*(4), 815–846, doi:10.1175/1520-0485(1979)009⟨0815:ADTSIM⟩2.0.CO;2.

Holland, D., L. Mysak, D. Manak, and J. Oberhuber (1993), Sensitivity study of a dynamic thermodynamic sea ice model, *J. Geophys. Res*, *98*(C2), 2561–2586.

Hunke, E., and J. Dukowicz (1997), An Elastic-Viscous-Plastic Model for Sea Ice Dynamics, *Journal of Physical Oceanography*, *27*(9), 1849–1867.

Häkkinen, S., and G. Mellor (1990), One hundred years of Arctic ice cover variations as simulated by a one-dimensional, ice-ocean model, *Journal of Geophysical Research-Oceans*, *95*(C9).

Kattsov, V., V. Ryabinin, C. Bitz, A. Busalacchi, J. Overland, M. Serreze, M. Visbeck, and J. Walsh (), RAPID LOSS OF SEA ICE IN THE ARCTIC.

Køltzow, M. (2007), The effect of a new snow and sea ice albedo scheme on regional climate model simulations, *Journal of Geophysical Research-Atmospheres*, *112*(D7), D07,110.

Laxon, S., N. Peacock, and D. Smith (2003), High interannual variability of sea ice thickness in the Arctic region, *Nature*, *425*(6961), 947–950.

Lindsey, R. (2005), Nimbus: 40th Anniversary, [Online; accessed 21-April-2010], `http://earthobservatory.nasa.gov/Features/Nimbus/nimbus.php`.

Liu, J., Z. Zhang, J. Inoue, and R. Horton (2006), Evaluation of snow/ice albedo parameterizations and their impacts on sea ice simulations, *International Journal of Climatology*, *27*(1), 81–91.

Maykut, G., and N. Untersteiner (1971), Some results from a time-dependent thermodynamic model of sea ice, *Journal of Geophysical Research*, *76*(6), 1550–1575.

Meier, W. (2005), Comparison of passive microwave ice concentration algorithm retrievals with AVHRR imagery in arctic peripheral seas, *IEEE Transactions on Geoscience and Remote Sensing*, *43*(6), 1324–1337.

Mellor, G., and L. Kantha (1989), An ice-Ocean Coupled Model, *Journal of Geophysical Research*, *94*(10), 937–10.

NASA web page, NSSDC (2010), DMSP 5D-2/F08, [Online; accessed 21-April-2010], `http://nssdc.gsfc.nasa.gov/nmc/spacecraftDisplay.do?id=1987-053A`.

NSIDC: Sea Ice Conc. (2010), Sea Ice Concentrations from Nimbus-7 SMMR and DMSP SSM/I Passive Microwave Data, [Online; accessed 22-April-2010], `http://nsidc.org/data/docs/daac/nsidc0051_gsfc_seaice.gd.html`.

NSIDC: Sea Ice Index (2008), Sea Ice Index, [Online; accessed 23-April-2010], `http://nsidc.org/data/docs/noaa/g02135_seaice_index/index.html`.

OSI SAF (2010), EUMETSAT Ocean and Sea Ice Satelitte Application Facility. Global sea ice concentration reprocessing dataset 1978-2007 (v1, 2010).

Overland, J., S. McNutt, J. Groves, S. Salo, E. Andreas, and P. Persson (2000), Regional sensible and radiative heat flux estimates for the winter Arctic during the Surface Heat Budget of the Arctic Ocean (SHEBA) experiment, *Journal of Geophysical Research*, *105*(C6), 14,093.

Parkinson, C., and D. Cavalieri (1989), Arctic Sea Ice 1973–1987: Seasonal, Regional, and Interannual Variability, *Journal of Geophysical Research*, *94*(C10).

Partington, K., T. Flynn, D. Lamb, C. Bertoia, and K. Dedrick (2003), Late twentieth century Northern Hemisphere sea-ice record from US National Ice Center ice charts, *J. Geophys. Res*, *108*(C11).

Perovich, D., R. Kwok, W.Meier, S. Nghiem, and J. Richter-Menge (2009), Sea Ice Cover, [Online; accessed 10-June-2010], `http://www.arctic.noaa.gov/reportcard/seaice.html`.

Roesch, A., and E. Roeckner (2006), Assessment of Snow Cover and Surface Albedo in the ECHAM5 General Circulation Model, *Journal of Climate*, *19*, 16.

Roesch, A., M. Wild, H. Gilgen, and A. Ohmura (2001), A new snow cover fraction parametrization for the ECHAM4 GCM, *Climate Dynamics*, *17*(12), 933–946.

Røed, L. P., and J. Debernard (2004), *Description of an integrated flux and sea-ice model suitable for coupling to an ocean and atmosphere model*, met.no report 4/2004, 51p, Norwegian Meteorological Institute, Oslo, Norway, ISSN 1503-8025.

Røed, L. P., and J. Debernard (2005), Simulations with a north atlantic coupled ice-ocean model, *RegClim, General Technical Report No. 8*, *8*, 69–81.

Semtner Jr, A. (1987), A Numerical Study of Sea Ice and Ocean Circulation in the Arctic, *Journal of Physical Oceanography*, *17*(8).

Smolarkiewicz, P., and L. Margolin (1998), MPDATA: A Finite-Difference Solver for Geophysical Flows, *Journal of Computational Physics*, *140*, 459–480.

Solomon, S., D. Qin, M. Manning, R. Alley, T. Berntsen, N. Bindoff, Z. Chen, A. Chidthaisong, J. Gregory, G. Hegerl, et al. (2007), Technical Summary. In Climate Change 2007: The Physical Science Basis. Contribution of Working Group 1 to the Fourth Assessment Report of the Intergovernmental Panel on Climate Change [Solomon, S. and Qin, D. and Manning, M. and Chen, Z. and Marquis, M. and Averyt, KB and Tignor, M. and Miller, HL].

Stroeve, J., M. Holland, W. Meier, T. Scambos, and M. Serreze (2007), Arctic sea ice decline: Faster than forecast, *Geophys. Res. Lett*, *34*.

TIROS Program/NASA (2000), Planet earth from tiros 1: First tv image, [Online; accessed 19-April-2010], `http://apod.nasa.gov/apod/image/0004/first_tiros1.jpg`.

Tonboe, R., and E. Nielsen (2010), Global Sea Ice Concentration Reprocessing, Validation Report, Version 1.1, *Tech. rep.*, DMI.

Uppala, S., P. Kaallberg, A. Simmons, U. Andrae, V. Da Costa Bechtold, M. Fiorino, J. Gibson, J. Haseler, A. Hernandez, G. Kelly, et al. (2005), The ERA-40 re-analysis, *Quarterly Journal of the Royal Meteorological Society*, *131*(612), 2961–3012.

Verserghy, D. (1991), Class-A Canadian land surface scheme for GCMS. I, Soil model, *International journal of climatology*, *11*(2), 111–133.

Yang, Z., R. Dickinson, A. Robock, and K. Vinnikov (1997), Validation of the snow submodel of the Biosphere–Atmosphere Transfer Scheme with Russian snow cover and meteorological observational data, *Journal of Climate*, *10*(2).

Yokoyama, Y., K. Lambeck, P. De Deckker, P. Johnston, and L. Fifield (2000), Timing of the Last Glacial Maximum from observed sea-level minima, *Nature*, *406*(6797), 713–716.

Øseth, E. (2010), Klimaendringer i norsk Arktis - Konsekvenser for livet i nord, (136).